INVESTIGATION OF GEOMETRICAL FACTORS FOR DETERMINING FRACTURE TOUGHNESS WITH THE MODIFIED RING TEST

A THESIS SUBMITTED TO
THE GRADUATE SCHOOL OF NATURAL AND APPLIED SCIENCES
OF
MIDDLE EAST TECHNICAL UNIVERSITY

BY

CEYDA ALPAY

IN PARTIAL FULFILLMENT OF THE REQUIREMENTS
FOR
THE DEGREE OF MASTER OF SCIENCE
IN
MINING ENGINEERING

SEPTEMBER 2008

Approval of the thesis:

INVESTIGATION OF GEOMETRICAL FACTORS AND SIZE EFFECT FOR DETERMINING FRACTURE TOUGHNESS WITH THE MODIFIED RING TEST

submitted by CEYDA ALPAY in partial fulfillment of the requirements for the degree of **Master of Science in Mining Engineering Department, Middle East Technical University** by,

Prof. Dr. Canan Özgen _____

Dean, Graduate School of **Natural and Applied Sciences**

Prof. Dr. Celal Karpuz _____

Head of Department, **Mining Engineering**

Assoc. Prof. Dr. Levent Tutluoğlu _____

Supervisor, **Mining Engineering Dept., METU**

Examining Committee Members:

Prof. Dr. Naci Bölükbaşı _____
Mining Engineering Dept., METU

Assoc. Prof. Dr. Levent Tutluoğlu _____
Mining Engineering Dept., METU

Prof. Dr. Celal Karpuz _____
Mining Engineering Dept., METU

Assoc. Prof. Dr. Aydın Bilgin _____
Mining Engineering Dept., METU

Assist. Prof. Dr. M. Ali Hindistan _____
Mining Engineering Dept., Hacettepe University

Date:

I hereby declare that all information in this document has been obtained and presented in accordance with academic rules and ethical conduct. I also declare that, as required by these rules and conduct, I have fully cited and referenced all material and results that are not original to this work.

Name, Last name: Ceyda Alpay

Signature :

ABSTRACT

INVESTIGATION OF GEOMETRICAL FACTORS FOR DETERMINING FRACTURE TOUGHNESS WITH THE MODIFIED RING TEST

Alpay, Ceyda

M.Sc., Department of Mining Engineering

Supervisor: Assoc. Prof. Dr. Levent Tutluoğlu

September 2008, 120 pages

Modified Ring specimens are of the shape of discs having a hole inside and flattened ends. These specimens are used for determination of Mode I fracture toughness. Finite element program, named ABAQUS, is used for numerical modeling for finding stress intensity factors. Varying disc geometries were used for the experiments and numerical modeling in which size of the flat ends, radius of the hole inside, and external radius of the specimen were varied.

Experiments were done by using pink Ankara andesite. Effects of internal hole radius, external disc radius and size of the flat ends on both stress intensity factor and fracture toughness were studied. In order to compare the results, fracture tests with semi-circular specimens under three point bending (SCB) were also performed. From a similar previous study, fracture toughness values of gray andesite were recalculated and compared to the fracture toughness values of pink andesite for varying geometrical factors. Size effect studies were performed as well for varying diameter of core specimens.

Fracture toughness values of andesite were found to increase with increasing specimen size. Fracture toughness of 100 mm specimens was determined as 1.11±0.07 MPa√m, whereas fracture toughness of 75 mm specimens was 0.96±0.08 MPa√m. 100 mm or larger diameter specimens were suggested for the fracture toughness determination with the modified ring tests.

Keywords: Stress Intensity Factor, Mode I Fracture Toughness, Modified Ring Test, Size Effect, Numerical Modeling

ÖZ

ÇATLAK TOKLUĞU TAYİNİ İÇİN GELİŞTİRİLMİŞ UYARLANMIŞ HALKA TESTİNE GEOMETRİK FAKTÖRLERİN ETKİSİNİN ARAŞTIRILMASI

Alpay, Ceyda

Yüksek Lisans, Maden Mühendisliği Bölümü

Tez Yöneticisi: Doç. Dr. Levent Tutluoğlu

Eylül 2008, 120 sayfa

Çatlak tokluğu tayini için geliştirilmiş halka numuneleri, içinde bir delik bulunan ve üst ve alt yüzeyleri düzeltilmiş disklerdir ve bu diskler Mod I çatlak tokluğu tayini için kullanılmaktadır. ABAQUS isimli sonlu eleman programı gerilme şiddet faktörünün belirlenmesinde kullanılmıştır. Farklı geometrilerde numuneler ile deneysel ve sayısal modelleme çalışmaları yapılmıştır. Bu numunelerde, düzeltilmiş kenarların boyutu, içerdeki deliğin yarıçapı, numunenin dış yarıçapı değiştirilmiştir.

Deneyler pembe Ankara andesiti kullanılarak yapılmıştır. Düzeltilmiş kenarların boyutunun, iç deliğin yarıçapının ve numunenin dış çapının gerilme şiddet faktörüne ve çatlak tokluğuna etkisi çalışılmıştır. Sonuçları karşılaştırmak amacıyla, çatlak tokluğu testleri, yarım-dairesel örneklerde eğilme deneyleri ile de yapılmıştır. Daha önceki benzer bir çalışmadan, gri Ankara andezitinin de çatlak tokluğu tekrar hesaplanmış ve bu değerler farklı

geometrilerde pembe andezitinkilerle karşılaştırılmıştır. Numune boyutunun çatlak tokluğuna etkisi de incelenmiştir.

Andezitin çatlak tokluğu değerinin artan numune çapıyla arttığı bulunmuştur. 100 mm'lik numunelerin çatlak tokluğu değeri 1.11±0.07 MPa√m olarak bulunurken, 75 mm'lik numunelerin çatlak tokluğu değeri 0.96±0.08 MPa√m olarak bulunmuştur. Uyarlanmış halka testlerinde 100 mm'lik numunelerin kullanılması uygun görülmüştür.

Anahtar Kelimeler: Gerilme Şiddet Faktörü, Mod I Çatlak Tokluğu, Uyarlanmış Halka Testi, Boyut Etkisi, Sayısal Modelleme

TO MY FAMILY

ACKNOWLEDGEMENT

During the writing of this thesis I was fortunate enough to obtain substantial guidance from my supervisor, Assoc. Prof. Dr. Levent Tutluoğlu, for his helpful comments and advice. I would like to take this opportunity to give him my deepest appreciation.

I want to thank to the examining committee the members, Prof. Dr. Celal Karpuz, Prof. Dr. Naci Bölükbaşı, Assoc. Prof. Dr. Aydın Bilgin and Assist. Prof. Dr. Mehmet Ali Hindistan, for being interested in this thesis.

For their help in my laboratory works, I'm grateful to Tahsin Işıksal, Hakan Uysal and Arman Koçal.

I have to give a lot of credit for what Çiğdem Alkılıçgil has done for me. She was there for me whenever I need help.

I'd like to show my gratitude to all my friends. They are always with me, in my best and worst times.

I truly appreciate to all my family, for their unconditional support during my thesis and all my life.

I want to express my deepest appreciation to Berk Alpay for his patience and love.

TABLE OF CONTENTS

LIST OF TABLES

LIST OF FIGURES

LIST OF SYMBOLS AND ABBREVIATIONS

a : Crack length

BDT : Uncracked Brazilian Disk Test

CB : Chevron Bend

CCBD : Central Cracked Brazilian Disc under diametral compression test

CCP : Centre Cracked Panel

CMOD : Crack Mouth Opening Displacement

CNBD : Chevron-Notched Brazilian Disc

CTOD : Crack Tip Opening Displacement

D : Specimen diameter

E : Young's Modulus

F : Applied load

F_{cr} : Critical load

F_{Imax} : First maximum load in the modified ring test

F_{max} : Maximum load

G : Strain energy release rate

ISRM : International Society for Rock Mechanics

J : J-integral

K : Stress intensity factor

K_{Ic} : Fracture toughness

K_I : Stress intensity factor in Mode I

K_{II} : Stress intensity factor in Mode II

K_{III} : Stress intensity factor in Mode III

K_{CB} : Fracture toughness of chevron bend specimen

K_{SR} : Fracture toughness of short rod specimen

L : Half length of flattened end of MR specimen

LEFM : Linear Elastic Fracture Mechanics

LVDT : Linear Variable Differential Transducer

MR : Modified Ring test

MTS : Material Testing System

r : Specimen Radius

r_e : External radius of the specimen

r_i : Inner hole radius

S : Support Span

SCB : Semi-Circular specimen under three-point bending

SR : Short Rod

t : Thickness of the specimen

T : Traction vector

T_0 : Tensile strength

u : Displacement vector

UCS : Uniaxial Compressive Strength

W : Strain energy density

μ : Shear modulus

ν : Poisson's Ratio

ε : Strain

σ : Applied stress

σ_{cr} : Critical stress

σ_{11} : Stress in horizontal (x) direction

σ_{22} : Stress in vertical (y) direction

τ : Shear stress

2γ : Surface energy

Γ : Arbitrary path around crack tip

CHAPTER 1

INTRODUCTION

1.1 General

Crack, in its dictionary meaning, is to break or burst with or without entire separation of the parts. Fracture mechanics is the science which examines the cracked bodies. Formation of cracks is important for many sciences and engineering uses.

Fracture toughness is a parameter to determine the stress required to drive a preexisting crack. It is an important parameter; because materials generally have a preexisting crack. Although, the ways to determine fracture toughness have been studied by many researchers, still there is no standard method. But some suggested methods are present.

Suggested methods for determination of fracture toughness are not very easy to perform. Modified ring test is not a suggested method; but this method use specimens which are easily prepared. Since there are not many studies on modified ring test, this method has to be improved.

1.2 Fracture Toughness Applications

Engineering materials are full of cracks. For civil engineering applications; although structures can be safely built with these materials, this fact is relevant for the design of a wide class of structures. The presence of stress

concentrations in notches, around holes, in connections, etc. require sophisticated design procedures. With the development of Fracture Mechanics, whether the cracks are stable or not becomes more important than if it exists or not. The high end in Fracture Mechanics applied to concrete indicates a great variety of models to simulate concrete behavior. These models require that parameters be obtained from concrete samples to characterize, basically, resistance to crack propagation. (Prado and Mier, 2003)

Medical use of fracture mechanics shows its importance in biomaterials such as stents. Stents are small tubes that are inserted into the body for several reasons. Inside the body, stents are exposed to many cycles of loading and sometimes some overloads which may result in fracture. After this point, fracture mechanics is the science which should be used.

Many researchers used strength or fracture toughness to find the toughness of bones. In 2006, Yan et al. stated in their paper, that they applied elastic-plastic fracture mechanics to find the fracture toughness of the bone. They used the J-integral, which is a parameter used to calculate energy per unit fracture surface area in a material, to quantify the total energy spent before bone fracture.

Fracture mechanics is also used for the determination of fracture properties of adhesively bonded aerospace material systems. In the paper of Choupani (2008), finite-element analyses of bonded joints and also mixed-mode fracture toughness tests of the specimens consisting of several combinations of adhesive, composite and metallic adherends were studied for the determination of interfacial mixed-mode fracture properties.

Fracture mechanics have several usages in material sciences. Application of fracture mechanics to adhesive joints is one of them. The effect on fracture toughness of joint geometry, section size, strain rate and fracture mode are discussed by Ripling et al. in 1963.

Fracture mechanics is used in analyzing problems such as rock slope stability and well bore stability. Also, the applications of fracture mechanics for designing operations like rock blasting, hydraulic fracturing are increasing. The most essential parameter in these studies is fracture toughness of rock material.

Fracture toughness studies are also used to study the energy requirement to break coal during crushing. Cutting results in dynamic breakage of rocks where drilling and blasting operations break the rock partly in tension along pre-existing or newly formed cracks which produces dust. Karl & Bieniawski (1986) studied effect of fracture toughness of coal to the formation of coal dust.

One of the most important use fields of fracture mechanics is undoubtedly hydraulic fracturing. Thiercelin (1989) showed the importance of the exact value for fracture toughness in hydraulic fracture. Abou-Sayed et. al. (1978) introduced a fracture mechanics approach to the hydraulic fracturing criterion assuming the existence of arbitrarily oriented cracks in rock. Rummel (1987) suggest that when the opening mode (Mode I) stress intensity factor K_I at the tip of the crack reaches a critical value, K_{IC} (fracture toughness), hydraulic fracturing will occur.

1.3 Statement of the Problem

Since rock fracture mechanics has been widely applied to many branches of civil and mining engineering, researchers are still studying to find a simple and

accurate standard method to determine fracture toughness. It is difficult to achieve accurate fracture toughness values in the case of soft and heterogeneous rocks. In the case of subsized specimens, the existence of a large process zone ahead of the crack tip makes the determination of the apparent fracture toughness crack-length dependent.

Most of the existing test techniques for fracture toughness determination require specimens with preliminary notches or cracks of different shapes. Preparation of specimens with these sophisticated notch shapes and fatigue pre-cracking for some test techniques, take a lot of effort and time. With its simplicity in specimen preparation and with its compressive loading procedure the modified ring testing method is a future candidate as one of the suggested methods of ISRM for fracture toughness testing on core-based specimens.

The Modified Ring Test uses the concept of effective crack length and considers an adequately long crack to be able to neglect subcritical crack propagation. This test also prevents development of a large process zone ahead of the crack tip (Thiercelin and Roegiers, 1986). It is easy to prepare modified ring test specimens compared to the other specimen geometries since there is a hole inside and crack initiates from this hole, there is no need to open a new crack. So crack forms by itself.

In order to become one of the suggested or standard methods for fracture testing extensive studies including effects of geometrical factors and specimen size are to be conducted. For this testing method, stress intensity factors for different specimen geometries and sizes should be computed and served for the universal applications of this specimen geometry.

1.4 Objective of the Thesis

The aim of this study is to investigate the effects of geometrical factors on Mode I fracture toughness of rocks. Effects of inner hole radius, size of loading ends, and specimen size, that is, the diameter of core specimens will be investigated. This way it is hoped here that contributions is made in efforts to develop another core-based testing technique, and in efforts to include this technique as one of the suggested methods of ISRM. The modified ring testing technique is expected to find wide applicability, since it does not require any preliminary notch or crack, provided that appropriate geometries and specimen sizes, and accurate stress intensity factors in general are determined and served for general use.

1.5 Methodology

Experimental studies for development of modified ring test start with cutting the rock blocks into smaller pieces so that cores can be taken. After the cores are taken, these cores are cut into discs with desired width. Then these discs are drilled with drill bits having different diameters. Following that the surfaces of the discs are flattened and polished, and then two ends of the specimens are flattened. After preparing the specimens, experiments start under compressive loading, the data are collected, and load - displacement graphs are drawn.

Tests are carried out with specimens having 54, 75, 100 and 125 mm diameter specimens. Like the size of the specimen, inner hole diameter and the size of the flat ends are changed.

ABAQUS program was used for numerical modeling. After drawing the geometry of the specimens in the program and giving their properties, load and

boundary conditions, stress intensity factor versus crack length graphs were drawn. From these graphs maximum stress intensity factor was computed. Using this maximum stress intensity factor together with the maximum load taken from the load-displacement graph of the experiments, fracture toughness was calculated. The same procedure was repeated for varying specimen diameters, inner hole diameters and flat end sizes.

Half-disc specimens were prepared for the semicircular bending tests under three point bending (SCB). Fracture toughness values obtained from modified ring tests are compared with the results of SCB tests.

1.6 Sign Convention

In rock mechanics, compressive stresses are accepted to be positive and tensile stresses are accepted to be negative. But in this study, since general linear elastic fracture mechanics and a finite element program; ABAQUS is used, stresses of compression and tension are negative and positive respectively.

1.7 Outline of the Thesis

This thesis begins with a brief introduction in Chapter 1 and continues with history and some basic principles of fracture mechanics. Chapter 3 covers some previous studies on fracture toughness determination. Explanation of the finite element program used and numerical modeling studies are given in Chapter 4. Laboratory work with experimental setup is elucidated in Chapter 5 and finally Chapter 6 covers the conclusion of this study and recommendations for further studies.

CHAPTER 2

FRACTURE MECHANICS

2.1 History

In 1913, C. E. Inglis noticed that, an elliptical hole at a thin plate of glass becomes greater when he pulled the plate at both ends. He found the points that are feeling the most stress. He then looked at other plates having non-elliptical holes and he found that the shape of the crack does not really matters in cracking. The important thing in cracking is the length of the crack in the direction perpendicular to the load and also the radius of curvature for the ends of the hole. He is the first man who discovered something about the relation between the load and cracking.

In 1920's A. A. Griffith started to do experiment with soft iron wire. He used two wires, both same type and with same dimensions. He put some scratches and small fractures on one of the wires. He pulled them until they yielded and found that the scratched one had quarter of the strength of the unscratched one. Griffith also introduced and formulated crack propagation by saying that if a crack could not found enough energy to create new crack surfaces, it propagates.

At the time of Griffith, the theoretical strength of a material was accepted to be one tenth of the material's Young's Modulus. But it was observed that the critical strength is 1000 times less that the predicted value. Griffith explained by stating that in every material there are many macroscopic cracks which lowers the overall strength of the material because stress concentration occurs when a load is applied to the cracks. Stress concentration occurs at a place

where stress is concentrated which is the crack tip for cracks. Cracks in the crack tip grow more quickly which results in fracture before reaching to the theoretical strength. It should be noted that Griffith was only considering elastic, brittle materials, in which no plastic deformation took place.

Griffith related crack length and applied stress with this formula:

$$\sigma = \sqrt{\frac{2\gamma E}{\pi a}} \tag{2.1}$$

where,
σ = applied stress
2γ = surface energy
E = Young's modulus
a = crack length

Because of the limitations of the Griffith's theory, in 1940's Irwin extended this theory also for ductile materials. He developed the concept of strain energy release rate; G. G is the rate of change in potential energy near the crack area for linear elastic materials. When G reaches a critical value; G_c, the crack propagates. Later, some researchers change G into K, which is the stress intensity factor. Irwin also formulates the stresses in the region near the tip of the crack as a general form:

$$\sigma_{ij} = \frac{K_I}{\sqrt{2\pi r}} f_{ij}(\theta) + \cdots \tag{2.2}$$

where,
r,θ = polar coordinates
K = stress intensity factor

After the first milestones of fracture mechanics have been set, scientist began to focus on plasticity of the crack tips. In United States, Rice (1968) modeled plastic deformation as a nonlinear elastic behavior and he extended the energy release rate method to those materials. He found a path-independent line integral, called the J-integral to indicate energy release rate. Also in Europe, a scientist named Wells noticed that the crack faces move apart before fracture. From these observations, he proposed Crack Tip Opening Displacement (CTOD) as a fracture criterion.

2.2 Linear Elastic Fracture Mechanics

Linear elastic fracture mechanics (LEFM) is based on the continuum mechanics of elastic bodies applied to specimens containing cracks. As the crack tips perform singularities where the stresses tend to infinite, complete failure of the specimen would be caused by incremental loads.

LEFM assumes the material to be isotropic and linearly elastic. Such materials have only two independent elastic constants; Young's Modulus (E) and Poisson's Ratio (ν). Some brittle fracture situations show a linear relation between stress and strain up to the point of fracture. In such cases LEFM is applicable up to that point. Sometimes large zones of plastic deformation develop before the crack grows, for this type of fractures Elastic Plastic Fracture Mechanics (EPFM) must be used.

By considering linear elastic theories, the stress field near the crack tip depends on the location, the loading conditions and the geometry of the specimen.

$$\sigma_{ij}{}^{cr.tip} = \sigma_{ij}{}^{cr.tip}\ (r, \theta, K) \tag{2.3}$$

where,

r and θ = polar coordinates

K = stress intensity factor which is calculated from loading and geometry

2.3 Fracture Modes

Linear Elastic Fracture Mechanics (LEFM) considers three different fracture modes. These are the only possible ways that a crack tip can deform.

In Mode I, tensile or opening mode, the forces are perpendicular to the crack plane resulting opening of the crack.

In Mode II, in-plane shear mode, the forces are parallel to the crack. One of the forces pushes the top part of the crack back and the other force pulls the bottom part of the crack forward on the same line. There is no out of plane deformation in this mode.

In Mode III, out-of-plane shear mode, forces cause the material to separate by shearing parallel to the crack front. This mode is also termed as tearing mode.

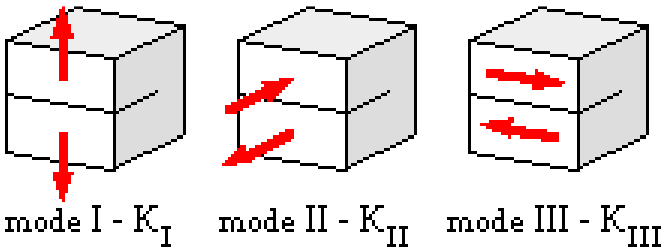

Figure 2.1 Fracture modes

Any combinations of these modes is called mixed mode.

2.4 Plane Stress and Plane Strain

Many problems in elasticity can be treated by plane theory of elasticity. Plane stress and plane strain are two general types for this plane analysis.

When a plate is too thin to sustain through-the-thickness stress, plane stress condition controls the fracture process. It means σ_{zz} is equal to "0".

In plane strain condition, for a thick plate, the strain normal to the x-y plane, ε_{zz} is assumed to be "0". Dams, tunnels and other geotechnical works are some important applications of plane strain.

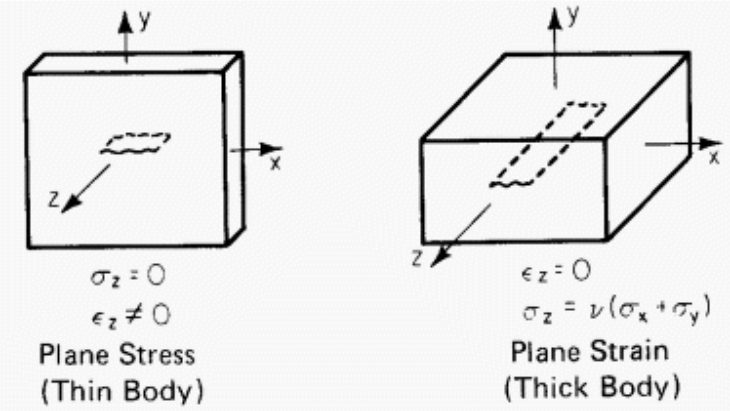

Figure 2.2 Plane stress and plane strain

2.5 Crack Tip Stress Fields in an Isotropic, Linear Elastic Solid

The loading conditions and geometry of the solid are not important for the distribution of the stress, displacement and strain fields when you get really close to the crack tip. The distribution is always the same.

Figure 2.3 shows a linear elastic solid containing a crack. The solid is loaded in infinity. As it is seen cylindrical- polar coordinates (r,θ,z) are used for expressing crack tip field.

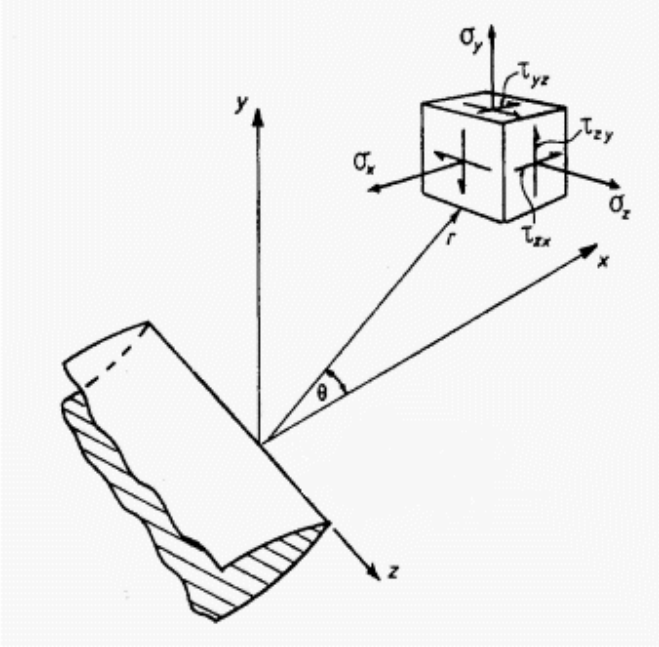

Figure 2.3 Local stresses near a crack tip

The stress field components near crack tip are given by

$$\sigma_{xx} = \frac{K_I}{\sqrt{2\pi r}}\cos\frac{\theta}{2}\left(1 - \sin\frac{\theta}{2}\sin\frac{3\theta}{2}\right) - \frac{K_{II}}{\sqrt{2\pi r}}\sin\frac{\theta}{2}\left(2 + \cos\frac{\theta}{2}cos\frac{3\theta}{2}\right) \quad (2.4)$$

$$\sigma_{yy} = \frac{K_I}{\sqrt{2\pi r}}\cos\frac{\theta}{2}\left(1 + \sin\frac{\theta}{2}\sin\frac{3\theta}{2}\right) + \frac{K_{II}}{\sqrt{2\pi r}}cos\frac{\theta}{2}\sin\frac{\theta}{2}\cos\frac{3\theta}{2} \quad (2.5)$$

$$\tau_{xy} = \frac{K_I}{\sqrt{2\pi r}}cos\frac{\theta}{2}\sin\frac{\theta}{2}\cos\frac{3\theta}{2} + \frac{K_{II}}{\sqrt{2\pi r}}cos\frac{\theta}{2}\left(1 - \sin\frac{\theta}{2}sin\frac{3\theta}{2}\right) \quad (2.6)$$

$$\tau_{yz} = -\frac{K_{III}}{\sqrt{2\pi r}}\sin\frac{\theta}{2} \quad (2.7)$$

$$\tau_{zx} = \frac{K_{III}}{\sqrt{2\pi r}}\cos\frac{\theta}{2} \quad (2.8)$$

in which K_I, K_{II} and K_{III} are Mode I, Mode II and Mode III stress intensity factors respectively.

Displacement components calculated by integrating the strains are:

$$u_x = \frac{K_I}{\mu}\sqrt{\frac{r}{2\pi}}\left[\kappa - 1 + 2sin^2\frac{\theta}{2}\right]cos\frac{\theta}{2} + \frac{K_{II}}{\mu}\sqrt{\frac{r}{2\pi}}\left[\kappa + 1 + cos^2\frac{\theta}{2}\right]sin\frac{\theta}{2} \quad (2.9)$$

$$u_y = \frac{K_I}{\mu}\sqrt{\frac{r}{2\pi}}\left[\kappa + 1 - 2cos^2\frac{\theta}{2}\right]sin\frac{\theta}{2} + \frac{K_{II}}{\mu}\sqrt{\frac{r}{2\pi}}\left[\kappa - 1 - sin^2\frac{\theta}{2}\right]cos\frac{\theta}{2} \quad (2.10)$$

$$u_z = \frac{K_{III}}{\mu}\sqrt{\frac{2r}{\pi}}sin\frac{\theta}{2} \quad (2.11)$$

$$\text{where } \kappa = \begin{cases} \frac{3-\nu}{1+\nu} & plane\ stress \\ 3 - 4\nu & plane\ strain \end{cases}$$

The displacement and stress near the crack tip can be characterized by three numbers, known as stress intensity factors. The `Mode I' stress intensity factor quantifies the crack opening displacements and stresses; the `Mode II' stress intensity factor characterizes in-plane shear displacements and stress; and the `Mode III' stress intensity factor quantifies out-of-plane shear displacement of the crack faces and anti-plane shear stresses at the crack tip. The stress intensity factors depend on the detailed shape of the solid, and the way that it is loaded.

2 .6 Stress Intensity Factor

Stress intensity factor (SIF,K) is a measure of the singularity of the stress field at a loaded crack tip. K is used in fracture mechanics to more accurately predict the stress state near the tip of a crack caused by a remote load or residual stresses. When this stress state becomes critical a small crack grows and the material fails.

Figures 2.4 a through h, shows stress intensity factor expressions for some common loading conditions.

a) Infinite Plate with a Center Through Crack under Tension

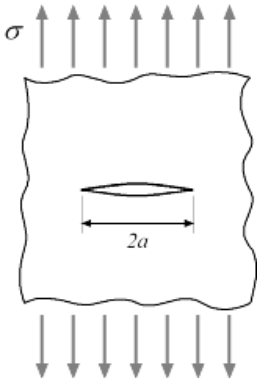

$$K_I = \sigma\sqrt{\pi a}$$

b) Infinite Plate with a Hole and Symmetric Double Through Cracks under Tension

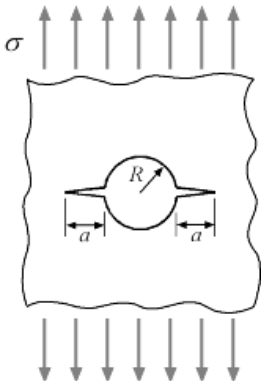

$$K_I = \sigma\sqrt{\pi a}\left[1+2.365\left(\frac{R}{R+a}\right)^{2.4}\right]$$

c) Semi-infinite Plate with an Edge Through Crack under Tension

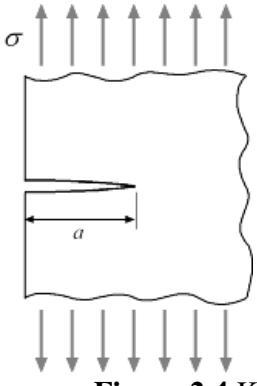

$$K_I = 1.12\sigma\sqrt{\pi a}$$

Figure 2.4 K_I expressions for some common loading conditions (www.efunda.com)

d) Infinite Stripe with a Center Through Crack under Tension

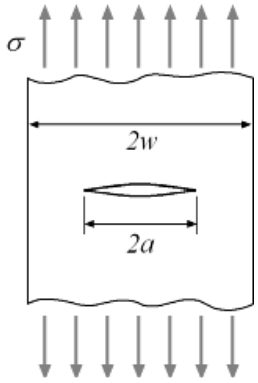

$$K_I = \sigma\sqrt{\pi a}\left[\frac{2w}{\pi a}\tan\left(\frac{a}{2w}\right)\right]^{1/2}$$

or

$$K_I = \sigma\sqrt{\pi a}\left[\sec\left(\frac{\pi a}{2w}\right)\right]^{1/2}\left[1-0.25\left(\frac{a}{w}\right)^2+0.06\left(\frac{a}{w}\right)^4\right]$$

e) Infinite Stripe with an Edge Through Cracks under Tension

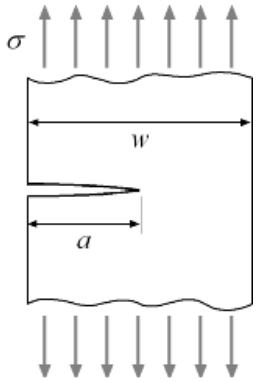

$$K_I = \sigma\sqrt{\pi a}\left(\frac{2w}{\pi a}\tan\left(\frac{\pi a}{2w}\right)\right)^{\frac{1}{2}}\left[\frac{0.752+2.02\frac{a}{w}+0.37\left(1-\sin\left(\frac{\pi a}{2w}\right)\right)}{\cos\left(\frac{\pi a}{2w}\right)}\right]$$

f) Infinite Stripe with Symmetric Double Through Cracks under Tension

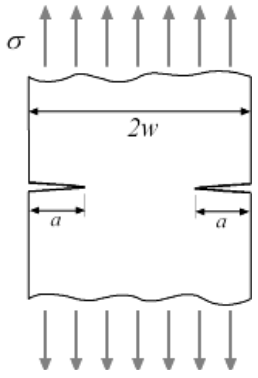

$$K_I = \sigma\sqrt{\pi a}\left(\frac{2w}{\pi a}\right)^{\frac{1}{2}}\left[\tan\left(\frac{\pi a}{2w}\right)+0.1\sin\left(\frac{\pi a}{w}\right)\right]^{\frac{1}{2}}$$

Figure 2.4(cont'd) K_I expressions for some common loading conditions

g) Single Edge Notched Specimen Under Tension

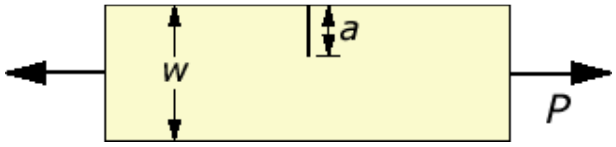

$$K_I = \frac{P}{B\sqrt{w}} \left\{ \frac{\sqrt{2\tan\left(\frac{\pi a}{2w}\right)}}{\cos\left(\frac{\pi a}{2w}\right)} \left[0.752 + 2.02\left(\frac{a}{w}\right) + 0.37\left(1 - \sin\left(\frac{\pi a}{2w}\right)\right)^3 \right] \right\}$$

h) Double Edge Notched Specimen Under Tension

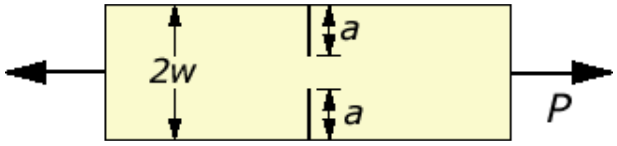

$$K_I = \frac{P}{B\sqrt{w}} \left\{ \frac{\sqrt{\frac{\pi a}{2w}}}{\sqrt{1-\frac{a}{w}}} \left[1.122 - 0.561\frac{a}{w} - 0.205\left(\frac{a}{w}\right)^2 + 0.471\left(\frac{a}{w}\right)^3 + 0.190\left(\frac{a}{w}\right)^4 \right] \right\}$$

Figure 2.4(cont'd) K_I expressions for some common loading conditions

2.8 Fracture Toughness

As the stress intensity factor reaches a critical value (K_c), unstable fracture occurs. This critical value of the stress intensity factor is known as the fracture toughness of the material. The dimension of K_c is given in Equation 2.12.

$$Dim[K_C] = \frac{Force}{Length^2}\sqrt{Length} = PL^{-3/2} = Stress \times \sqrt{Length} = Pa\sqrt{m} \qquad (2.12)$$

K_c changes with the specimen thickness until the thickness exceeds some critical dimension. Once the thickness exceeds the critical dimension, the value of K_I becomes relatively constant and this value, K_{IC}, is a true material property which is called the plane-strain fracture toughness.

When K reaches K_{IC}, crack growth occurs. This means if a structure is designed where K is kept below K_{IC} then it is safe; but if K exceeds K_{IC}, a failure or fragmentation is expected.

2.7.1 Fracture Toughness Values of Some Rock Types

Fracture toughness values are found by researchers with some different techniques like chevron bending, semicircular bending, modified ring testing etc. Some of these values and testing methods are given in Table 2.1.

Table 2.1 Fracture toughness values of some rock types with related testing method (Modified from Alkılıçgil, 2006)

Rock Type	Testing Method	K_{IC} (MPa$\sqrt{m}$)	Source
Johnstone (w =18%)	SECB	0.05	Harberfield & Johnstone, 1990
Johnstone (w =18%)	SCB	0.06	Lim, et. al., 1994
Fine grained sandstone	SCB	0.28	Singh & Sun, 1990
Coarse grained sandstone	SCB	0.35	Singh & Sun, 1990
Fine grained sandstone	SC3PB	0.56	Whittaker, 1992
Fine grained sandstone	CCBD	0.62	Fowell & Chen, 1990
Sandstone	BDT	0.67	Whittaker, 1992
Alvdalen sandstone	CB	0.73	Ouchterlony, 1987
Ruhr sandstone	CB	1.03	Müller & Rummel, 1984
Ryefield sandstone	SECBD	1.04	Whittaker, 1992
Flechtingen sandstone	CB	1.15	Backers, et al., 2003
Montcliffe sandstone	CB	1.18	Bearman, 1999
Grimsby sandstone	SR	1.47	Gunsallus & Kulhawy, 1984
Alvdalen sandstone	SR	1.91	Ouchterlony, 1987
Pennant sandstone	CB	2.1	Bearman, 1999
Pennant sandstone	SR	2.56	Meredith, 1983
Saudi Arabia limestone	SENRBB	0.39	Khan & Al-Shayea 2000
Middleton limestone	CB	0.73	Bearman, 1999
Harrycroft limestone	CB	0.82	Bearman, 1999
Welsh limestone	SCB	0.85	Singh & Sun, 1990
Indiana limestone	SECB	0.97	Ingraffea & Schmidt, 1979
Indiana limestone	CCP	0.97	Sun & Ouchterlony, 1986
Indiana limestone	SC3PB	0.99	Whittaker, 1992
Irondequoit limestone	SR	1.36	Gunsallus & Kulhawy, 1984
White limestone	BDT	1.38	Whittaker, 1992
Shelly limestone	SR	1.44	Meredith, 1983
Gray limestone	BDT	1.58	Whittaker, 1992
Wredon limestone	CB	1.7	Bearman, 1999
Klinthagen limestone	SR	1.87	Ouchterlony, 1987
Reynales limestone	SR	2.06	Gunsallus & Kulhawy, 1984

Table 2.1 (Cont'd) Fracture toughness values of rocks with related testing method

Rock Type	Testing Method	K_{IC} (MPa$\sqrt{m}$)	Source
Siltstone	SECBD	0.8	Whittaker, 1992
Fine grained marble	BDT	1	Whittaker, 1992
Coarse grained marble	BDT	1.12	Whittaker, 1992
Carrara marble	CB	1.38	Müller & Rummel, 1984
Treuchtlingen marble	CB	1.7	Müller & Rummel, 1984
Ekeberg marble	CB	1.76	Ouchterlony, 1987
Ekeberg marble	SR	2.25	Ouchterlony, 1987
Utinga granite (Rift plane)	CNBD	0.6	Almeida, et al., 2006
Falkenberg granite	CB	0.65	Müller & Rummel, 1984
Utinga granite (Grain plane)	CNBD	0.73	Almeida, et al., 2006
Utinga granite (Hardway plane)	CNBD	0.82	Almeida, et al., 2006
Favela granite (Grain plane)	CNBD	0.9	Almeida, et al., 2006
Favela granite (Rift plane)	CNBD	0.97	Almeida, et al., 2006
Iidate granite	SR	1.12	Takahashi et al, 1986
Favela granite (Hardway plane)	CNBD	1.16	Almeida, et al., 2006
Daejeon granite	BDT	1.18	Yoon & Jeon, 2004
Cornwall granite	CB	1.32	Müller & Rummel, 1984
Bohus granite	CB	1.42	Ouchterlony, 1987
Falkenberg granite	CB	1.52	Müller & Rummel, 1984
Granite	SECBD	1.65	Whittaker, 1992
Newhurst granite	SCB	1.72	Whittaker, 1992
Iidate granite	CB	1.73	Müller & Rummel, 1984
Epprechtstein granite	CB	1.74	Müller & Rummel, 1984
Stripa granite	SECRBB	1.74	Sun & Ouchterlony, 1986
Merrivale granite	SR	1.8	Meredith, 1983
Westerly granite	SR	1.82	Meredith, 1983
Penryn granite	CB	1.83	Bearman, 1999
Pink granite	SR	2.03	Meredith, 1983
TGP granite	SENRBB	2.08	Yu,2001
Krakemala granite	CB	2.16	Ouchterlony, 1987
Straht Halladale granite	SR	2.19	Meredith, 1983
Krakemala granite	SR	2.22	Ouchterlony, 1987
Iidate granite	CB	2.26	Takahashi et al, 1986

Table 2.1 (Cont'd) Fracture toughness values of rocks with related testing method

Rock Type	Testing Method	K_{IC} (MPa$\sqrt{m}$)	Source
Westerly granite	SR	2.27	Ouchterlony, 1987
Stripa granite	SR	2.36	Sun & Ouchterlony, 1986
Bohus granite	SR	2.4	Ouchterlony, 1987
Stripa granite	SR	2.7	Ouchterlony, 1987
Westerly granite	CT	2.7	Schmidt & Lutz, 1979
Westerly granite	CT	2.7	Sun & Ouchterlony, 1986
Rasjö granite	SR	2.8	Ouchterlony, 1987
Colorado oil shale	SCB	1.02	Chong,et al., 1987
Ogino tuff	SR	1.06	Matsuki et al, 1987
Ogino tuff	CB	1.08	Matsuki et al, 1987
Göynük tuff	SR	1.29	Şantay, 1990
Falkirk dolostone	SR	1.66	Gunsallus & Kulhawy, 1984
Kankakee dolostone	SR	1.66	Gunsallus & Kulhawy, 1984
Oatka dolostone	SR	1.78	Gunsallus & Kulhawy, 1984
Markgraf dolostone	SR	1.8	Gunsallus & Kulhawy, 1984
Romeo dolostone	SR	2.47	Gunsallus & Kulhawy, 1984
Tampomas andesite	CB	1.26	Abrahamsson, et al, 1987
Gray Ankara andesite	MR	1.59	Şener, 2002
Gray Ankara andesite	SCB	1.3	Het, 2008
Pink Ankara andesite	SCB	0.93	Alkılıçgil, 2006
Pink Ankara andesite	SNBD	0.96	Alkılıçgil, 2006
Tampomas andesite	CB	1.68	Abrahamsson, et al, 1987
Whitwick andesite	CB	2.17	Bearman, 1999
Bolton hill diorite	CB	2.22	Bearman, 1999
Cliffe hill diorite	CB	2.77	Bearman, 1999
Äspö diorite	SENRBB	3.21	Nordlund, et al., 1999
Finnsjön granodiorite	SR	3.35	Ouchterlony, 1987
Basalt	SECBD	1.8	Whittaker, 1992
Basalt	SC3PB	2.27	Whittaker, 1992
Basalt	BDT	3.01	Whittaker, 1992
Ingleton graywacke	CB	2.38	Bearman, 1999
Cornish graywacke	CB	3.15	Bearman, 1999

Table 2.1 (Cont'd) Fracture toughness values of rocks with related testing method

Rock Type	Testing Method	K_{IC} (MPa$\sqrt{m}$)	Source
Kallax gabbro	SR	3.23	Yi, 1987
Gray norite	SR	2.69	Meredith, 1983
Whin Sill dolerite	SR	3.26	Meredith, 1983

BDT : Uncracked Brazilian Disk Test

CB : Chevron Bend

CCBD : Central Cracked Brazilian Disc under diametral compression test

CCP : Centre Cracked Panel

CNBD : Chevron-Notched Brazilian Disc

CT : Compact Tension

MR : Modified Ring test

SC3PB : Single edge straight through cracked rectangular plate in three-point bending test

SCB : Semi-Circular Bend test

SECB : Single Edge Cracked Beam under three-point bending test

SECBD : Single edge cracked Brazilian disk in diametral Compression

SECRBB : Single Edge Cracked Round Bar Bend

SENRBB : Single Edge Notched Round Bar in Bending

SNBD : Straight-Notched Brazilian Disc

SR : Short Rod

CHAPTER 3

PREVIOUS STUDIES

Fracture toughness values can sometimes be obtained from the literature or materials properties databases. But, it is preferable to determine K_c by experiment for the particular material. Testing methods are still being studied to find the most easy and accurate way to find K_c.

K_{IC}, K_{IIC} and K_{IIIC} define Mode I, Mode II and Mode III fracture toughness values respectively which are referring to opening, shear and antiplane modes. K_{IC} is mostly studied but still there is no standard method to determine it. There are only some test methods suggested by ISRM which are:

- Suggested Method for Determining Fracture Toughness Using Chevron Bend (CB) Specimens
- Suggested Method for Determining Fracture Toughness Using Short Rod (SR) Specimens
- Suggested Method for Determining Fracture Toughness Using Cracked Chevron Notched Brazilian Disc (CCNBD) Specimens

There are some different methods that were previously used to find Mode I fracture toughness. Some of them are:

- Modified Ring (MR) Test (Thiercelin and Roegiers, 1986)
- Diametral Compression Method (Singh and Pathan, 1988)

- Semi–Circular Core in Three Point Bending (SCB) (Chong and Kuruppu,1984, Lim et al., 1994 , Khan and Al-Shayea, 2000)
- Brazilian Disc Test (BDT) (Guo et al., 1993, Chang et al., 2002)

3.1 ISRM Suggested Methods

3.1.1 Chevron Bend (CB) Specimen Tests

Ouchterlony (1988) asserted the chevron bend specimens. The specimens have a chevron or V-shaped notch perpendicular to the core axis which are opened by a diamond wheel saw. Loading process is done by a testing machine in which both load and displacement rates can be controlled. Specimens are loaded under three-point bending so three support rollers are used. These rollers shall be capable of rotating to maintain the rolling contact during the test. Chevron Bend specimen geometry is given in Figure 3.1.

Crack mouth opening displacement (CMOD) is measured by a clip gauge where the vertical displacement is measured by two linear variable differential transformers (LVDT).

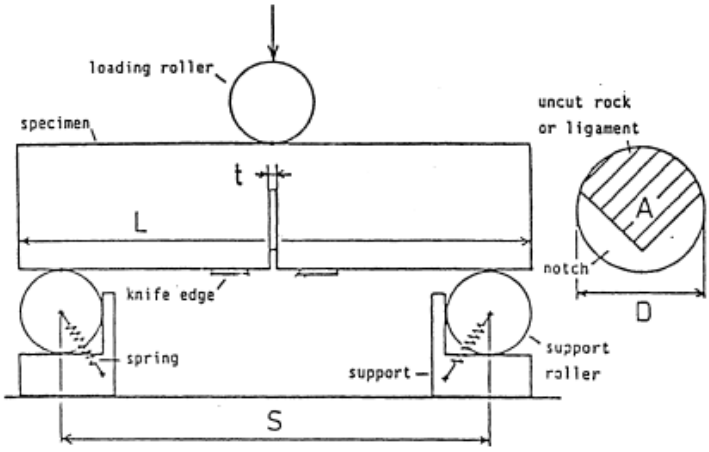

Figure 3.1 CB specimen geometry (Ouchterlony, 1988)

In 1989, Ouchterlony calibrated and suggested the standard proportions for CB specimens which are:

$S = 3.33D \pm 0.02D$ $\quad\quad$ $2\theta = 90.0° \pm 1.0°$

$a_0 = 0.15D \pm 0.10D$ $\quad\quad$ $t \leq 0.03D$ or 1mm, whichever is greater

where

S = distance between support points

a_0 = initial crack length

2θ = chevron notch angle

CB specimens can only be used to determine the Mode I fracture toughness of materials with the formula below:

$$K_{CB} = C_K 24.0 F_{max}/D^{1.5} \quad (3.1)$$

where

K_{CB} = fracture toughness of chevron bend specimen (MPa√m)

F_{max}= failure load (kN)

D = specimen diameter (cm)

C_K= correction factor to account for the size variation of the specimen;

$$C_K = \left(1 - \frac{0.6\Delta W}{D} + \frac{1.4\Delta a_0}{D} - 0.01\Delta\theta\right) \quad (3.2)$$

where

ΔW = variation in specimen height

Δa_0 = initial position of chevron notch apex

$\Delta\theta$ = chevron notch angle

By using load – CMOD curves a correction factor is calculated and the corrected fracture toughness is calculated as:

$$K_{CB}^{c} = \sqrt{\frac{1+p}{1-p}} K_{CB} \tag{3.3}$$

where $p = \Delta x_0 / \Delta x$

3.1.2 Short Rod (SR) Specimen Tests

Short Rod rock specimen configuration is suggested by ISRM (Ouchterlony, 1988). For SR specimens, a V-shaped or chevron notch is opened along the core axis as in CB specimens. A view of SR specimen is given in Figure 3.2.

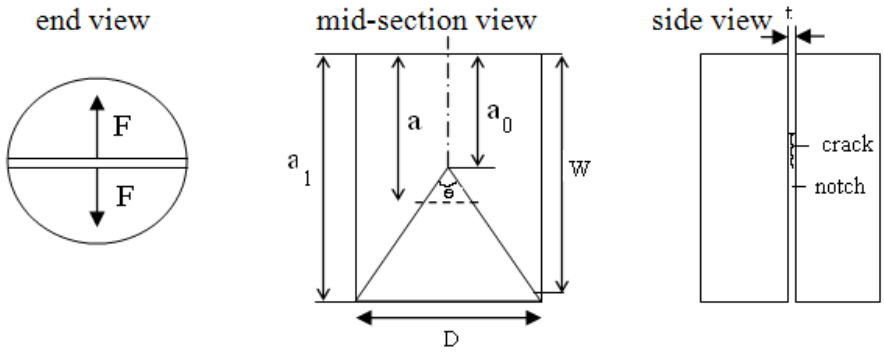

Figure 3.2 Geometry of SR specimen (Ouchterlony, 1988)

Fracture toughness is calculated by equations 3.1 to 3.3 by changing K_{CB} to K_{SR}. Yi et al. (1992) observed that fracture toughness K_{SR} should be size-independent if the specimen is larger than a certain value and also K_{SR}^{c} should be size-independent. K_{SR} is found during the Level 1 testing of the experiment in which maximum load during bending is recorded. K_{SR}^{c} is found after load and displacement measurements are collected and evaluated in Level 2 testing.

3.1.3 Cracked Chevron Notched Brazilian Disc (CCNBD) Specimen

Shetty et al. (1985) developed a new specimen type called Cracked Chevron Notched Brazilian Disc (CCNBD) to determine the fracture toughness of ceramics. ISRM suggested this method which only requires recording of the maximum load during the experiment (Fowell, 1995). The method uses a specimen with a chevron or V-shaped notch along the core diameter with the following geometry:

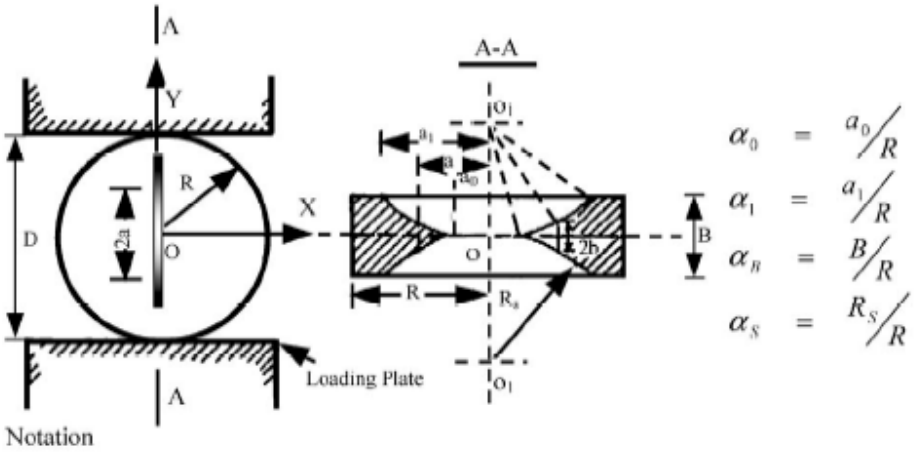

Figure 3.3 Geometry of CCNBD Specimen (Iqbal & Mohanty, 2006)

The restrictions of the dimensionless factor, α, are given in Equation 3.4. A graph can be drawn according to these restrictions (Figure 3.4). When a specimen's α values are inside the closed shape formed by five lines, then that specimen will give a valid test.

$$
\begin{aligned}
&\alpha_1 \geq 0.4 && \text{Line 0} \\
&\alpha_1 \geq \alpha_B/2 && \text{Line 1} \\
&\alpha_B \leq 1.04 && \text{Line 2} \\
&\alpha_{1 \leq} 0.8 && \text{Line 3} \\
&\alpha_B \geq 1.1729 \cdot \propto_1^{1.6666} && \text{Line 4} \\
&\alpha_B \geq 0.44 && \text{Line 5}
\end{aligned}
\tag{3.4}
$$

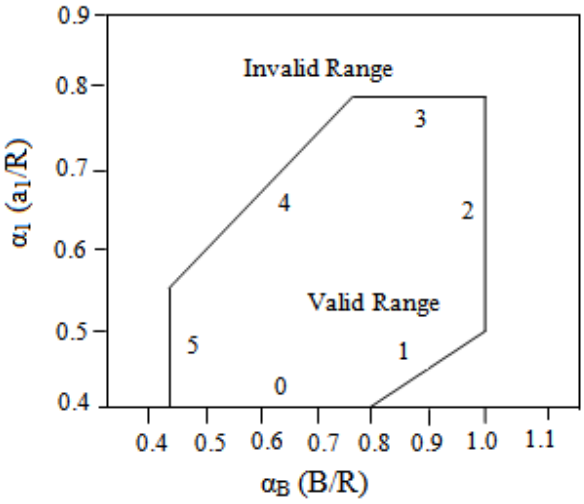

Figure 3.4 Valid geometrical ranges for CCNBD

Fowell at al. (2006) pointed out that for fracture toughness testing, the minimum SIF value (Y*) is important. Because Y* corresponds to the failure load recorded during testing. Equation 3.5 is used to calculate fracture toughness of a CCNBD specimen.

$$K_C = \frac{F_{max}}{B \cdot \sqrt{R}} \cdot Y_m^* \tag{3.5}$$

ISRM (1995) suggested an equation to calculate Y_{min}* as follows:

$$Y^*_{min} = u \cdot e^{v \cdot \alpha_1} \tag{3.6}$$

where, u and v are constants determined by a_0/R and B/R.

Above equation can be applied to all fracture modes; Mode I, II, III or mixed mode.

3.2 Semicircular Core in Three Point Bending (SCB)

Chong and Kuruppu (1984) proposed a fracture toughness determination method which uses semicircular core specimens with a single edge notch subjected to a three point loading (Figure 3.5).

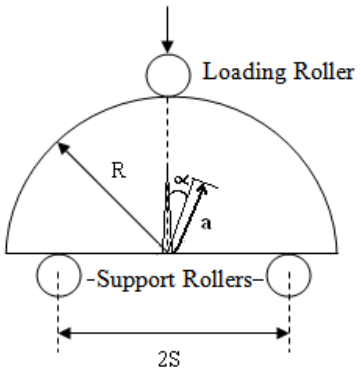

Figure 3.5 SCB specimen

Mode I fracture toughness (K_{IC}) can be calculated from Equation 3.7 which is developed by Lim et al. (1994). This equation can be used for $0.05 \leq a/D \leq 0.3$ and S/D = 0.25, 0.305, 0.335 or 0.4.

$$K_{IC} = \frac{F_{max}\sqrt{\pi a}}{Dt} Y_I \tag{3.7}$$

where

Y_I = dimensionless stress intensity factor which is determined by the dimensionless notch length (a/D), notch inclination angle (α) and the span (s).
F_{max} = load at fracture (kN)
D = 2R (diameter of the specimen) (mm)
t = specimen thickness (mm)

Chang et al. (2002) concluded that, since in SCB tests no precracking is performed, the fracture toughness values obtained are smaller than those from CCNBD tests. The reason is; crack tips obtained from precracking are in crystal grains which usually resist crack propagation. But they also found that this only happens for hard rocks so precracking should be done for SCB tests of hard rocks.

3.3 Modified Ring Test Studies

Diametral loading is the basic characteristic of modified ring (MR) tests. Although there are not many MR studies in the literature, diametrally loaded discs were used to determine fracture toughness by some researchers.

Singh and Pathan (1988) used 38 mm, 49 mm, 50.5 mm and 51.4 mm disc specimens with thicknesses varying between 10 mm and 50 mm of Ryefield sandstone. The geometry of the specimen is given in Figure 3.6. The two

loading faces were ground and a groove with a_0 depth was opened through one face of the disc along the loading axis.

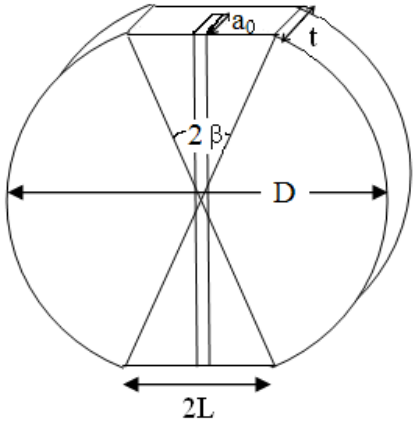

Figure 3.6 Specimen geometry for diametral compression test

Singh and Pathan (1988) used the formula in Equation 3.8 and 3.9 for strip and line loading respectively to determine fracture toughness. From the results of the experiments, they found that fracture toughness first increases but then level off as specimen thickness increases.

$$K_{IC} = 1.264\ (\sin 2\beta - \beta) P \cdot \sqrt{a}/2L \cdot t \tag{3.8}$$

$$K_{IC} = 1.264 \times F \times \sqrt{a}/t \times D \tag{3.9}$$

where

K_{IC} = fracture toughness ($MN/m^{3/2}$)
F = failure load (MN)
a = crack length at failure (m)
2L = length of flat loading surface (m)
t = thickness of the disc (m)
$\alpha = \sin^{-1}$ (t/D) in radians
D = diameter of the disc (m)

Thiercelin and Roegiers (1986) proposed Modified Ring test to prevent the development of a large process zone in the specimen. The geometry of the specimen they used is given in Figure 3.7. To normalize the specimen geometry, they used ratios α and β which are internal hole radius (r_i) to external hole radius (r_e) and the half length of the loading surface (L) to external radius (r_e) respectively. 6.5 mm and 5 mm r_i, 7mm L are used for specimens having 38.5 mm r_e. For specimens having 50 mm r_e, r_i and L is 13 mm. Stress intensity factor (K_I), which is normalized with F, to half crack length graph shows that K_I increases with increasing crack length meaning unstable crack propagation and to control the crack growth the load has to be decreased. As the crack length continue to increase, K_I/F decreases indicating that crack grows in a stable manner. At the point of maximum K_I/F, fracture toughness (K_{Ic}) is determined. As a result, Thiercelin and Roegiers (1986) concluded that the fracture toughness values obtained from Modified Ring Test are not affected by a variation in specimen size.

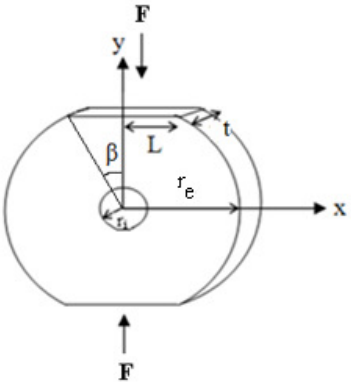

Figure 3.7 Modified ring test geometry

Proveti and Michot (2006) used Brazilian test to determine the toughness of a material and its brittle to ductile transition. In the plane y = 0, σ_{yy} is constant and equal to $F/\pi r_e t$, except at $X = \pm r_e$. At these points σ_{yy} tends to infinity which results in easy development of cracks at the contact points. To decrease these stress localizations, loading was done from two flat surfaces (Figure 3.8).

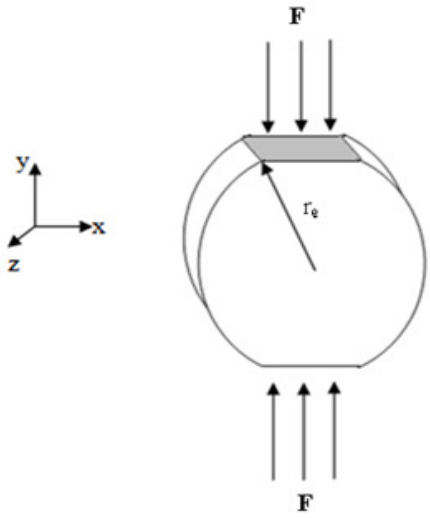

Figure 3.8 Modified Brazilian test with machined flat contact surfaces

CHAPTER 4

NUMERICAL MODELING AND STRESS INTENSITY FACTOR COMPUTATION

Numerical modeling is used for estimating stress intensity factors for different Brazilian disc geometries. In this study a package program called ABAQUS is used. Before using this program, to check the results of ABAQUS modeling work, it was compared with another finite element program called FRANC2D/L. A simple model with well known stress intensity factor solution was prepared and run by ABAQUS CAE and FRANC2D/L programs.

4.1 Finite Element Programs

Finite Element Analysis (FEA) is a computer simulation technique generally used for engineering purposes. This type of analysis, use a numerical technique which is called Finite Element Method. While being an approximate method, the accuracy of the FEA method can be improved by refining the mesh in the model using more elements and nodes.

Finite element packages are the complex programs doing Finite Element Analysis. ABAQUS, ANSYS, FRANC2D/L, FRANC3D, AXISVM, SYSTUS, GO-MESH are some examples of these packages. A common use of them is for the determination of stress and displacements in mechanical object and systems.

The common steps of finite element packages begin with the formation of the geometry in 2D or 3D. The other steps are; defining the material properties,

boundary and load conditions and meshing. Meshing is where you define a finite number of elements to represent the geometric structure. Number of elements is an important factor in the accuracy of the problem. More elements mean higher accuracy; but it also means more time for computation so it is not always the best to have many number of elements. For meshing, different type of elements can be used for different programs and also some programs let you to decide the type of elements between some certain geometric shapes such as tetrahedral, hexahedral, etc.

4.1.1 ABAQUS CAE

ABAQUS is a 3D modeling program in general. Since, the modified ring tests do not need 3D modeling and 2D analyses are adequate, 2D plane strain analyses were performed in the work here. ABAQUS results were tested by modeling some verification examples that have known analytical solutions. ABAQUS was also compared to another finite element program; FRANC2D/L. When it was seen that the results were compatible, ABAQUS was decided to be used for numerical modeling work, since it has better capabilities for input processes, more user friendly PC interfaces, more reliable crack tip modeling, more powerful user-defined subroutines and also complex surface and contact behaviors.

ABAQUS uses J-integral method to compute stress intensity factors which was presented by Rice (1968). J is calculated on linear bodies of linear or nonlinear elastic material free of body forces and subjected to either plane strain or plane stress. J measures the strength of the singular stresses and strains near a crack tip. J is defined for a body containing an edge crack like in Figure 4.1.

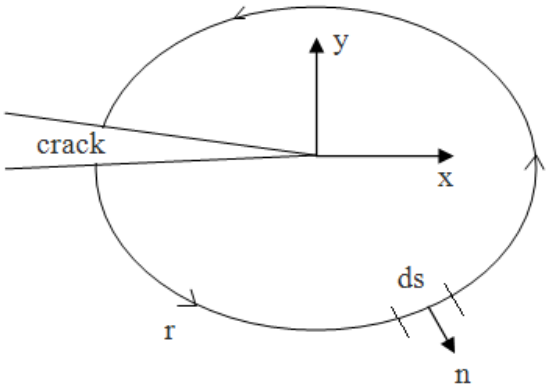

Figure 4.1 Crack tip coordinate system and typical line integral contour

Strain energy density, W is defined as:

$$W = W(x, y) = W(\varepsilon) = \int_0^{\varepsilon} \sigma_{ij}\, \partial\varepsilon_{ij} \tag{4.1}$$

where, ε = infinitesimal strain tensor. J integral is defined as:

$$J = \int_{\Gamma} \left(W\partial y - T\frac{\partial u}{\partial x}\partial s \right) \tag{4.2}$$

where,

Γ = arbitrary path around the crack tip

T = traction vector, ($T = \sigma_{ij}n_j$)

u = displacement vector

ds = an element arc length along Γ

Rice (1968) found that for small-scale yielding the stress energy release rate G is equal to the J-integral. Therefore, the stress intensity factor can be evaluated as shown in Equations 4.3 and 4.4.

$$J = G = \frac{K_I^2}{E^*} \tag{4.3}$$

$$K_I = \sqrt{JE^*} \tag{4.4}$$

where $E^* = \frac{E}{1-V^2}$ for plane strain and $E^* = E$ for plane stress.

ABAQUS is composed of several modules. In this thesis the 9 modules of the program were used. Geometry of the specimen was created and edited in the Part Module. The material properties such as Elastic Modulus and Poisson's Ratio are defined in the Property Module. In the Assembly Module, the parts that are created in the Part Module are positioned relative to each other. The propagation of the crack was also developed in the Assembly Module. To perform a sequence of one or more analysis steps; Step Module is used. Interaction Module is used for defining the interaction between the upper surface of the specimen with the formerly created analytical rigid part. The stress is given to the specimen in the Load Module. Also the boundary conditions and axes symmetries are given in this module. Mesh Module is used to generate the mesh. Number of elements, element types and mesh technique are determined in Mesh Module. Submission of the analysis was done in the Job Module. If an error occurs in the submission ABAQUS monitors the error. Finally Visualization Module shows the results with shapes, contours, graphs and animations. Results of the stress intensity factor are also viewed in the Visualization Module.

4.1.2 Verification Problem

Verification of the ABAQUS program was done by an example having an analytical solution which is Infinite Plate with a Hole and Symmetric Double through Cracks under Tension. The geometry of this example is given in Figure 4.2. This example was chosen because cracks emanating from the circular holes in the Brazilian Disc type specimens are under a similar tensile stress field. The tensile stress can be taken to be comparable or proportional to $\sigma = F / \pi R$ which is the tensile stress acting perpendicular to the crack forming at the center of the regular Brazilian Disc type specimens due to the indirect compression at the specimen ends. This is illustrated in Figure 4.3.

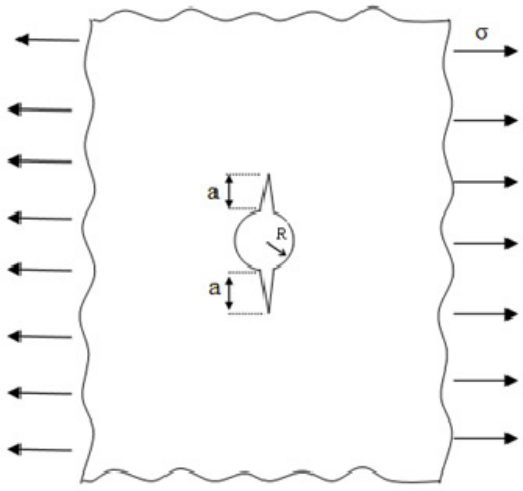

Figure 4.2 Geometry of the verification example

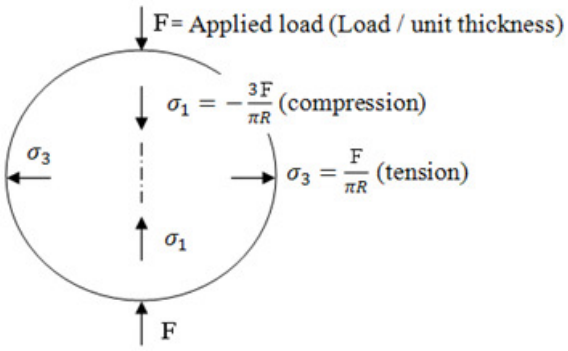

Figure 4.3 Brazilian disc stress field around the crack tip

As it is seen from Figure 4.2, the infinite plate having a hole inside is in tension and two symmetric cracks are present in the direction perpendicular to the pulling direction. This model has the analytical solution given for "Infinite plate with a hole and symmetric double through cracks under tension" which is given in chapter 2.6. Equation 4.5 shows the solution.

$$K_I = \sigma \sqrt{\pi a} \left[1 + 2.365 \left(\frac{r_i}{r_i + a}\right)^{2.4}\right] \tag{4.5}$$

The same example is modeled in ABAQUS. For simplifying the model, quarter of it was drawn and symmetry option was used. Mechanical properties of the example were chosen to represent the andesite for which Elastic modulus and Poisson's ratio are 12300 MPa and 0.16, respectively. Plane strain solution was performed and compared with the analytical solution. Figure 4.4 shows the ABAQUS model with boundary conditions.

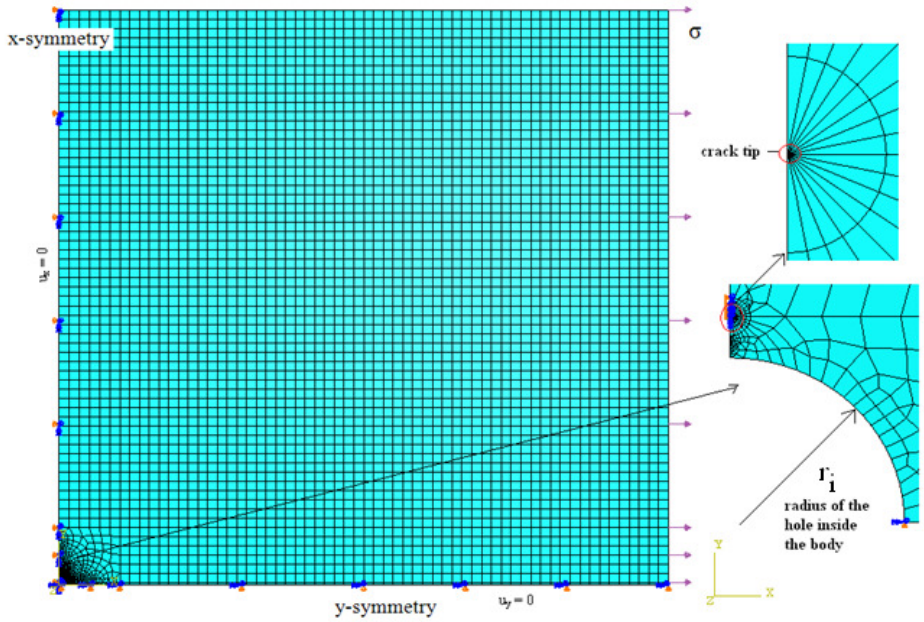

Figure 4.4 Boundary conditions and crack region of the verification example

In ABAQUS there is no unit limitation; one will get the results in the units as it is given. For this example the stress was given as 1. The radius (r_i) of the inner hole is 1. The length and width of the plate are taken as 250 which is assumed to be sufficient to simulate infinite plane. The crack length (a) starts from 0.25 and goes to 7. When all these values were substituted in Equation 4.5 the different K_I values for different crack lengths (a) were computed analytically. And when it was calculated from ABAQUS, the program also gave different K_I values for different crack lengths.

There is no analytical solution for the modified ring specimen geometry,. However, stress intensity factors for this geometry will be computed by ABAQUS models here, and they will be compared to stress intensity factors given by Thiercelin and Roegiers (1986).

Thiercelin and Roegiers (1986) studied the fracture toughness determination with modified ring test. The specimen they worked on had an external radius (r_e) of 38.5 mm, internal hole radius (r_i) of 5 mm and half of the flattened area length (L) of 7 mm. The geometry of the specimen is given in Figure 4.5.

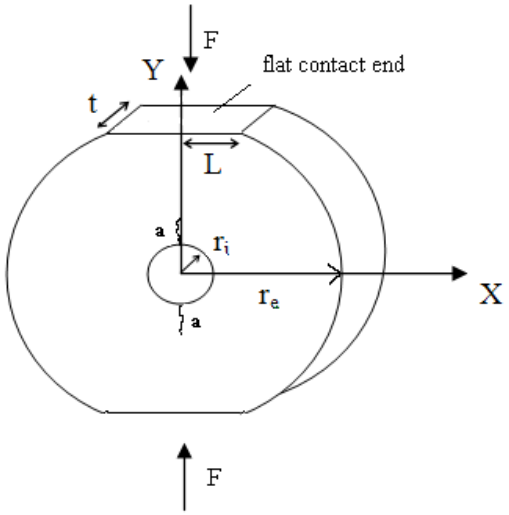

Figure 4.5 Geometry of MR specimen

The stress intensity factor results of Thiercelin and Roegiers (1986) were modified and plotted by reading the values from the graph in their article and is given in Figure 4.6. In the same figure, results from ABAQUS plane strain models are also plotted. Later on in the fracture toughness computations, points marked as K_{Imax} will be important. As seen in the figures maximums from two different computations have a difference of about 8%. ABAQUS maximum point is a little lower than the maximum of Thiercelin and Roegiers (1986).

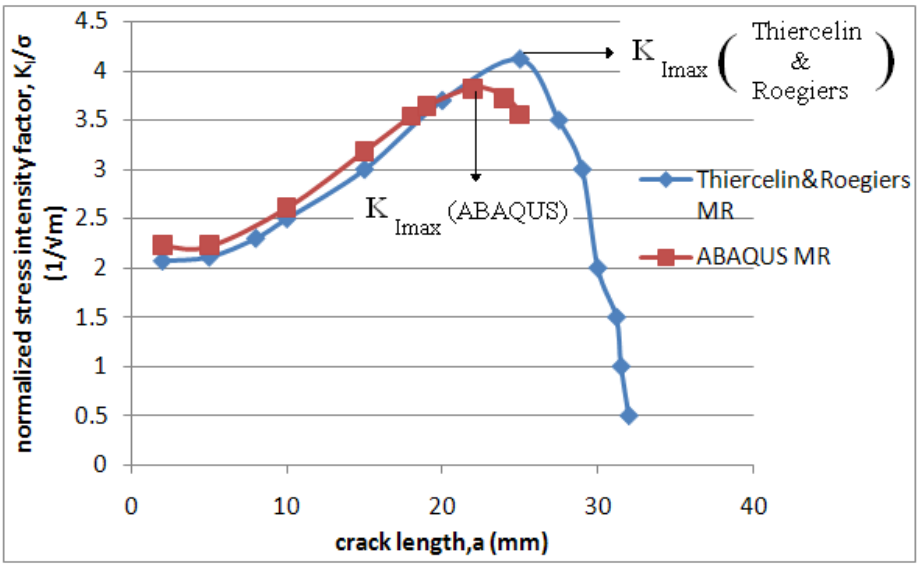

Figure 4.6 Stress Intensity Factor vs crack length

To chenck the accuracy of numerical computations, K_I values computed from analytical solution and from the infinite plate modeled in ABAQUS are given in Table 4.1. Results of Thiercelin and Roegiers (1986) and ABAQUS numerical modeling results of a modified ring specimen, which has the same geometry with Thiercelin and Roegiers's (1986) specimen are also given in Table 4.1.

Table 4.1 Comparison of analytical solution with numerical modeling solutions

	Analytical soln. (infinite plate)	**ABAQUS (infinite)**	**Thiercelin and Roegier's Results for MR specimen geometry**		**ABAQUS numerical results for MR specimen geometry**	
a/r_i	**K_I/σ ($1/\sqrt{m}$)**	**K_I/σ ($1/\sqrt{m}$)**	**a/r_i**	**K_I/σ ($1/\sqrt{m}$)**	**a/r_i**	**K_I/σ ($1/\sqrt{m}$)**
0.00	0.00	0.00	0.00	0.00	0.00	0.00
0.25	2.11	1.99	0.40	2.07	0.40	2.22
0.50	2.37	2.26	1.00	2.11	1.00	2.22
1.00	2.57	2.57	1.60	2.30	2.00	2.61
1.50	2.74	2.81	2.00	2.50	3.00	3.19
2.00	2.93	3.05	3.00	3.00	3.60	3.54
5.00	4.09	4.16	4.00	3.70	3.80	3.64
7.00	4.76	4.70	5.00	4.12	4.40	3.82
			5.50	3.50	4.80	3.73
					5.00	3.56

The graph in Figure 4.7 is obtained from Table 4.1. Stress intensity factor (K_I) is normalized with the stress (σ) where crack length (a) is normalized with internal hole radius (r_i).

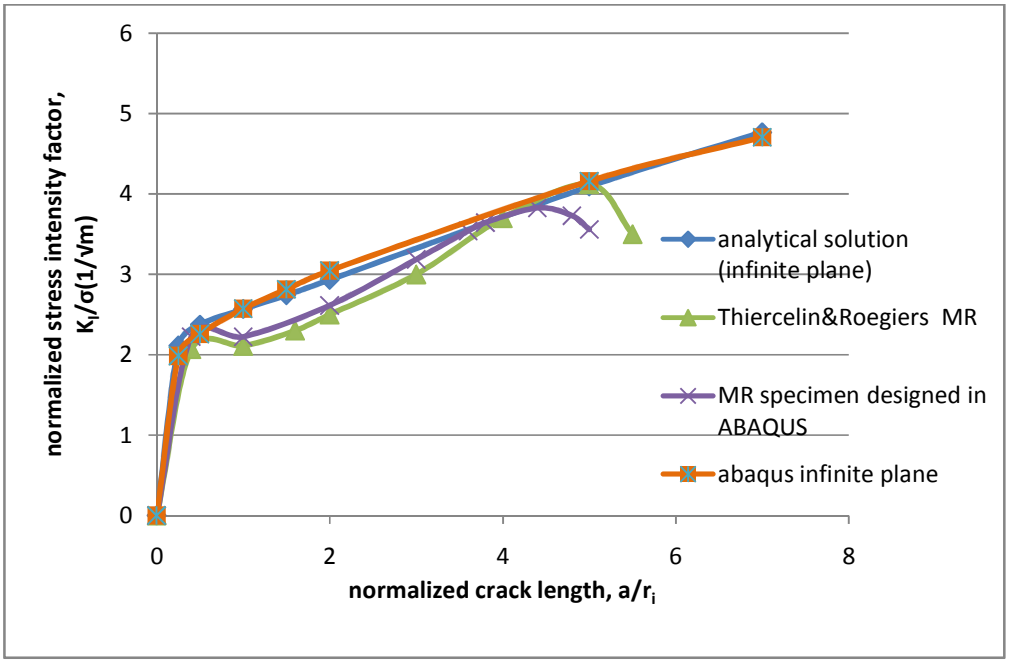

Figure 4.7 Plot of comparison of K_I results;for r_e=38.5mm, r_i=5mm,2L=14mm

These infinite plane stress intensity factors were determined in order to be compared to the factors of modified ring test specimen geometry which is a geometry with finite specimen dimensions. When the percent errors are calculated, it is seen that the difference between ABAQUS solutions of the infinite plate and analytical solutions is changing from 1.2% to 5.7%. This difference is possibly due to the plate width limitation of the numerical model to simulate infinite extent of the analytical model. On the other hand the difference between ABAQUS numerical results of the MR specimen geometry and the results of Thiercelin & Roegiers (1986) come up to 13.59 %. Due to the different boundary types of infinite plate example and modified ring model, it is of course expected to have slight differences in K_I values. However, this infinite plane example is the closest geometry and problem type with a known analytical solution. A check like this was thought to be necessary, since stress

intensity factors given by Thiercelin and Roegiers (1986) were slightly different from the values found from ABAQUS models.

For infinite plate example, as it is seen from the graph in Figure 4.7, K_I values steeply increase initially with the crack length until a specific crack length value, and then continue to increase, but with a moderate slope indicating unstable crack propagation. The numerical modeling results of ABAQUS and the analytical solution show a good match in that figure indicating that numerical modeling with ABAQUS yields quite accurate results for stress intensity factor computations under sophisticated problem conditions including crack-hole combinations.

4.1.3 FRANC2D/L

FRANC2D/L is a finite element program which can make two-dimensional analysis of structures. The program was developed at Cornell University by Paul Wawrzynek.

To run a model in FRANC2D/L, firstly the geometry is formed in another unit of the program which is called CASCA. Mesh is also formed in CASCA. Then, that model is called from FRANC2D/L and the other properties such as material properties, boundary conditions and load applications are given here. Cracks are also defined in FRANC2D/L.

Some capabilities of FRANC2D/L are; simulation of linear elastic and elastic-plastic crack growth, elastic and elastic-plastic material response. The program has Pre-process, Modify, Analysis and Post-Process options. Material properties, boundary conditions, load applications are some sub-menus of

Pre-Process. Modify option is used for defining cracks. The linearity or nonlinearity is selected from Analysis menu. And Post-process option gives the results such as contours or stress intensity factors.

In order to compare ABAQUS CAE results with another finite element program, FRANC 2D/L was used. Fischer et al. (1996) studied finite element model of the modified ring test by using interactive finite element program FRANC (FRacture ANalysis Code).

As in ABAQUS, geometry is created first. After completing the model, cracks are defined at the top and bottom of the inner hole. Crack propagation continues towards the ends of the specimen if the automatic option is used.

In this model; the external radius (r_e) of the specimen is 38.5 mm, r_i of the specimen is 5 mm and the flattening angle is 10.45° to give the flattened length (2L) as 14 mm. 0.1 mm displacement was applied to the top and bottom loading surfaces. Plane strain analysis was selected and the model was run. The maximum K_I value was found as 0.679 MPa$\sqrt{m}$. The deformed and undeformed shape of the model is given in Figure 4.8.

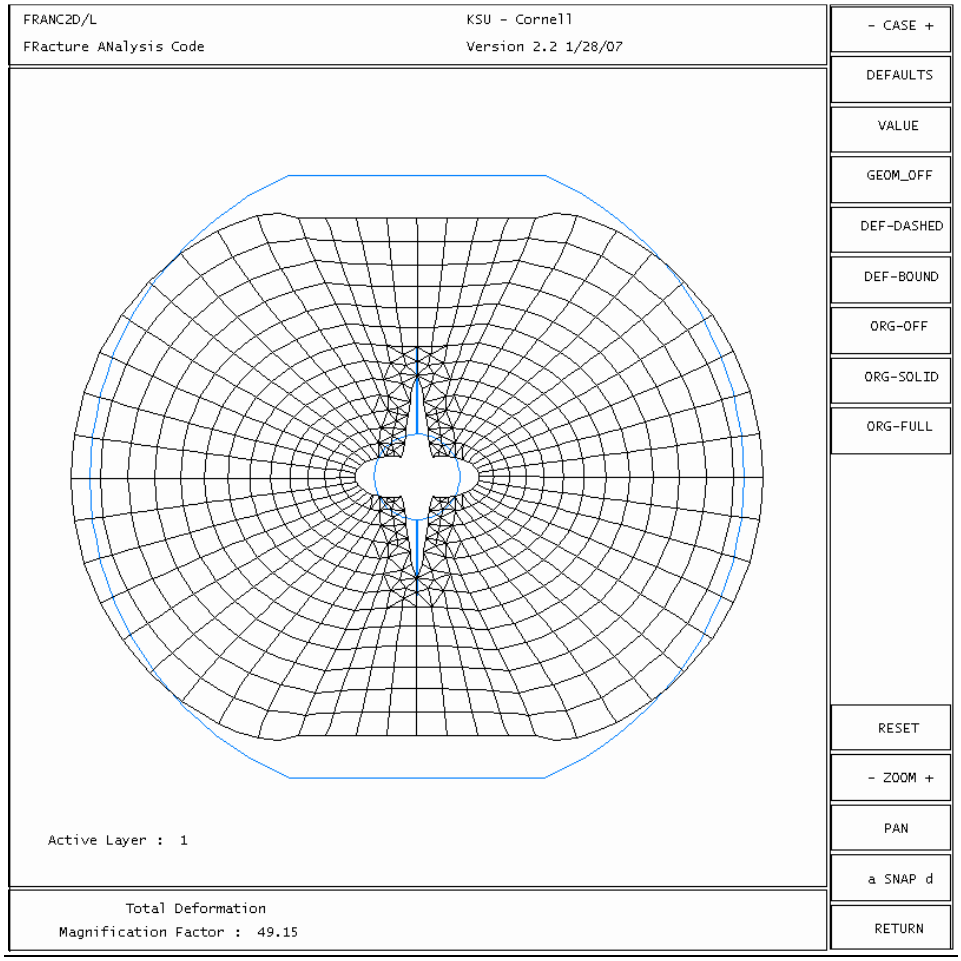

Figure 4.8 Deformed and undeformed model in FRANC2D/L

The same model was also formed in ABAQUS CAE to compare the results. Again a displacement of 0.1 mm was given to top and bottom loading surfaces. Computing the model under plane strain the maximum K_I value was found as 0.679 MPa$\sqrt{m}$ which is same as the FRANC result. The mesh, boundary conditions and deformed shape of the ABAQUS modified ring specimen model are given in Figure 4.9.

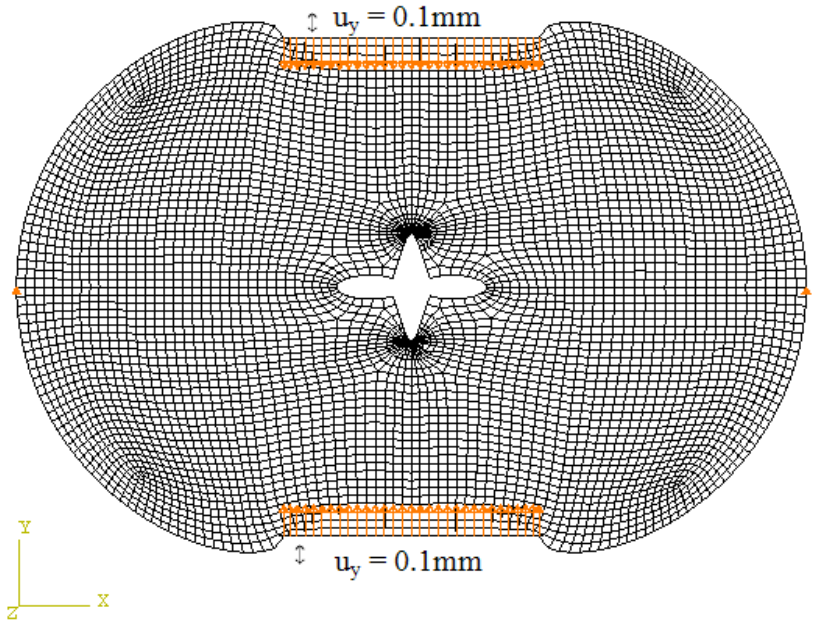

Figure 4.9 Mesh, boundary conditions, and the deformed shape of ABAQUS modified ring specimen model

4.2 Numerical Modeling of the Modified Ring Specimens

Series of specimens with different internal hole radius (r_i) and different L/r_e ratios ($\sin\beta$) are designed in ABAQUS. For each specimen, firstly a quarter 2D models without a crack is modeled and submitted. Due to the symmetry, a quarter of the specimen geometry is enough for modeling purposes.

Forming a model starts from the formation of the parts in the Part Module. For modified ring specimens geometry of a quarter of the specimen is formed in this module. Also a rigid line is assigned on the top of the flattened part of the specimen. This line is attached there to set the interaction between the specimen and the loading platen. Then, by using the Property Module the specimen is

defined to be elastic and the elastic properties are given which are a Young's Modulus value of 12.3 GPa and a Poisson's ratio of 0.16. These material properties are assigned in this module in the section option. Assembly Module is for the creation of part instances and positioning them. Crack is created in this module from the engineering features option. Crack front is selected to be the center of the contour region and crack extension direction is selected to show the positive y direction. The red dot in Figure 4.10 shows the crack front and the red arrow shows the extension direction. Also partitions and contour regions are formed in Assembly Module. Partitions are set to ease the formation of mesh.

A sequence of analysis steps is performed in the Step Module. In this study two steps are used. One of them is the initial step and the other is step-1. Step module has an ability to specify output requests. In this study to obtain stress intensity factor data, a history output request is defined in step module. Interaction between the rigid line, simulating the loading platen, and the specimen is defined in the Interaction Module. A friction coefficient of 0.4 is given for this interaction for this platen-specimen contact. In the Load Module, loads and boundary conditions are defined. Figure 4.10 shows the load given from the reference point defined at the top of the specimen and the boundary conditions.

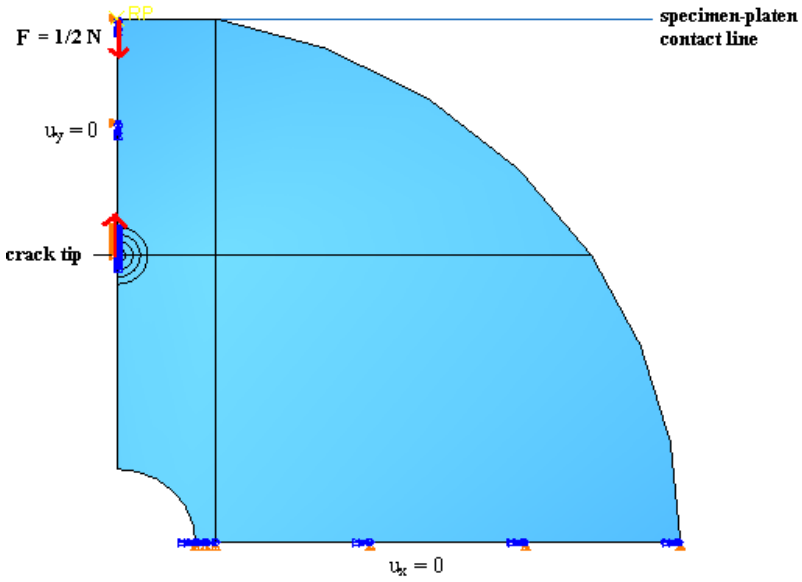

Figure 4.10 Crack front, crack extension direction and boundary conditions

As stated above, Symmetry option is utilized to model the whole specimen as a quarter part which decreases computing time and increases the simplicity of preparations. The model is said to be symmetric in x and y direction but for y-symmetry the selection should start from the crack tip so that the crack boundary can freely move. Figure 4.11 shows the symmetry conditions for an uncracked and 10 mm cracked model.

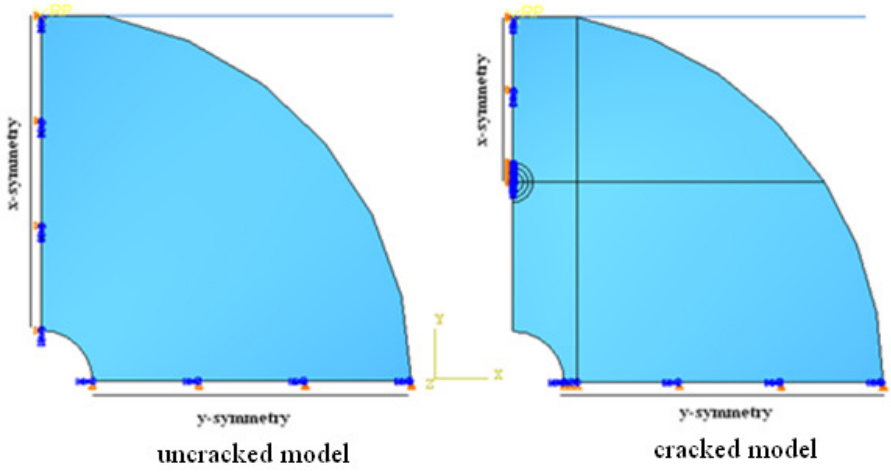

Figure 4.11 Symmetry conditions for uncracked and cracked model

Mesh Module is used to generate meshes on parts and assemblies of the model. Seeds, element types, and mesh techniques are selected in this module. Since crack tips cause high stress concentrations mesh should be finer while getting closer to the crack tip. To construct the mesh around the crack front and to control the singularity at the crack tip, a contour region formed from half circles is generated. Inside the smallest ring, the meshing technique called sweep is used. Figure 4.12 shows a typical mesh for a 75 mm diameter specimen having a 10 mm hole inside, with a flattening angle of 10° (L/r_e=0.174) and a crack length of 10 mm.

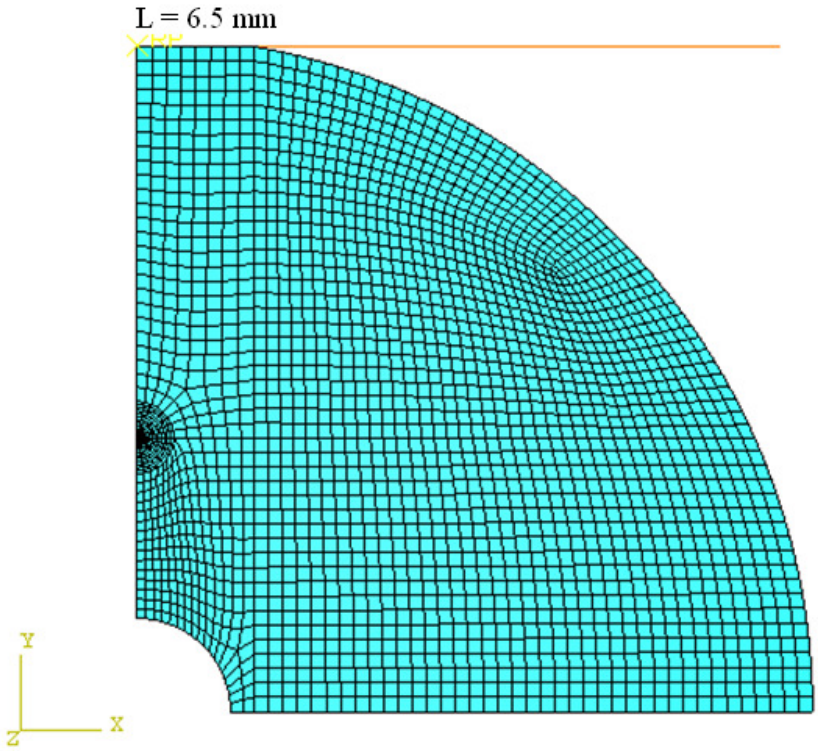

Figure 4.12 Mesh of a specimen with r_e = 37.5 mm, r_i = 5 mm, $\beta = 10°$

All the input data up to this point are submitted and analyzed in the Job Module. If there is a warning or an error, the program shows where the error is. For each new crack length a new job should be created and submitted.

Crack propagation is made by propagating the contour region which firstly, starts from a small distance from the upper part of the inner hole. This process is done in the Assembly Module. Figure 4.13 shows the contour region and how the crack is propagated.

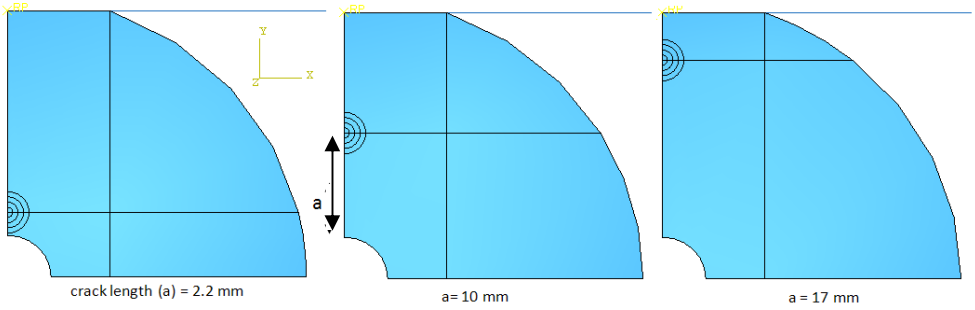

Figure 4.13 Crack propagation and contour region

At the end of job submission of each model, the results of the analysis in terms of deformed shapes, contours, graphs and animations are examined in the Visualization Module.

4.2.1 Geometry of the Models

Modified ring specimens differ from each other according to their external radius (r_e), internal hole radius (r_i) and flattening angle (β). The r_e values used in numerical modeling were chosen according to the diameters used in the experiments which are; 54, 75, 100 and 125 mm. Internal hole radius (r_i) is changed from 8 mm to 20 mm. Flattening angle (β) differs from 10° to 25°.

4.2.2 Stress Intensity Factor Computation

To compute stress intensity factors, in the visualization module, history output request is used. K_I results which are Mode I stress intensity factors are selected from the history outputs and averaged. So for each crack length a new stress intensity factor is obtained. Figure 4.14 shows the graph of K_I versus a/r_e for a model with r_e = 37.5 mm, r_i=5 mm and β = 10°. As it is seen from the graph, K_I value increases with increasing crack length up to a point. This increase indicates unstable crack propagation. Thiercelin and Roegiers (1986) stated that

the load has to be decreased to control the crack growth at this point. This results in a decrease of K_I with increasing crack length. After the point of maximum stress intensity factor, the crack grows in a stable manner. This peak point of K_I – a/r_e curves is important, since it is used in the computation of fracture toughness value. All of the K_I values for a specific model are collected in an Excel sheet and K_I value versus crack length to radius ratio (a/r_e) graph is plotted. The maximum stress intensity factor (K_{Imax}) is found from this graph. To find the maximum value for K_I more accurately, the equation obtained from the trendline with maximum R^2 (correlation coefficient) is solved in MATLAB program and the maximum point of the equation of the graph which corresponds to the maximum stress intensity factor is obtained.

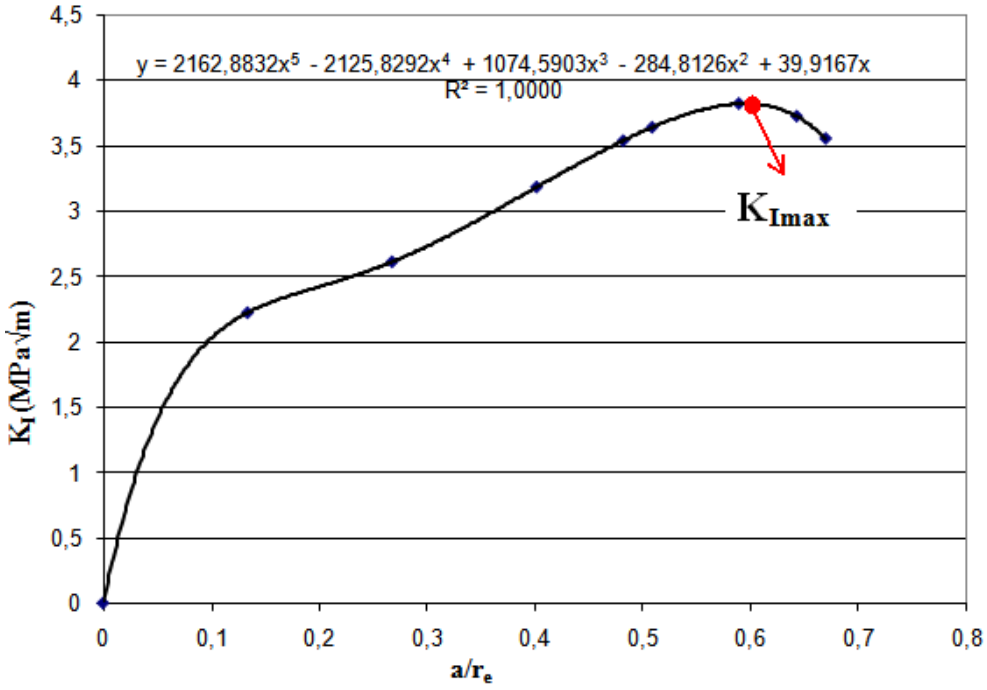

Figure 4.14 Stress intensity factor versus a/r_e

4.3 Stress Distributions at the Crack Front

In order to study the mechanism of fracture propagation for MR test stress distributions at the crack front were examined in detail. A specimen geometry with a constant inner hole diameter of 16 mm is considered and external diameter of the models is changed as 54, 75, 100, and 125 mm in order to generate different r_e/r_i ratios in the graph.

The change of vertical and horizontal stresses while moving away from the crack tip is examined. To see the effect of external radius on the crack front stresses. Horizontal (σ_{xx}) and vertical (σ_{yy}) stresses are observed for specimens having exactly the same r_i (= 8mm) and β (= 16°) but different r_e values. Figure 4.15 shows the change of vertical stress with the distance from the crack front in positive y direction. These stresses are observed at the moment where K_{Imax} is achieved.

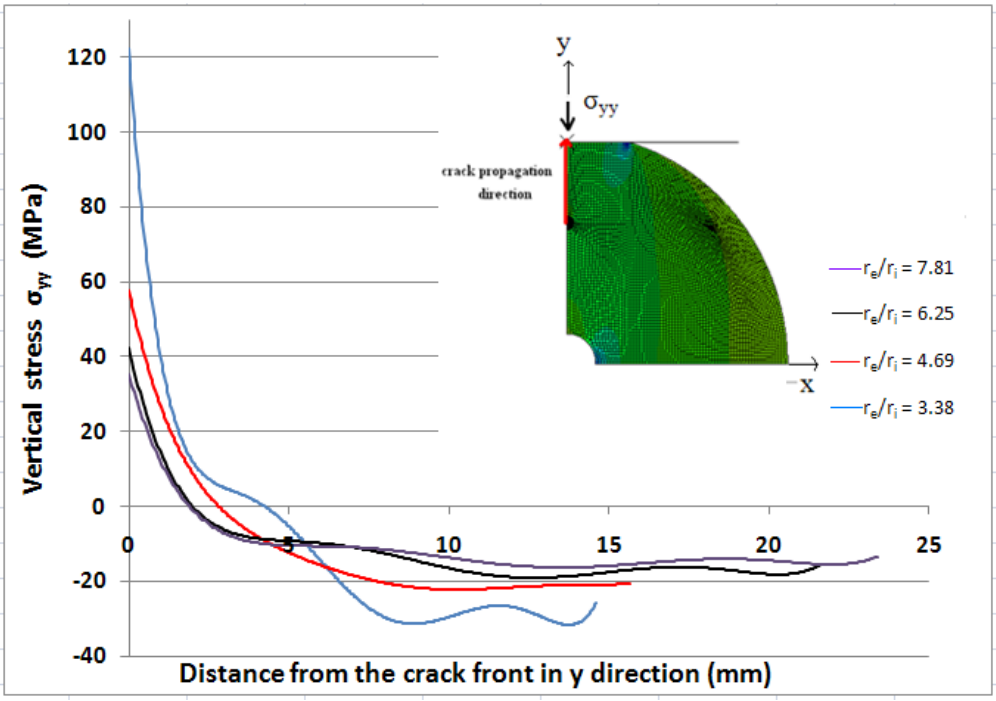

Figure 4.15 Distribution of σ_{yy} at the crack front for different r_e/r_i ratios

Vertical stress (σ_{yy}) is the largest at the crack tip. Checking the difference in maximum vertical stress between models having different external radius, it is obvious that the one with the smallest external radius has the largest value of vertical stress at the crack tip. σ_{yy} decreases while moving away from the crack tip in the direction of crack propagation. When it is moved a bit away from the crack tip and get closer to the point of loading the vertical stress becomes compression. Like the tension values, compression values are also high in case of small external radius.

Figure 4.16 shows the horizontal stress (σ_{xx}) change with the distance from the crack tip in positive y direction. Like in vertical stress, horizontal stress decreases while moving away from the crack tip. Positive values of σ_{xx} indicate

that every point observed is in tension. The model having the smallest r_e/r_i ratio thus the smallest external radius, has the largest value of σ_{xx} at the crack tip.

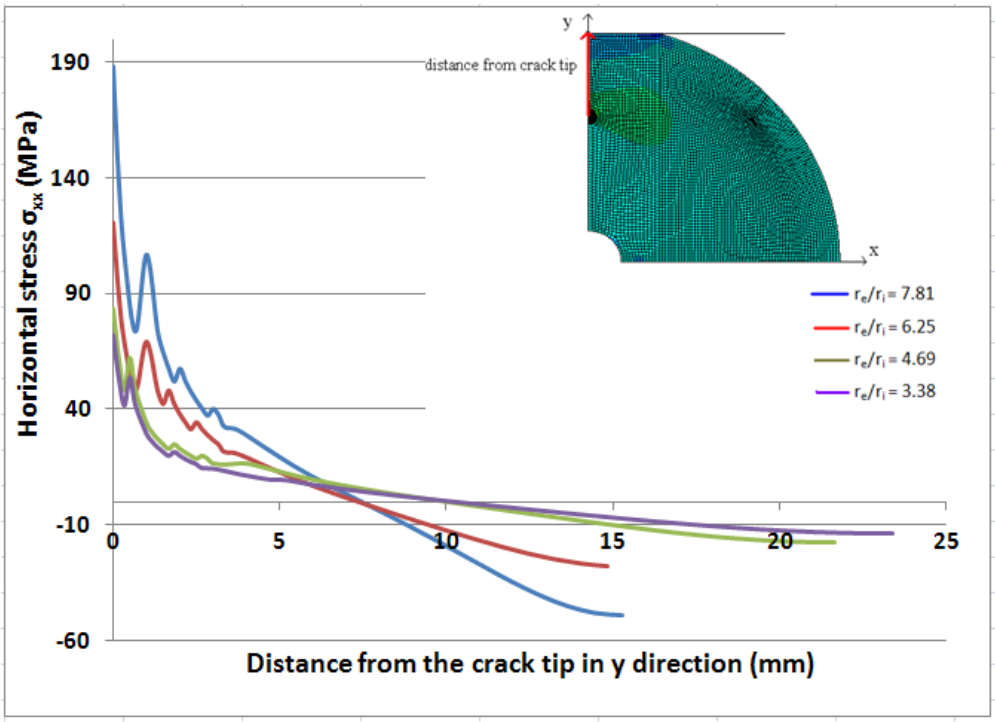

Figure 4.16 Distribution of σ_{xx} at the crack front for different r_e/r_i ratios

4.4 Variation of Stress Intensity Factor with Geometrical Parameters of MR Specimens

When all the stress intensity factor computations are completed, the thing is to find what factor affects K_{Imax} value. Internal hole radius, external hole radius and flattening angles are the variables in the models created with ABAQUS and also in the specimens used in the experiments.

Figure 4.17 shows the calculated K_{Imax} change of 54 mm diameter specimens. For a specific internal hole radius, stress intensity factor decreases with

increasing L/r_e ratio. It is also obvious that K_{Imax} values are higher for larger internal hole radii (r_i). In case readers are interested, exact numerical values of maximum stress intensity factors (K_{Imax}) used in constructing Figure 4.17, can be picked from Table 5.4 in Chapter 5.

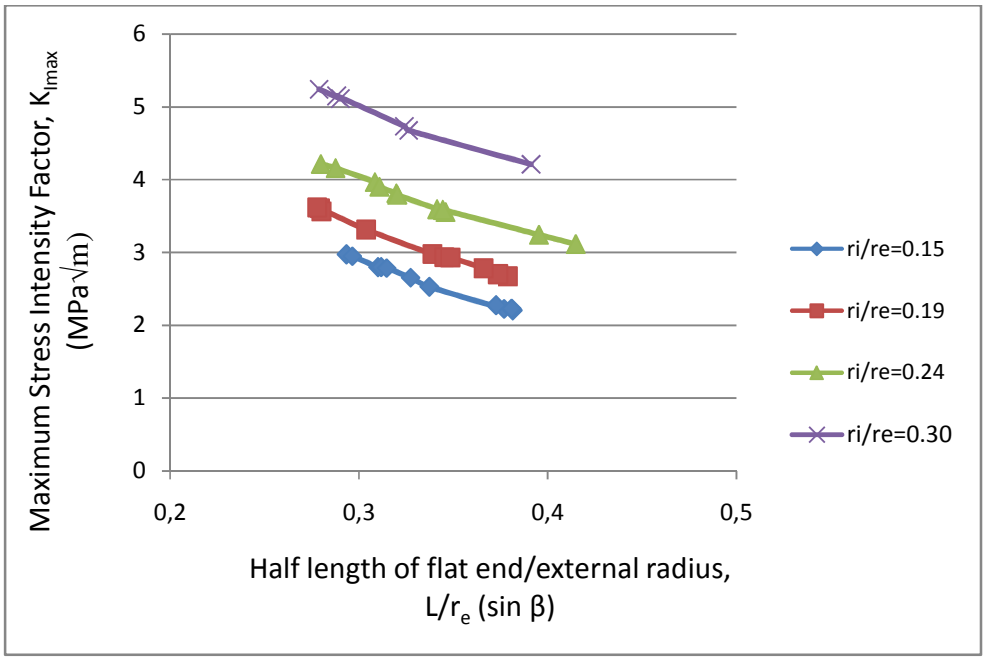

Figure 4.17 Variation of K_{Imax} with respect to L/r_e ratio

When L/r_e is kept constant and effect of r_i/r_e is examined, it is seen from Figure 4.17 that K_{Imax} increases with increasing r_i/r_e ratio. So this means K_{Imax} increases with increasing internal hole radius.

Variation of stress intensity factor with respect to L/r_e (sinβ) together with respect to r_i/r_e can be seen in a single graph. Since there are three variables, this graph should be three dimensional. By using TableCurve3D program, three dimensional graphs and their analytical functions are obtained. Figure 4.19

shows the 3D graph for 54 mm (r_e = 27 mm) specimens and Figure 4.20 shows the same graph for 75 mm (r_e = 37.5 mm) specimens.

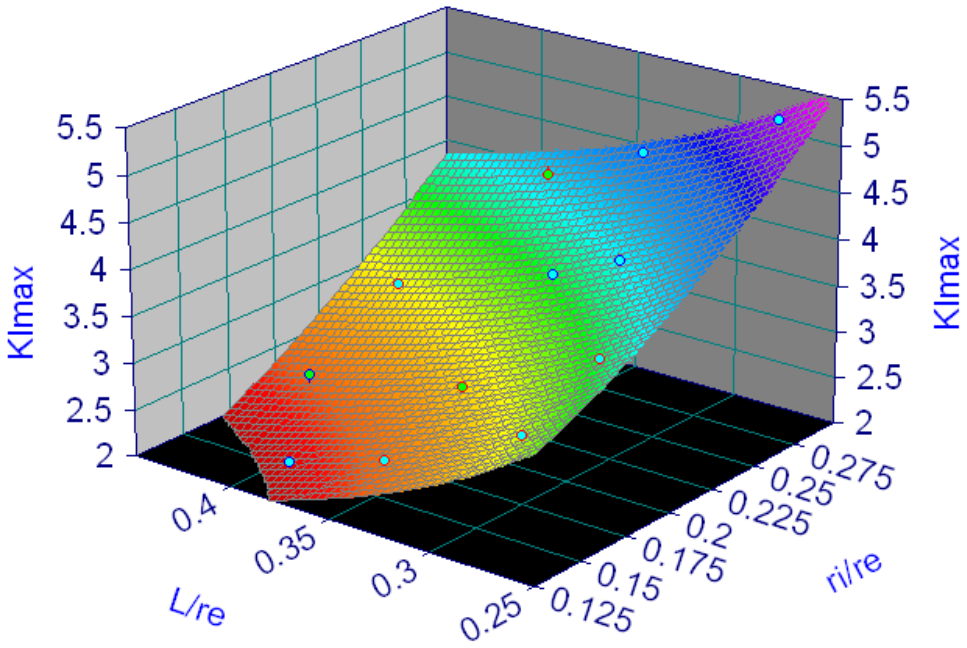

Figure 4.18 3D Graph of K_{Imax} for different L/r_e and r_i/r_e for 54 mm specimens

$$K_{Imax} = -1.1042 + 30.6654(r_i/r_e)^2 + 0.9950/(L/r_e) \quad (4.6)$$

Within the range $0.125 < r_i/r_e < 0.300$ and $0.25 < L/r_e < 0.45$ with $R^2 = 0.9965$.

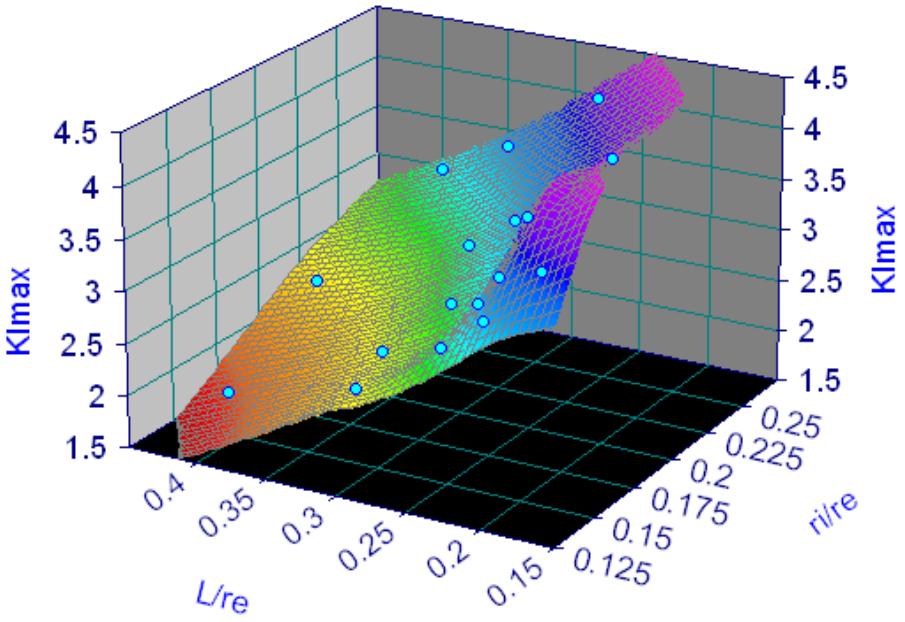

Figure 4.19 3D Graph of K_{Imax} for different L/r_e and r_i/r_e for 75 mm specimens

$$K_{Imax} = -3.6184 + 15.7980\,(r_i/r_e)^{1.5} + 2.834/(L/r_e)^{0.5} \qquad (4.7)$$

Within the range $0.125 < r_i/r_e < 0.275$ and $0.15 < L/r_e < 0.45$ with $R^2 = 0.9682$.

From the Equations 4.6 and 4.7, if r_i/r_e ratio and L/r_e are known for a 54 mm or a 75 mm specimen, the maximum stress intensity factor can be calculated.

To see how external radius affects maximum stress intensity factor the graph in Figure 4.21 is plotted. For this graph internal hole radius (r_i) and flattening angle (β) are kept constant while changing the external radius. Each blue diamond in the line above shows the average of stress intensity factors calculated for 54, 75, 100 and 125 mm specimens. As it can be seen from the

graph, K_{Imax} gets the largest value for the smallest r_e (= 54/2 = 27 mm) and smallest value for the largest r_e (= 125/2 = 62.5 mm).

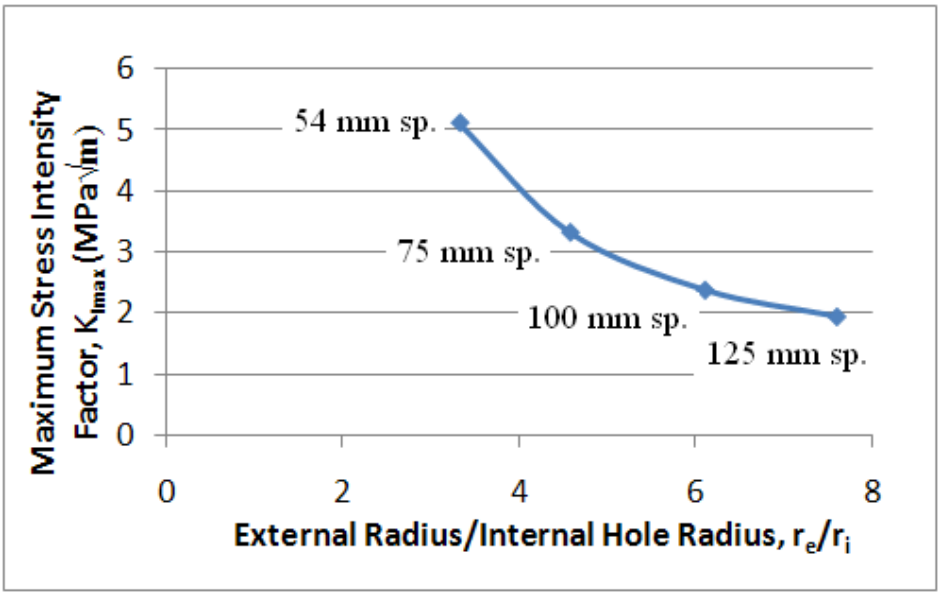

Figure 4.20 Stress intensity factor change with respect to r_e/r_i ratio

CHAPTER 5

EXPERIMENTAL STUDIES

Pink colored Ankara andesite is used for the experiments. The blocks that have been used were taken from a quarry near Gölbaşı region which is 20 km far from Ankara. Two types of specimens were used in the experiments. One of them is Modified Ring (MR) specimen and the other is Semicircular Bend (SCB) specimen. SCB tests were commonly used by the other researchers, so SCB specimens were tested to compare the results to the Modified Ring tests. Modified Ring experiments were also done by the other researchers but effects of the inner hole diameter, size of the flat loading end, and size effects by changing external diameter were not studied before.

5.1 Physical and Mechanical Properties of Pink Ankara Andesite

Before doing fracture tests mechanical and physical properties of the pink Ankara andesite should be known. In order to determine these properties two types of tests were done.

i- Uniaxial Compressive Strength (UCS) Test
ii- Indirect Tensile Strength (Brazilian) Test

5.1.1 Uniaxial Compressive Strength (UCS) Test

Uniaxial Compressive Strength, Young's Modulus (E) and Poisson's Ratio (ν) were determined by conducting the ISRM's (1979) suggested methods. Three NX-sized (≈54mm) specimens with L/D ≥2 were uniaxially loaded by MTS 815 Material Testing System. In order to measure axial strain two axial extensometers were used, and to measure circumferential strain a bracelet shaped circumferential extensometer was used.

Figure 5.1 Uniaxial compressive test

Load and displacement data were taken from the data acquisition system; DaqBook and were converted to stress and strain. Stress-strain curves were

plotted and from these curves, UCS, E and ν were calculated. Tangent of both E and ν were calculated separately. Stress-strain graph of UCS1 is given in Figure 5.2.

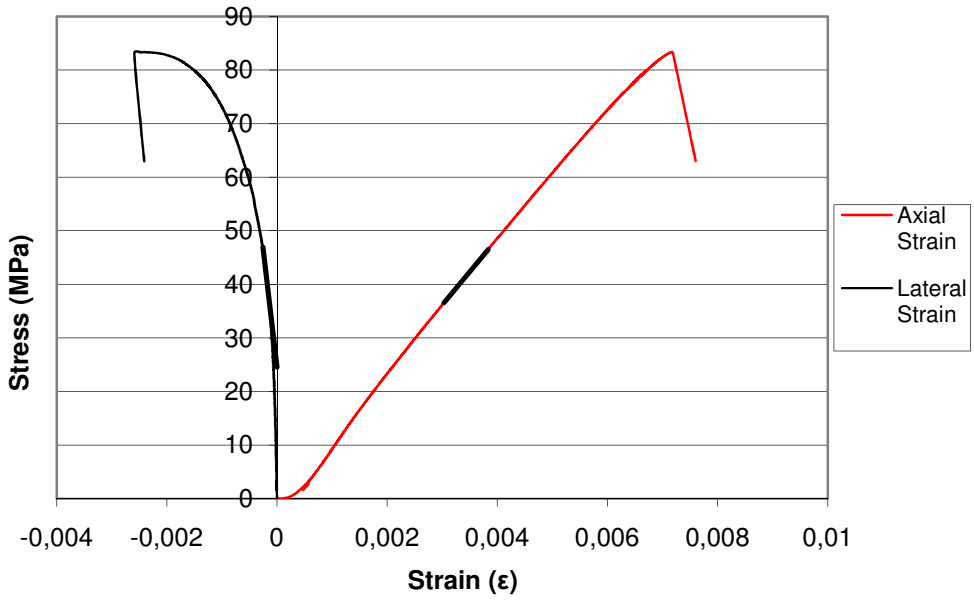

Figure 5.2 Stress-Strain graph of UCS1

Table 5.1 shows geometry measurements and calculated Elastic Modulus and Poisson's ratio values of UCS specimens.

Table 5.1 UCS Test Data and Results

Name	SPECIMEN Diameter mm	Length mm	Elastic Modulus(E) GPa	Poisson's Ratio(v)	UCS MPa
UCS1	54.79	143.81	12.40	0.14	83.31
UCS2	54.46	134.17	12.28	0.16	79.97
UCS3	54.46	141.86	12.30	0.17	86.18
		Average	**12.33**	**0.16**	**83.16**

5.1.2 Indirect Tensile Strength (Brazilian) Test

According to ISRM's (1978) suggested method, Brazilian tests were done to find the tensile strength. NX specimens with D/t = 2 approximately were loaded inside the Brazilian apparatus. MTS 815 was used in loading. Two external LVDT (internal linear variable differential transformer) transducers were used to measure the vertical displacement.

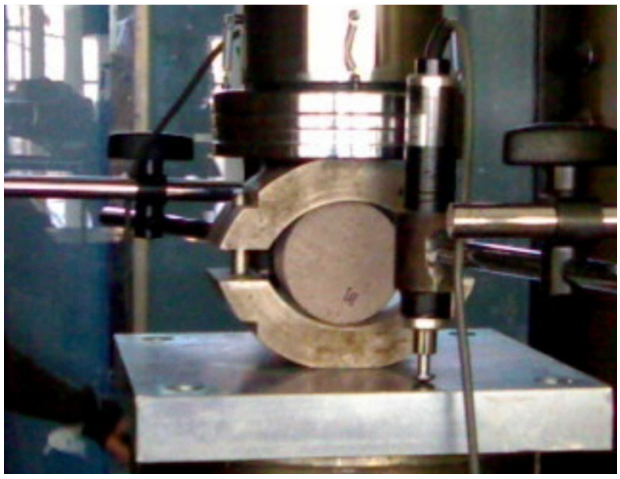

Figure 5.3 Indirect tensile strength test

From the load-displacement curves, the point where the maximum load occurs indicates the failure load. And from the maximum load, tensile strength was computed. Figure 5.4 gives a stress-displacement graph of a Brazilian Test. Three specimens with the same geometry were tested and the results given in Table 5.2 are obtained.

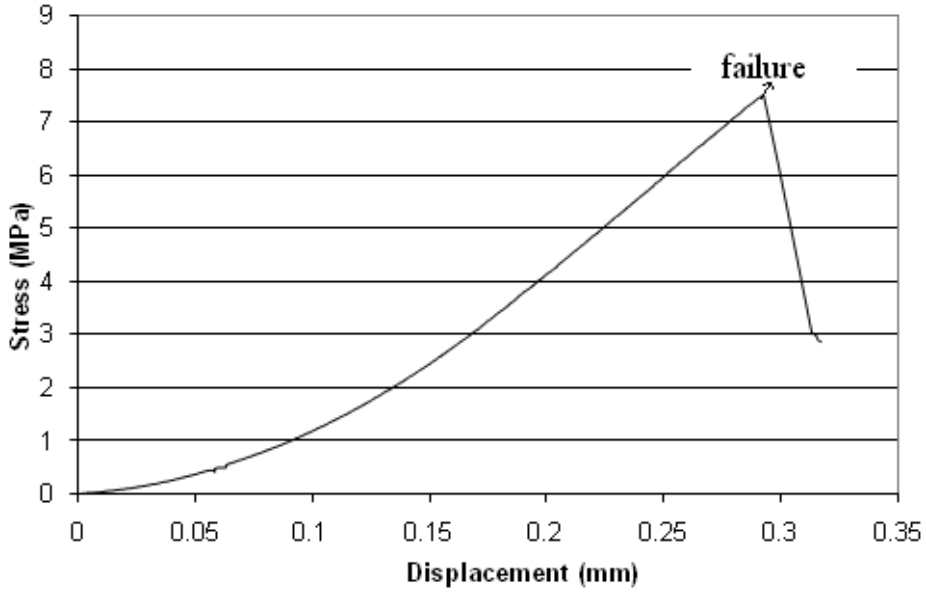

Figure 5.4 Stress–displacement graph of one of the Brazilian tests

Table 5.2 Brazilian test results

Name	SPECIMEN Diameter(D) mm	Thickness(t) mm	D/t	T_0 MPa
Braz-1	54.45	28.08	1.94	6.11
Braz-2	54.41	28.21	1.93	8.27
Braz-3	54.43	28.32	1.92	7.51
			Average	**7.29 ±1.09**

5.2 Fracture Toughness Tests

The blocks that were taken from Gölbaşı were brought to the laboratory. But these blocks were very large to put into the coring machine, so the blocks were cut by the cutting saw. Using different diameters of core bits, core samples were taken from the blocks by coring machine. The inner diameters of the core bits were 75 mm for SCB tests, and 54 and 75 mm for the Modified Ring tests.

Figure 5.5 Coring machine

After the cores were taken, they were cut by using Smartcut 1004 Precision Diamond Saw to the required thickness. If the required thickness could not have been achieved or if some deflections had occurred after the cutting, then by using grinding machine the specimens were polished.

Figure 5.6 Grinding machine

5.2.1 SCB Specimen Preparation

To obtain SCB specimens; 75 mm cores were sliced into 37.5 mm thickness discs. By using geniometer a diameter line was drawn. By using Smartcut 1004, the discs were cut into two from the diameter line. Then these semicircular specimens were put into the apparatus which was specially designed for opening notches. The apparatus was moved manually to back and front while the saw was operating. Notch lengths were adjusted by a digital caliper which was mounted on the saw.

Figure 5.7 Opening of notches to SCB specimen

Finally the measurements were done, noted, the lines of loading were drawn and the specimens were coded. An example coding is shown above:

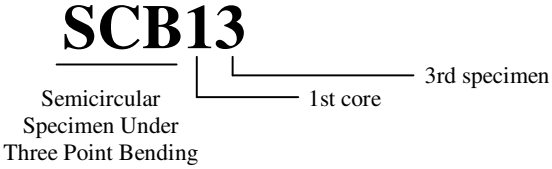

5.2.2 Modified Ring Specimen Preparation

For MR test specimens, 75 mm cores were sliced into 37.5 mm thickness discs and 54 mm cores were sliced into 27 mm thickness discs.

For opening the internal holes, drill bits were used. 8, 10, 13 and 16 mm drill bits were used for 54 mm specimens and 10, 13, 16 and 20 mm drill bits were

used for 75 mm specimens. The holes were barely opened in the lathe and then completely opened in drilling frame.

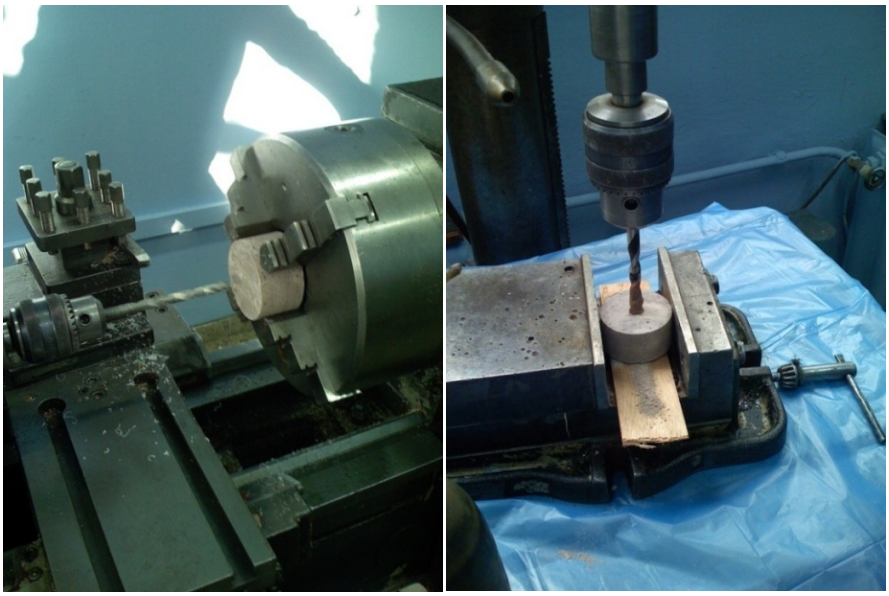

Figure 5.8 Lathe and drilling frame

After opening the holes, the required flattening amount was calculated from the angle of flattening, then upper and lower parts of the specimens were flattened accordingly by grinding machine. Some points of the specimen were marked and the measurements were done from these points. Finally, the specimen was coded. An example coding is shown above:

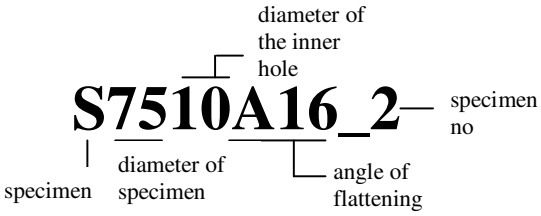

Figure 5.9 Flattening of the ends of the specimen in the grinding machine

5.2.3 SCB Specimen Geometries

Specimens were cut in order to get almost the same thickness values with the radius which is 27 mm. Eight specimens with same geometries were prepared. Notch lengths (a) were around 5 mm, and the spans were around 26 mm to make the S/R ratio equal to 0.7.

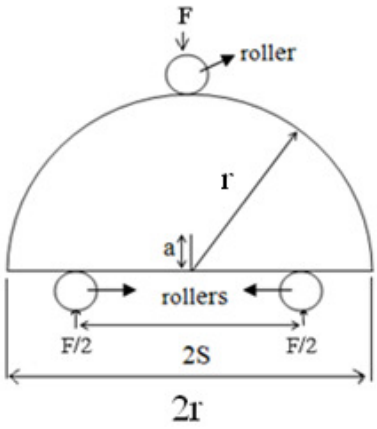

Figure 5.10 Geometry of SCB specimen

where

r = specimen radius

2S = span length

F = load

5.2.4 MR specimen Geometries

Specimens having r_e values of 54, 75, 100 and 125 mm, inner hole radius (r_i) varying from 4 mm to 10 mm and half length of the flattened end (L) ranging from 7 mm to 14mm were prepared. The geometry of MR specimens are as shown in Figure 5.11.

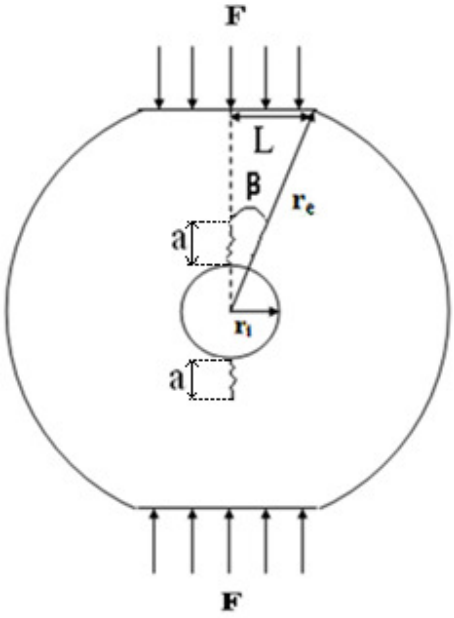

where;

F = load (kN)

r_e = external radius (mm)

r_i = internal radius (mm)

a = crack length (mm)

β = flattening angle (degrees)

L = half length of the flattened surface (mm)

Figure 5.11 Geometry of the MR specimen

5.3 Rock Fracture Testing

Many researchers studied rock fracture toughness using different specimen geometries. In this study, for rock fracture toughness determination SCB tests were done firstly. Because SCB test is a well known test. But the main subject is the Modified Ring Test. SCB tests were done just to compare the results to the results of the MR tests.

5.3.1 SCB Tests

To perform the three point bending test, a special apparatus was used. This apparatus has a bottom part with two rollers and an upper part with one roller. One of the rollers at the bottom was movable in loading axis in order to avoid misalignments. The top roller was attached to a steel block which has magnets on the top to completely attach the upper loading platen of MTS.

5.3.2 SCB Test Results

In order to obtain fracture toughness values for these specimens, firstly stress intensity factors are necessary. A formula for calculating normalized stress intensity factors (Y_1) is given in Equation 5.3. (Alkılıçgil, 2006)

$$Y_1 = \frac{0.615 - 9.676\left(\frac{a}{r}\right) + 18.904\left(\frac{a}{r}\right)^2 - 9.987\left(\frac{a}{r}\right)^3 + 5.235\left(\frac{S}{r}\right)}{1 - 1.136\left(\frac{a}{r}\right) + 0.876\left(\frac{a}{r}\right)^2 - 0.866\left(\frac{a}{r}\right)^3 - 0.019\left(\frac{S}{r}\right)} \qquad (5.3)$$

within the range $0.1<a/r<0.8$ and $0.5<S/r<0.8$ with $R^2 = 0.9995$.

Three point bending tests were performed for eight SCB specimens, and their load-displacement graphs were obtained. A typical load-displacement graph of a SCB test is shown in Figure 5.13.

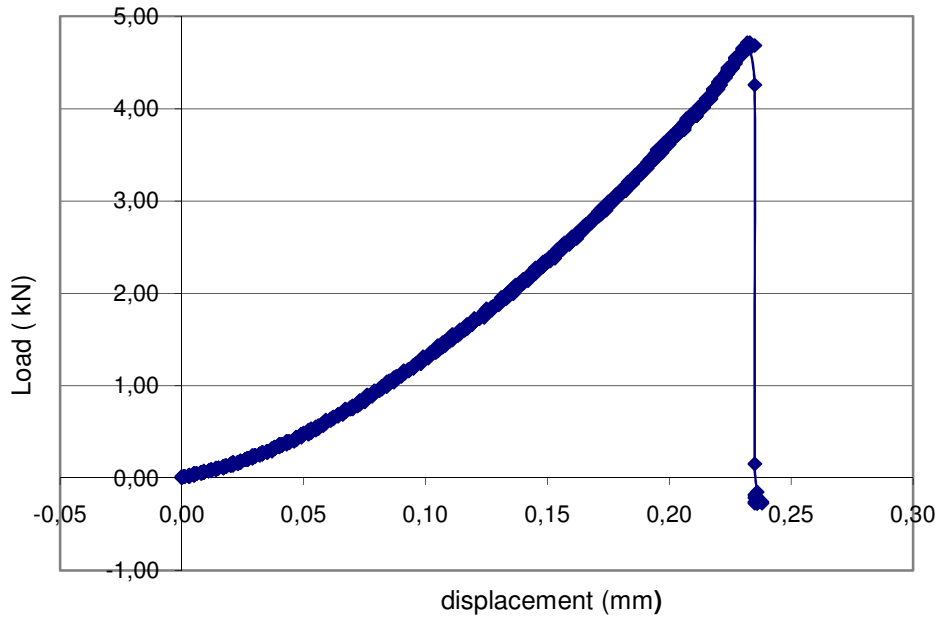

Figure 5.12 Load-Displacement graph of SCB-14

By using maximum load (i.e critical load) and Y_1 values, fracture toughness (K_{Ic}) of the pink Ankara andesite was calculated from Equation 5.4 (Alkılıçgil, 2006).

$$K_{IC} = Y_I \, \sigma_{cr} \sqrt{\pi a} \tag{5.4}$$

where

Y_I = normalized stress intensity factor

$\sigma_{cr} = \frac{F_{cr}}{2rt}$

F_{cr} = load at fracture (maximum load)

r = specimen radius

t = specimen thickness

Table 5.3 gives geometry measurements, maximum load values and calculated σ_{cr}, Y_I and K_{IC} values for each SCB specimen with a core diameter of about 75 mm..

Table 5.3 Fracture data for SCB specimens

	r (mm)	t (mm)	2S (mm)	a (mm)	a/r	2S/r	F_{cr} (kN)	Y_I	σ_{cr} (MPa)	K_{Ic} (MPa√m)
SCB-11	37.49	37.75	26.24	5.80	0.155	0.7	5.24	3.859	1.85	0.96
SCB-12	37.48	37.90	26.24	5.85	0.156	0.7	5.44	3.858	1.91	1.00
SCB-13	37.52	37.83	26.26	5.61	0.150	0.7	5.14	3.865	1.81	0.93
SCB-14	37.50	37.90	26.25	5.78	0.154	0.7	4.72	3.860	1.66	0.86
SCB-21	37.55	37.90	26.28	5.33	0.142	0.7	4.96	3.876	1.74	0.87
SCB-22	37.65	37.75	26.36	5.70	0.151	0.7	4.77	3.863	1.68	0.87
SCB-23	37.52	37.51	26.26	5.25	0.140	0.7	6.85	3.879	2.43	1.21
SCB-24	37.56	37.67	26.29	5.54	0.148	0.7	6.32	3.868	2.23	1.14

where

r = specimen radius

t = specimen thickness

2S = span length

F_{cr} = critical load

σ_{cr} = critical stress = F_{cr} /2rt

K_{IC} = fracture toughness

From these eight fracture toughness tests; average K_{IC} of pink Ankara andesite is calculated as 0.98 ± 0.13 MPa√m. This is very close to the 0.93 MPa√m value found by Alkılıçgil (2006) from tests using SCB specimens with 50 mm radius, and 100 mm diameter.

5.3.3 Modified Ring Tests

In 1987, Thiercelin stated the problems that occur in fracture toughness experiments. The first one was the fact that the specimens shouldn't have been subsized, because the size of the process zone ahead of the crack tip should be negligible compared to the crack length. The second problem was that the rock should not yield under the applied confining pressure due to excessive compressive stress concentrations. And the third problem was the difficulty in measuring axial and crack opening displacements due to the confining pressure. Considering these MR tests seem to be favorable, since crack forms automatically around the holes without any need for notches.

The MR test requires a hollow cylindrical shaped specimen in which the upper and lower parts were flattened in order to have flat loading surfaces. The specimen is loaded across its diameter by applying an axial displacement at a constant rate. As the tangential stress exceeds the tensile strength, the crack initiates at the top and bottom parts of the inner hole and propagates along the loading axis. As discussed before, stress intensity factor (K_I) changes with crack length during the propagation of the crack. Numerical modeling is required at this point to find the changes. The stress intensity factor increases with crack length in first part of the experiment showing that first propagation is unstable and sudden. In the second part, the SIF decreases with crack length which means for crack propagation to continue, additional loading is needed.

Under this stable crack propagation part the load increases gradually again till the crack reaches the loaded boundary and final splitting occurs. (Thiercelin&Roegiers, 1986)

5.3.4 MR Method Testing Procedure

After being sure that the loading surfaces are parallel and the specimen is completely dry, it was put between the loading platens of MTS. Before starting the experiment a program was written in the MicroProfiler 418.91. The program controls all the experiment so once the experiment is started, no other intervention is needed. Firstly, a number was given to program, to be its name. Then, whether a rate, or a level together with time should be given. In MR tests, a rate of 0.0005 mm/s was given. This rate controls the experiment rate. According to this rate, time for a typical experiment is about 10-15 minutes. If it is wanted to perform the experiment under constant axial displacement rate, then the "control" under the AC Controller should be selected. SCB and MR tests were both displacement controlled.

Upper platen of the MTS is spherical shaped so that it is movable to avoid loading axis misalignments. Specimens were put between two platens, and then by using AC displacement controller, the gap between the upper flattened part of the specimen and upper platen were manually closed. It was stopped at the point where two surfaces barely touching each other. Following that, two external LVDT transducers were placed, one of them to the front and one to the back. Then the data acquisition system was set to get the required data which were load, right displacement transducer, and left displacement transducer. The name of the specimen was typed to determine the place where the data is collected. When the data acquisition system was ready, "programmed" option

was selected from MicroProfiler mode selection. The function selection was taken to “Run Enable” mode, and then the program number was typed. By pressing “Run Program” button from MicroProfiler, shortly after to “Run” button from MicroConsole, the experiment was initiated.

The increasing load was followed from the screen of MicroConsole. When it was observed the load reaches a point and drops suddenly, that point was the point of maximum SIF, then the loading continues for a while. Finally unloading was done by pressing “Return to 0” button from the MicroProfiler. In some of the experiments, specimen yielded before unloading.

At the end of the experiments, the collected data was exported to Excel and load-displacement graphs were plotted.

5.3.5 MR Test Results

76 experiments with varying flattening angle (β), inner hole diameters and external diameters were done. For obtaining accurate results statistically; 3 experiments with the same geometry were performed.

Two different external diameters were used in these experiments; 54 mm and 75 mm. 54 mm specimens have 8, 10, 13 and 16 mm inner hole diameters and flattening angles varying from 16 to 24 degrees. These angles correspond to half flat end size of 15 mm to 22 mm for 54 mm specimens, and 21 mm to 30.1 mm for 75 mm specimens.

For each listed specimen, load values were transferred directly from MTS to DaqBook and vertical displacement values were measured by two external

LVDT transducers and then transferred to DaqBook. The capacities of LVDT transducers are $\pm$ 5 mm with 0.005 mm accuracy.

Figure 5.13 gives an example load-displacement curve for a specimen with 54 mm external diameter, 10 mm internal hole diameter and flattening angle of 16°.

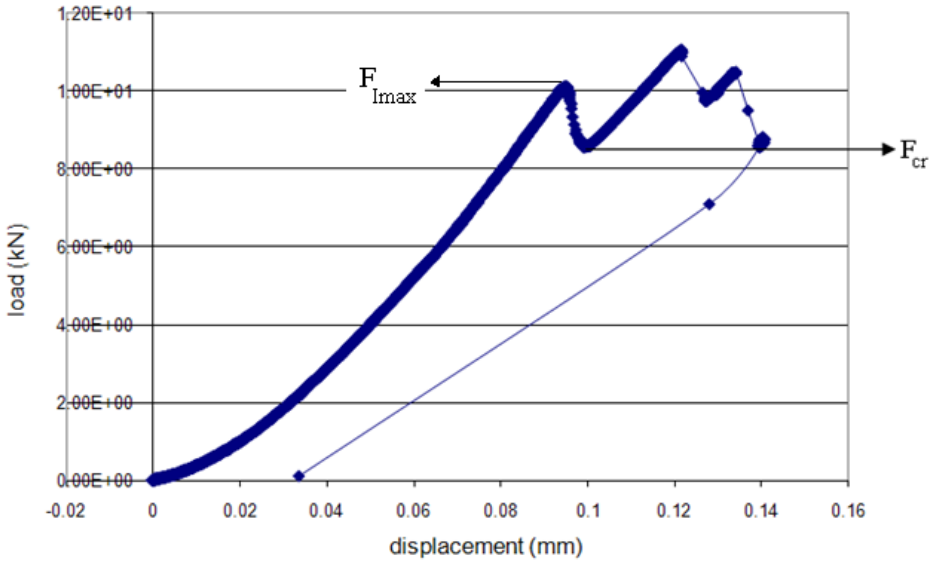

Figure 5.13 Load-displacement graph of S5410A16

As seen from the graphs, there are noise bands both for load and displacement. For displacement the observed noise band is about 0.0025 mm and for load the observed band is about 0.2 kN. These numbers give an idea about the accuracy of the fracture toughness determinations.

From the graphs, it is seen that since the specimen was compressed at a constant displacement rate, the load is nonlinearly increasing with displacement until the time that cracks initiate from the top and bottom of the central hole. These cracks propagate unstably starting at a load level F_{Imax} as shown in

Figure 5.13. Then, after a decrease in load to F_{cr} occurs crack growth becomes stable. At the point of F_{cr}, interaction between the cracks and the crack-normal compressive stress field near the loading surfaces causes the Mode I stress intensity factor (K_I) to decrease with increasing crack length. After that decrease, for cracks to propagate further loading is required. If loading continues, cracks propagate stably after that time.

5.3.6 Computation of Fracture Toughness Values for MR Tests

F_{cr} values will give the σ_{cr} values when divided to the loading area where σ_{cr} is the stress acting on the upper and lower flat ends under critical loads. σ_{cr} is the only required data from the experiments to determine the fracture toughness of the specimens according to Equation 5.5.

$$\left(\frac{\sigma_{cr}}{K_{Imax}}\right)_{model} = \left(\frac{\sigma_{cr}}{K_{Ic}}\right)_{lab} \tag{5.5}$$

where,

σ_{cr} = Stress calculated at load F_{cr}

K_{Imax} = Maximum stress intensity factor found from numerical modeling

K_{IC} = Fracture toughness

For an example computation for K_{IC}, K_{Imax} values for each specimen were found from the Equation 4.6 and 4.7 and given in Chapter 4. For the specimen, S7516A16_1, the r_i/r_e ratio is 0.219; the L/r_e ratio is 0.273, so the calculation of K_{Imax} can be done from Equation 4.7:

$$K_{Imax} = -3.6184 + 15.7980(0.219)^{1.5} + 2.8339/(0.273)^{0.5}$$
$$= 3.47MPa\sqrt{m}$$

The critical stress; σ_{cr} for the model is calculated from the load given in the model. Since a unit load is given in the numerical model, and since it is a 2D model in which thickness is 1, σ_{cr} is 1/(2xLx1). $(\sigma_{cr})_{lab}$ is calculated as F_{cr}/(2xLxt). The thickness of the specimen 37.58 mm and the F_{cr} was determined as 11.6 kN. Now Equation 5.5 becomes:

$$\left(\frac{1/(2\times 10\times 1)}{3.47}\right)_{model} = \left(\frac{11.6\times 10^{3}/(2\times 10\times 37.58\times 10^{-3})}{K_{Ic}}\right)_{lab} \qquad (5.6)$$

From Equation 5.6, K_{IC} for the specimen S7516A16_1 is determined as 1.072 MPa√m.

5.4 Effects of Geometric Parameters on Fracture Toughness

A total of 35 experiments were carried out on 54 mm core specimens. Half of the flat loading end size (L) changed from the smallest 7.6 mm to the highest 11.3 mm for these tests. Inner hole radius (r_i) changed from 4.07 mm to 8.23 mm.

During the specimen preparation, due to the mechanical difficulties, it is difficult to machine the flat loading end to the desired dimensions. Since a brittle material is being machined, variations in the size of flat loading end and inner hole radius are unavoidable. For this reason, number of tests was kept high, and effects of changing L and r_i on fracture toughness were investigated.

Table 5.4 gives geometry measurements, F_{cr}, σ_{cr}, K_{Imax} and K_{IC} values of MR specimens with 54 mm diameter.

Table 5.4 Fracture data for MR specimens with 54 mm diameter

Name	r_i mm	r_i/r_e mm	L mm	L/r_e mm	t mm	F_{cr} kN	σ_{cr} MPa	$K_{\imath max}$ MPa√m	K_{IC} MPa√m
S548A17_1	4.07	0.15	7.99	0.29	26.54	8.19	19.31	2.97	0.92
S548A17_2	4.11	0.15	8.07	0.30	25.90	7.84	18.75	2.95	0.89
S548A18_1	4.09	0.15	8.45	0.31	26.29	7.89	17.77	2.80	0.84
S548A18_2	4.14	0.15	8.49	0.31	26.42	8.38	18.68	2.80	0.89
S548A18_3	4.20	0.15	8.57	0.31	26.76	5.57	12.15	2.79	0.58
S548A19_1	4.17	0.15	8.92	0.33	24.78	7.84	17.73	2.65	0.84
S548A19_2	4.07	0.15	9.19	0.34	25.33	11.20	24.07	2.53	1.12
S548A22_1	4.09	0.15	10.28	0.38	26.10	10.30	19.20	2.23	0.88
S5410A16_1	5.27	0.19	7.60	0.28	26.65	7.86	19.40	3.61	1.06
S5410A16_2	5.20	0.19	7.63	0.28	26.61	8.59	21.15	3.56	1.15
S5410A16_3	5.25	0.19	7.57	0.28	26.55	7.81	19.44	3.62	1.06
S5410A18_1	5.26	0.19	8.28	0.30	25.91	8.42	19.64	3.32	1.08
S5410A20_1	5.27	0.19	9.23	0.34	26.53	5.04	10.29	2.98	0.57
S5410A20_2	5.29	0.19	9.39	0.35	26.11	7.43	15.16	2.94	0.84
S5410A20_3	5.34	0.20	9.49	0.35	25.55	8.09	16.68	2.93	0.93
S5410A22_1	5.28	0.19	10.32	0.38	26.84	9.48	17.12	2.67	0.94
S5410A22_2	5.26	0.19	10.18	0.37	27.09	8.21	14.89	2.70	0.82
S5410A22_3	5.32	0.20	9.97	0.37	26.46	8.35	15.83	2.79	0.88
S5413A16_1	6.52	0.24	7.61	0.28	25.21	3.94	10.28	4.21	0.66
S5413A16_2	6.61	0.24	7.84	0.29	24.95	5.55	14.20	4.16	0.93
S5413A18_1	6.69	0.25	8.41	0.31	24.15	4.56	11.23	3.97	0.75
S5413A18_2	6.61	0.24	8.47	0.31	26.48	5.74	12.80	3.90	0.85
S5413A18_3	6.62	0.24	8.72	0.32	24.97	5.57	12.79	3.81	0.85
S5413A19_1	6.59	0.24	8.74	0.32	24.78	3.42	7.90	3.79	0.52
S5413A20_1	6.57	0.24	9.42	0.35	25.53	6.01	12.50	3.56	0.84
S5413A20_2	6.57	0.24	9.31	0.34	24.92	4.06	8.75	3.59	0.59
S5413A20_3	6.60	0.24	9.38	0.34	26.43	5.57	11.24	3.58	0.76
S5413A23_1	6.65	0.24	10.75	0.40	26.25	4.59	8.13	3.25	0.57
S5413A24_1	6.64	0.24	11.29	0.41	25.42	5.94	10.35	3.12	0.73
S5416A16_1	8.19	0.30	7.59	0.28	28.07	5.11	11.99	5.24	0.95
S5416A17_1	8.18	0.30	7.87	0.29	24.34	3.66	9.55	5.11	0.77
S5416A17_2	8.23	0.30	7.85	0.29	27.47	3.37	7.82	5.15	0.63
S5416A17_3	8.21	0.30	8.23	0.30	24.70	2.53	6.22	4.98	0.51
S5416A18_3	8.21	0.30	8.79	0.32	27.27	4.49	9.37	4.66	0.77
S5416A23_1	8.18	0.30	10.64	0.39	27.44	5.26	9.01	4.21	0.81

r_i : inner hole radius
L : half length of flattened end
t : thickness of the specimen
F_{cr} : critical load
σ_{cr} : critical stress
$K_{\imath max}$: maximum stress intensity factor
K_{IC}: fracture toughness

A plot of K_{IC} values versus L/r_e ratios of 54 mm diameter specimens is given in Figure 5.14. Considering large variations and observing no specific trends, this figure shows that changing the inner hole size doesn't affect fracture toughness within the range of tested inner hole sizes. In addition it can be seen that fracture toughness is independent of L/r_e ratio within the limits of tested flat loading end sizes.

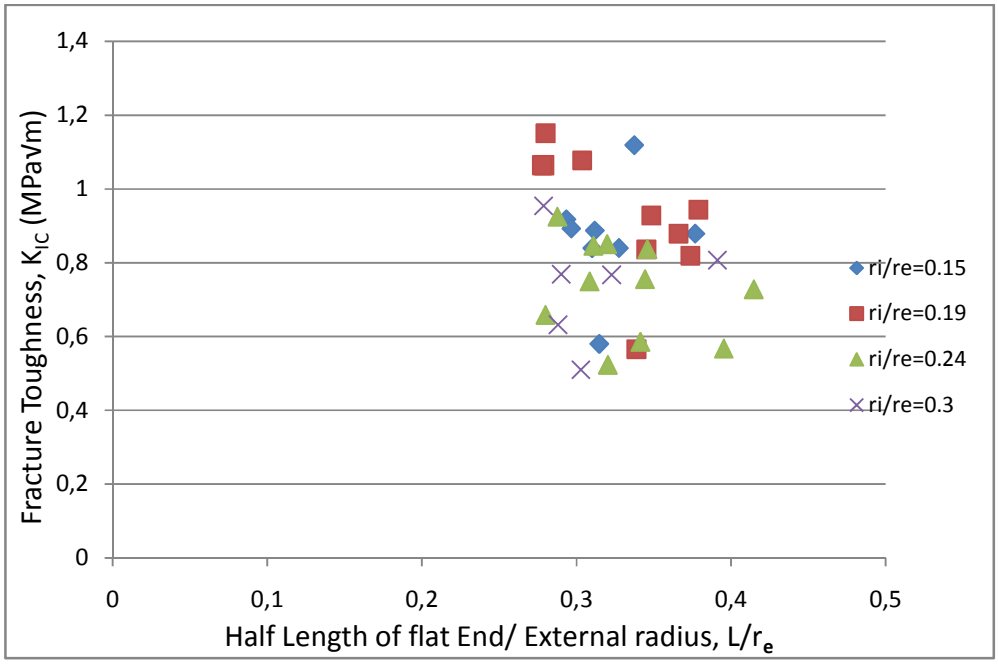

Figure 5.14 Fracture Toughness versus L/r_e for 54 mm diameter specimens

38 experiments were carried out on 75 mm core specimens. For these specimens, inner hole radius varied between 5.0 mm to 10.49 mm, and the half of the flat loading end size (L) varied from 7.6 mm to 14.61 mm.

Table 5.5 gives geometry measurements, F_{cr}, σ_{cr}, K_{Imax} and K_{IC} values of MR specimens with 75 mm diameter.

Table 5.5 Fracture data for MR specimens with 75 mm diameter

Name	r_i	r_i/r_e	L	L/r_e	t	F_{cr}	σ_{cr}	$K_{\imath max}$	K_{IC}
	mm	mm	mm	mm	mm	kN	MPa	MPa√m	MPa√m
S7510A14_1	5.17	0.14	9.30	0.25	37.51	12.20	17.49	2.88	0.94
S7510A16_1	5.10	0.14	10.24	0.27	30.08	13.30	21.60	2.59	1.15
S7510A17_1	5.15	0.14	11.20	0.30	37.58	14.90	17.70	2.37	0.94
S7510A20_1	5.00	0.14	12.63	0.34	35.14	17.40	19.60	2.02	1.00
S7510A21_1	5.00	0.13	13.34	0.36	34.16	16.80	18.43	1.90	0.93
S7512A18_1	6.04	0.16	11.61	0.31	37.68	15.10	17.26	2.49	1.00
S7512A18_2	6.10	0.16	11.90	0.32	37.25	14.50	16.36	2.45	0.95
S7513A12_1	6.58	0.18	7.61	0.20	37.5	10.20	14.71	3.83	1.04
S7513A14_1	6.58	0.18	9.25	0.25	37.25	13.10	17.35	3.24	1.14
S7513A16_1	6.62	0.18	10.14	0.27	37.64	12.70	15.66	3.00	1.01
S7513A16_3	6.65	0.18	10.77	0.29	36.45	11.60	13.83	2.84	0.91
S7513A18_1	6.60	0.18	11.50	0.31	34.67	14.90	17.32	2.66	1.14
S7513A20_1	6.63	0.18	12.41	0.33	33.22	16.20	19.65	2.48	1.21
S7513A22_1	6.54	0.18	13.76	0.37	37.6	15.00	14.12	2.21	0.88
S7513A22_2	6.59	0.18	14.13	0.38	37.46	16.90	15.91	2.16	0.97
S7513A22_3	6.57	0.18	14.18	0.38	36.9	17.90	17.10	2.15	1.04
S7516A14_1	8.22	0.22	8.67	0.23	36.98	10.90	16.63	3.89	1.15
S7516A14_2	8.18	0.22	8.86	0.24	37.6	10.60	15.87	3.82	1.08
S7516A14_3	8.29	0.22	8.88	0.24	36.81	10.60	14.41	3.85	1.11
S7516A16_1	8.17	0.22	10.00	0.27	37.58	11.60	15.20	3.48	1.07
S7516A16_2	8.26	0.22	10.16	0.27	36.08	10.50	13.24	3.46	1.01
S7516A17_1	8.24	0.22	10.99	0.30	37.93	11.50	12.89	3.24	0.98
S7516A17_2	8.00	0.21	11.16	0.30	35.11	10.00	12.76	3.13	0.89
S7516A18_1	8.26	0.22	11.76	0.31	37.11	10.50	10.61	3.08	0.87
S7516A21_1	8.15	0.22	13.33	0.36	38.21	13.00	12.05	2.74	0.93
S7516A22_1	8.22	0.22	14.12	0.38	37.27	15.50	14.78	2.62	1.09
S7516A22_2	8.16	0.22	14.07	0.38	36.6	14.50	14.08	2.61	1.03
S7520A16_1	10.45	0.28	10.17	0.27	34.55	8.96	12.22	4.15	1.08
S7520A16_2	10.44	0.28	10.62	0.28	36.72	9.46	12.16	4.03	1.04
S7520A16_3	10.24	0.27	10.60	0.28	34.43	8.42	11.11	3.97	0.97
S7520A17_1	10.39	0.28	11.01	0.30	35.62	9.22	11.10	3.92	1.02
S7520A18_1	10.40	0.28	11.66	0.31	34.67	9.03	10.30	3.78	0.98
S7520A20_1	10.24	0.27	12.64	0.34	36.44	10.60	11.49	3.52	1.02
S7520A20_2	10.49	0.28	12.66	0.34	34.5	8.33	8.74	3.60	0.87
S7520A22_1	10.32	0.28	13.82	0.37	33.8	8.00	8.65	3.34	0.79
S7520A22_2	10.17	0.27	13.68	0.37	33.98	11.90	11.99	3.31	1.16
S7520A23_1	10.33	0.28	14.61	0.39	36.52	10.90	10.39	3.21	0.96
S7520A23_2	10.41	0.28	14.37	0.38	35.22	11.50	11.36	3.27	1.07

r_i : inner hole radius
σ_{cr} : critical stress
L : Half length of flattened end
$K_{\imath max}$: maximum stress intensity factor
t : thickness of the specimen
K_{IC}: fracture toughness
F_{cr} : critical load

A plot of K_{IC} values versus L/r_e ratios of 75 mm diameter specimens is given in Figure 5.15. As in 54 mm specimens, it is seen that L/r_e ratio and the inner hole radius do not affect fracture toughness within the limits of tested hole and flat loading end sizes.

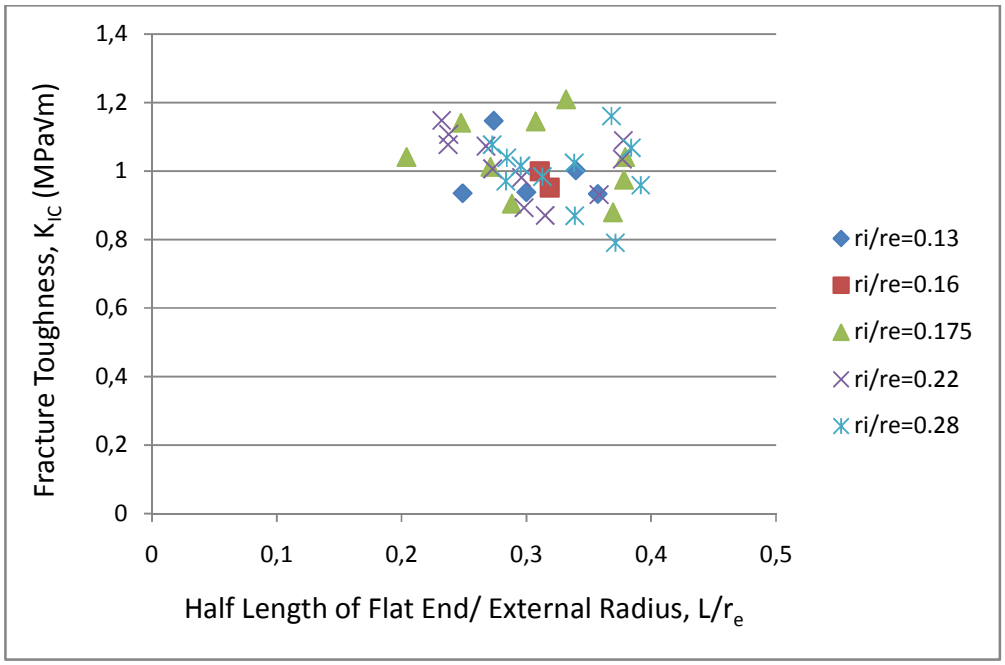

Figure 5.15 Fracture toughness versus L/r_e for 75 mm specimens

When 54 mm diameter and 75 mm diameter specimens were considered separately, the average K_{IC} value for 54 and 75 mm diameter specimens was calculated as 0.82 ± 0.17 MPa√m, and 1.01 ± 0.09 MPa√m, respectively. The K_{IC} value obtained from SCB tests was 0.98 ± 0.13. When an average of individual K_{IC} values is considered for 54 mm and 75 mm groups separately, it is seen from Figure 5.16 that a wider variation exists for 54 mm group.

Figure 5.16 shows the fracture toughness values for all specimen sizes plotted against r_i/r_e values. Since it was found that L/r_e ratio does not affect K_{IC}, the points on this graph correspond to the individual average values of all specimens having same r_i/r_e ratios, but different L/r_e ratios. Each average value is obtained from about 6-9 experiments.

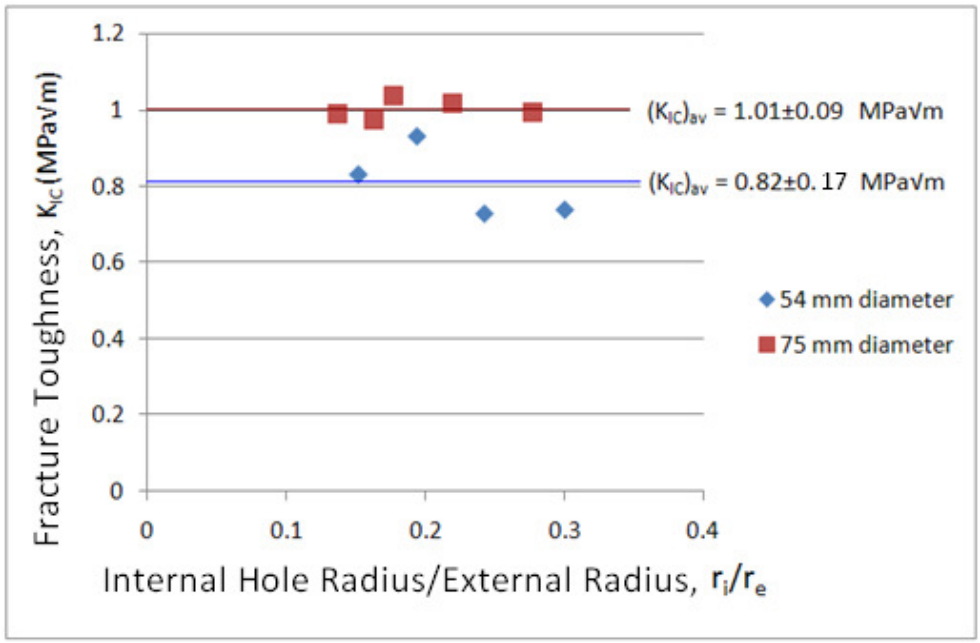

Figure 5.16 Fracture Toughness versus r_i/r_e

Fracture toughness value for 54 mm diameter core specimens was a little low. Therefore, it was decided to carry out a size effect investigation later on by including tests with larger diameters.

5. 5 Analysis with the Results of a Previous Study

Şener (2002) carried out a similar investigation for the modified ring tests. Gray Ankara andesite core specimens with different diameters and hole sizes were tested. According to Şener (2002), gray Ankara andesite had the mechanical properties below in Table 5.6:

Table 5.6 Mechanical properties of gray Ankara andesite

Uniaxial Compressive Strength, UCS (MPa)	Elastic Modulus,E (GPa)	Poisson's Ratio ,v
63.81±3.5	19.85	0.15

In the thesis of Şener (2002), stress intensity factor (K_{Imax}) values were calculated with a boundary element program. When the same geometries were modeled in ABAQUS CAE, the obtained K_{Imax} values are higher than the boundary element results. But, for calculating fracture toughness (K_{IC}) values, Şener (2002) used the first maximum load (F_{Imax}) in the load-displacement graph as F_{cr} instead of the load in the dropped part of the load-displacement graph. So, when lower values for K_{Imax} and higher values for F_{cr} were used, they compensated each other, and K_{IC} values became compatible with the SCB test results of gray Ankara andesite, which was studied by Het (2008).

In order to add the contribution of the results of this previous similar work to the investigation here, new numerical models were prepared and run, and from the load-displacement graphs available in Şener (2002), the corrected F_{cr} values were read. Then, K_{IC} values were recalculated.

Şener (2002) used specimens with external diameters of 75, 100, 125 and 150 mm. 10, 13 and 16 mm inner hole diameters in 75 mm specimens, inner hole diameters of 13 and 16 mm in 100 mm specimens, inner hole diameters of 16, 25 and 33 mm in 125 mm specimens, and inner hole diameters of 25, 33 and 37 mm in 150 mm specimens were used. For each r_i/r_e ratio 4-15 experiments were performed by Şener (2002) with nearly the same L/r_e ratios. Some of these experiments are analyzed here for recalculating the fracture toughness. K_{IC} values given in Table 5.7 are the averages of these experiments which were recalculated with corrected F_{cr} and K_{Imax}. An explanation for the code of the specimens is given below:

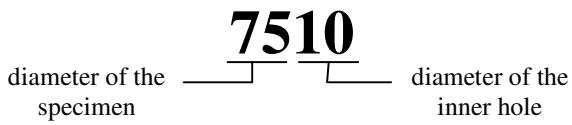

Table 5.7 Corrected fracture toughness values of gray Ankara andesite

Name	Number of tests	L mm	L/r_e	Average K_{ic}(MPa√m)
7510	4	8	0.21	1.24 ± 0.18
7513	5	9	0.24	1.06 ± 0.16
7516	5	8	0.21	1.13 ± 0.11
10013	5	12	0.24	1.52 ± 0.12
10016	5	11	0.22	1.29 ± 0.16
12516	5	12	0.19	1.54 ± 0.43
12525	5	15	0.24	1.27 ± 0.22
12533	4	14	0.22	1.25 ± 0.25
15025	5	16	0.21	1.30 ± 0.17
15033	4	15	0.20	1.35 ± 0.14
15037	5	15	0.20	1.31 ± 0.16

From Table 5.7, the average of all K_{IC} values is 1.30 MPa√m. To compare with another K_{IC} value computed for gray Ankara andesite, SCB test results of Het

(2008) were taken into consideration. Het (2008) found an average K_{IC} value of 1.31 MPa√m; result found here compares well with Het (2008) for the gray andesite. When average K_{IC} values are compared; it is seen that average K_{IC} of gray Ankara andesite is higher than average K_{IC} of pink Ankara andesite.

5.6 Size Effect Studies

It was found that K_{IC} value was not affected by r_i/r_e and L/re ratios. To see the effect of external diameter of the specimen on K_{IC}, it was decided to take a specific internal hole radius which is 8 mm and a specific flattening angle which is 17°. Then 10 specimens; 5 of them with 100 mm external diameter and 5 of them with 125 mm external diameter were prepared with that specific inner hole diameter and flattening angle. This way, it was aimed to carry out a size effect study for the modified ring testing method.

For stress intensity factors (K_I), numerical model of each specimen was prepared and run separately. The same geometry with the specimen's exact dimensions was modeled in ABAQUS and stress intensity factor was calculated.

The same procedure with previous experiments was carried out for these specimens, and the results for the pink andesite used here are given in Table 5.8.

Table 5.8 K_{IC} values of pink Ankara andesite with internal hole radius of 8 mm (r_i = 8 mm; diameter = 16 mm)

Name	r_e/r_i	L/r_e	t	L	F_{cr}	σ_{cr}	K_I	K_{IC}	$(K_{IC})_{av}$
	mm	mm	mm	mm	kN	MPa	MPa√m	MPa√m	MPa√m
S5416A16_1	3.32	0.28	28.07	7.59	5.11	11.99	5.24	0.95	
S5416A17_1	3.32	0.29	24.34	7.87	3.66	9.55	5.11	0.77	
S5416A17_2	3.31	0.29	27.47	7.85	3.37	7.82	5.15	0.63	0.73±0.17
S5416A17_3	3.31	0.30	24.70	8.23	2.53	6.22	4.98	0.51	
S5416A18_1	3.38	0.32	27.27	8.79	4.49	9.37	4.66	0.77	
S7516A16_1	4.58	0.27	37.58	10.00	11.60	15.20	3.47	1.07	
S7516A16_2	4.51	0.27	36.08	10.16	10.50	13.24	3.46	1.00	
S7516A17_1	4.51	0.30	37.93	10.99	11.50	12.89	3.23	0.98	0.96±0.08
S7516A17_2	4.68	0.30	35.11	11.16	10.00	12.76	3.13	0.89	
S7516A18_1	4.52	0.31	37.11	11.76	10.50	10.61	3.08	0.87	
S10016A17_1	6.11	0.29	47.62	14.43	21.30	15.50	2.33	1.04	
S10016A17_2	6.08	0.30	50.67	14.96	23.60	15.56	2.25	1.05	
S10016A17_3	6.12	0.29	50.85	14.67	24.00	16.09	2.29	1.08	1.11±0.07
S10016A17_4	6.25	0.25	50.42	12.52	23.30	18.45	2.65	1.22	
S10016A17_5	6.25	0.29	50.35	14.30	24.80	17.23	2.35	1.16	
S12516A17_1	7.62	0.28	61.43	17.46	40.90	19.07	1.98	1.31	
S12516A17_2	7.52	0.28	61.36	17.45	42.60	19.89	1.98	1.38	
S12516A17_3	7.63	0.30	60.55	18.48	42.00	18.77	1.86	1.29	1.29±0.12
S12516A17_4	7.69	0.25	62.57	15.42	39.20	20.32	2.23	1.40	
S12516A17_5	7.69	0.26	62.28	16.43	32.30	15.79	2.11	1.09	

From Şener's thesis (2002), the gray andesite specimens with 8 mm internal hole radius (r_i) were reanalyzed. As it was told before the stress intensity factors of these specimens were recalculated with ABAQUS and are corrected. Table 5.9 was obtained from the studies of Şener (2002).

Table 5.9 K_{IC} values of gray Ankara andesite with internal hole radius of 8 mm (r_i = 8 mm; diameter = 16 mm)

Name	r_e/r_i mm	L/r_e mm	t mm	L mm	F_{cr} kN	σ_{cr} MPa	K_I MPa√m	K_{IC} MPa√m	$(K_{IC})_{av}$ MPa√m
7516_1	4.69	0.21	37.00	8.00	10.80	36.49	4.09	1.19	
7516_2	4.69	0.21	37.00	8.00	11.00	37.16	4.09	1.22	
7516_3	4.69	0.21	37.00	8.00	9.10	30.74	4.09	1.01	1.13±0.12
7516_4	4.69	0.21	37.00	8.00	11.00	37.16	4.09	1.22	
7516_5	4.69	0.21	37.00	8.00	9.00	30.41	4.09	0.99	
10016_1	6.25	0.24	51.00	12.00	24.90	40.69	2.73	1.33	
10016_2	6.25	0.22	52.00	11.00	18.00	31.47	2.94	1.02	
10016_3	6.25	0.23	54.00	11.50	25.70	41.38	2.73	1.30	1.29±0.15
10016_4	6.25	0.20	51.00	10.00	22.70	44.51	3.16	1.41	
10016_5	6.25	0.19	52.00	9.50	21.80	44.13	3.28	1.37	
12516_1	7.81	0.19	61.00	12.00	35.00	47.81	2.72	1.56	
12516_2	7.81	0.19	60.00	12.00	35.00	48.61	2.72	1.59	
12516_3	7.81	0.19	61.00	12.00	35.10	47.95	2.72	1.57	1.54±0.05
12516_4	7.81	0.19	64.00	12.00	34.70	45.18	2.72	1.47	
12516_5	7.81	0.19	62.00	12.00	34.90	46.91	2.72	1.53	

Figure 5.17 is obtained from Table 5.8 and from Şener (2002)'s results for 8 mm internal hole radius in 75, 100 and 125 mm specimens given in Table 5.9. Red squares show Şener's (2002) results with gray andesite and blue diamonds show results of pink andesite used in this study. Statistical Fits are shown in Figure 5.17.

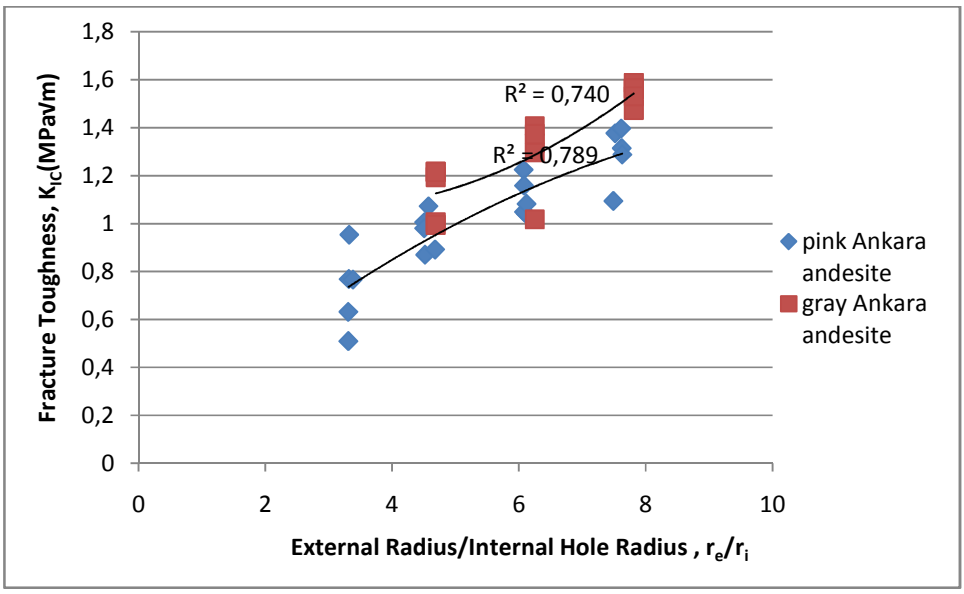

Figure 5.17 Fracture Toughness vs. r_e/r_i for r_i = 8 mm

As seen from Figure 5.17, K_{IC} increases with increasing r_e/r_i ratio. This means, for a constant r_i value, which is 8 mm K_{IC} increases with increasing r_e value. The trend is the same for both pink and gray andesites.

When all experiments for both pink and gray Ankara andesites were considered together, regardless of inner hole size and size of the flat loading end, the average K_{IC} values become as shown in Figure 5.18. A size effect is observed for gray andesite; K_{IC} value for 75 mm is lower (K_{IC} = 1.14 MPa√m) compared to the average value of K_{IC} of 100 mm, 125 mm, and 150 mm specimens (K_{IC} = 1.36 MPa√m). This shows that for modified ring tests, a specimen size of D = 100 mm should be considered in order to reach the constant value or the value tended at larger diameters. Results show a definite size effect for pink andesite, however, a tendency value for larger diameters cannot be identified clearly, since a larger diameter result such as D = 150 mm cannot be added to the

analysis due to the specimen shortage following the large number of tests performed here, so far.

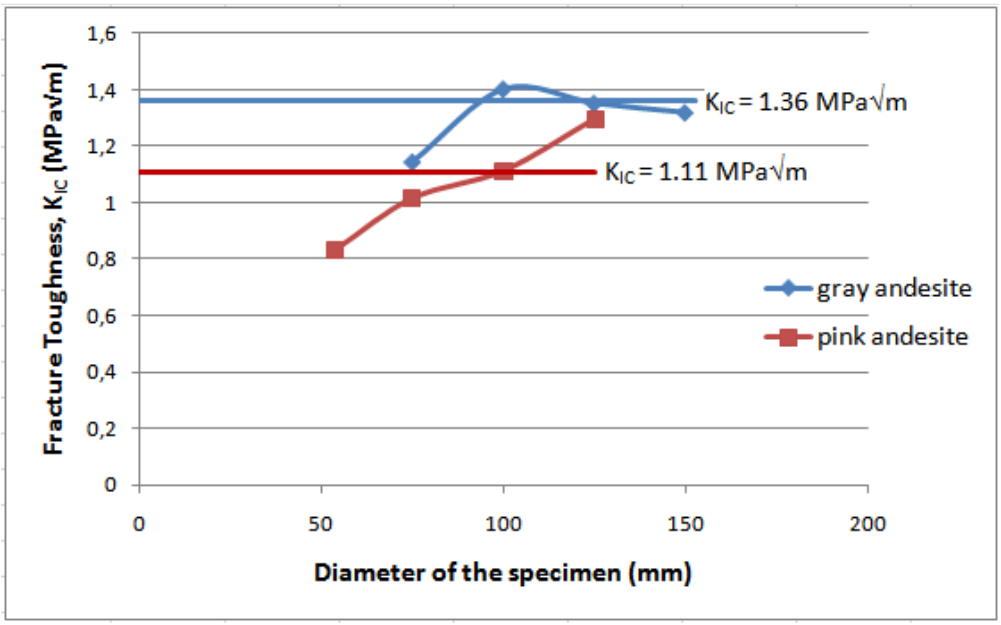

Figure 5.18 Average fracture toughness of all specimens with varying r_i and L vs. diameter of the specimen

In Figure 5.18, a tendency to a value is seen for K_{IC} values of gray andesite. Since 75 mm specimens have a lower K_{ic} value, the tendency is towards the average of the values obtained from 100, 125 and 150 mm specimens. This is towards to a value of $(K_{IC})_{av(100,125,150)}$ = 1.36 MPa√m, which is very close to the value 1.32 MPa√m found by Het (2008) for gray Ankara andesite with SCB tests.

For pink Ankara andesite, a tendency could not be clearly identified, since 150 mm specimens for this investigation were not available due to the shortage of specimen preparation rock blocks. Therefore, K_{IC} value calculated for 100 mm

specimens was considered to be the value tended. $(K_{IC})_{100}$ = 1.11 MPa√m for 100 mm diameter specimen size, which was close to the K_{IC} value obtained from SCB tests of pink Ankara andesite as 0.98 MPa√m, was concluded to represent Mode I fracture toughness of this rock type.

CHAPTER 6

CONCLUSIONS AND RECOMMENDATIONS

Fracture toughness of pink Ankara andesite was determined by using modified ring testing method. Modified ring specimens are core based and they do not need a notch to be opened before the experiments. Because of these advantages, this study was made to improve the Modified Ring Test method.

3D numerical modeling was carried out with a finite element program called ABAQUS. Stress intensity factor variation with respect to crack length was observed. Effects of L/r_e ratio (sin β) and r_i/r_e ratio on SIF were investigated. When numerical models were analyzed, it was seen that for a constant L/r_e ratio, maximum SIF (K_{Imax}) value increases with increasing r_i/r_e ratio, which means for a constant L and r_e, K_{Imax} increases with internal hole radius (r_i). It was also observed that K_{Imax} gets larger values for small flat loading end sizes. To see the effect of the external radius (r_e) or specimen size on SIF, flat loading end size and inner hole radius (r_i) were kept constant, and the size of the specimens was changed by changing the specimen diameter; it was seen that K_{Imax} is the largest for the largest r_e, and the smallest for the smallest r_e.

A well-known specimen type; SCB specimens were subjected to the fracture toughness experiments to check the reliability of the MR tests. From SCB tests, the average fracture toughness value (K_{IC}) was determined as 0.98 ± 0.13 MPa√m.

From the experiments with modified ring method, K_{IC} value of 54 mm specimens was found as 0.89±0.17 MPa√m, and K_{IC} value of 75 mm specimens was found as 1.01±0.09 MPa√m. K_{IC} value of 100 mm specimens was determined as 1.11±0.07 MPa√m, and K_{IC} value of 125 mm specimens was found as 1.29±0.12 MPa√m . This size effect can possibly be explained by studying crack tip stress distributions. Lower tensile stresses exist at the crack tip for larger diameter (larger r_e) specimens. This means that yield zone or process zone for smaller specimens is possibly larger, which possibly results in lower fracture toughness values for subsized specimen goemetries.

Based on the results of this study, it is concluded that the size of the flat loading end at the upper and lower boundaries of the specimen, and inner hole radius (r_i) do not affect the fracture toughness in tests with the modified ring method.

Considering a similar study conducted by Şener (2002) with gray Ankara andesite, K_{IC} values of gray Ankara andesite were recalculated. From these values, a tendency towards an average value of 1.36 MPa√m from 100 mm, 125 mm, and 150 mm specimens was observed. Results compared well with the results of a previous study in which fracture toughness was reported to be found as 1.32 MPa √m which was found by Het (2008) for gray Ankara andesite with SCB tests.

According to the results of the work on gray Ankara andesite, 100 mm diameter or larger specimens are suggested for the modified ring tests, because when size of the specimens exceeds 100 mm, $K_{ıc}$ value tends to a specific value. To see this tendency for pink Ankara andesite, it is recommended to extend the study

to the larger size specimens. It is also recommended to study the size effect for SCB testing method. Further investigations must be carried out to study the effect of loading rate on K_{IC}. Also, performing MR test with other rock types will improve the method.

REFERENCES

ABAQUS Analysis User's Manual, Version 6.5 Documentation.

ABAQUS/CAE User's Manual, Version 6.5 Documentation.

ABAQUS, Inc., "Modeling Fracture and Failure with ABAQUS", 2006.

ABAQUS Technology Brief, "Fracture Mechanics Study of a Compact Tension Specimen Using ABAQUS/CAE", 2004.

Abou-Sayed, A. S., Brechtel, C. E., Clifton,R. J., "In Situ Stress Determination by Hydrofracturing: A Fracture Mechanics Approach", J. Geophys. Res., Vol.83, pp. 2851-2862, 1978.

Alkılıçgil, Ç., "Development of a New Method for Mode I Fracture Toughness Test on Disc Type Rock Specimens", M.S. Thesis, METU, Ankara, 145 p, 2006.

Barker, L.M., "A Simplified Method for Measuring Plane Strain Fracture Toughness", Engng. Fracture Mech., Vol. 9, 361-369, 1977.

Boone, T.J., Wawrzynek, P.A., Ingraffea, A.R., "Simulation of the Fracture Process in Rock with Application to Hydrofracturing", International Journal of Rock Mechanics Mining Sciences & Geomechanics Abstracts, Vol.23, No. 3, pp. 255-265, 1986.

Chang, S. H., Chung-In Lee, Jeon, S., "Measurement of rock fracture toughness under modes I and II and mixed-mode conditions by using disc-type specimens", Engineering Geology, Vol. 66, pp. 79–97, 2002.

Chong, K.P, and Kuruppu, M.D., "New Specimen for Fracture Toughness Determination for Rock and Other Materials", Int. J. Fract., Vol. 26, R59-R62, 1984.

Choupani, N., "Interfacial Mixed-Mode Fracture Characterization of Adhesively Bonded Joints", International Journal of Adhesion and Adhesives, Vol. 28, Issue 6, pp. 267-282, 2008.

Cornell Fracture Group, "FRANC3D&BES Benchmarking", Version 2.6, 2003.

DBK Option Cards & Modules User's Manual, 2003.

EFunda Engineers, Fracture Mechanics. EFunda Engineering Fundamentals. http://www.efunda.com/formulae/solid_mechanics/fracture_mechanics.

Fischer, M. P., Elsworth, D., Alley, R. B., Engelder, T., "Finite Element Analysis of the Modified Ring Test for Determining Mode I Fracture Toughness", International Journal of Rock Mechanics Mining Sciences & Geomechanics Abstracts, Vol.33, No. 1, pp. 1-15, 1996.

Fowell, R. J., "Suggested Method for Determining Mode I Fracture Toughness Using Cracked Chevron Notched Brazilian Disc (CCNBD) Specimens", International Journal of Rock Mechanics Mining Sciences & Geomechanics Abstracts, Vol.32, No. 1, pp. 57-64, 1995.

Fowell, R.J., "An Update on the Fracture Toughness Testing Methods Related to the Cracked Chevron-notched Brazilian Disk (CCNBD) Specimen, Pure and Applied Geophysics, Vol. 163, pp. 1047-1057, 2006.

Guo, H., Aziz, N.I., Schmidt, L.C., "Rock Fracture-Toughness Determination by the Brazilian Test", Engineering Geology, Vol. 33, No. 3, pp. 177-188, 1993

Het, K., "Effects of Geometrical Factors on Fracture Toughness Using Semi-circular Bending Type Specimens", M.S. Thesis, METU, Ankara, 158 p., 2008.

Iqbal, M.J., Mohanty, B., "Experimental Calibration of Stress Intensity Factors of the ISRM Suggested Cracked Chevron-Notched Brazilian Disc Specimen Used for Determination of Mode-I Fracture Toughness", Department of Civil Engineering and Lassonde Institute, University of Toronto, Canada, 2006.

ISRM Commission on Standardization of Laboratory and Field Tests, "Suggested Methods for Determining Tensile Strength of Rock Materials", Int. J. Rock Mech. Min. Sci. & Geomech. Abstr., Vol. 15, pp. 99-103, 1978.

ISRM Commission on Standardization of Laboratory and Field Tests, "Suggested Methods for Determining the Uniaxial Compressive Strength and Deformability of Rock Materials", Int. J. Rock Mech. Min. Sci. & Geomech. Abstr., Vol. 16, pp. 135-140, 1979.

ISRM Commission on Testing Methods, "Suggested Method for Determining Mode I Fracture Toughness Using Cracked Chevron Notched Brazilian Disc (CCNBD) Specimens", Int. J. Rock Mech. Min. Sci. & Geomech. Abstr., Vol. 32, pp. 57-64, 1995.

Karl, Z. J. and Bieniawski, Z. T., "Mixed Mode Testing for Fracture Toughness of Coal Based on Critical Density", Proc. 27th U.S Symposium on Rock Mechanics, Alabama pp. 16-23, 1986.

Karpuz, C., Bozdağ, T., "A Comparison on the Double Cantilever Beam and Short Rod Fracture Toughness Test results of Ankara Andesite", Eurock'96, Barla, Rotterdam, 1996.

Khan, K. and Al-Shayea, N. A., "Effect of Specimen Geometry and Testing Method on Mixed Mode I-II Fracture Toughness of a Limestone Rock from Saudi Arabia", Rock Mech. Rock Engng., Vol. 33, pp. 179-206, 2000.

Lim, I.L., Johnston, I.W., Choi, S.K. and Boland, J.N., "Fracture Testing of a Soft Rock with Semi-circular Specimens Under Three-point Bending. Part I-Mode I", Int. J. Rock Mech. Min. Sci. & Geomech. Abstr., Vol. 31, No. 3, pp. 185-197, 1994.

Lim, I.L., Johnston, I.W., Choi, S.K. and Boland, J.N., "Fracture Testing of a Soft Rock with Semi-circular Specimens Under Three-point Bending. Part II-Mixed Mode", Int. J. Rock Mech. Min. Sci. & Geomech. Abstr., Vol. 31, No. 3, pp. 199-212, 1994.

Lim, I.L., et.al, "Stress intensity factors for semi-circular specimens under three-point bending", Engineering Fracture Mechanics, Vol. 44, No. 3, pp. 363-382, 1993.

Ma, F., "The Fracture Toughness and Fracture Assessments of Different Specimens", Engineering Fracture Mechanics, Vol. 51, No. 3, pp. 487-495, 1995.

NDT Resource Center, "Fracture Toughness", www.ndt-ed.org.

Ouchterlony, F., "Suggested Methods for Determining the Fracture Toughness of Rock", Int. J. Rock Mech Min. Sci., ISRM Working Group Report, Vol. 25, pp 71-96, 1988.

Prado, E. P., Mier, J. G. M., "Effect of Particle Structure on Mode I Fracture Process in Concrete", Engineering Fracture Mechanics, Vol. 70, No.14, pp. 1793-1807,2003.

Proveti, J., Michot,G., "The Brazilian Test: A Tool for Measuring the Toughness of a Material and Its Brittle to Ductile Transition", International Journal of Fracture, Vol.139, pp.455-460, 2006.

Rice, J.R., "A Path Independent Integral and the Approximate Analysis of Strain Concentration by Notches and Cracks", J. App. Mech., Vol. 35, pp. 379-386, 1968.

Ripling,E. J. ; Mostovoy,S. ; Patrick,R. L., "Application Fracture Mechanics to Adhesive Joints. Part I", Materials Research Lab Inc. Richton Park Ill, 1963.

Riveros, G.A., "Numerical Evaluation of Stress Intensity Factors (K_I) J-Integral Approach", US Army Corps, 2006.

Rummel, F., "Fracture Mechanics Approach to Hydraulic Fracturing Stress Measurements, in Fracture Mechanics of Rock (Edited by B.K. Atkinson)", Academic Press, London, pp. 217-239, 1987.

Rummel, F., Baumgartner, J., Alheid, H. J., "Hydraulic Fracturing Stress Measurements Along the Eastern Boundary of the SW-German Block", Hydraulic Fracturing Stress Measurements, National Academy Press, Washington, D. C., pp. 3-17, 1983.

Singh, R. N. and Pathan, A. G., "Fracture Toughness of Some British Rocks by Diametral Loading of Discs", Mining Science and Technology, Vol. 6, pp. 179-190, 1988.

Sousa, J.L.A, Bittencourt, T.N., "Experimental Analysis of Fracture Process in Concrete", Journal of the Brazilian Society of Mechanical Sciences, Vol.23, no.4, Rio de Janerio, 2001.

Shetty, D. K., Rosenfield, A. R., Duckworth, W. H., "Fracture Toughness of Ceramics Measured by a Chevron Notched Diametral Compression Test", J. Am. Ceram. Soc., Vol. 68, pp. c325-c443, 1985.

Şener, S., "Fracture Toughness Tests on Brazilian Discs of Ankara Andesite", M.S. Thesis, METU, Ankara, 122 p., 2002.

Thiercelin, M.,"Fracture Toughness Under Confining Pressure Using the Modified Ring Test", 28th US Symposium on rock Mechanics, Tucson, 1987.

Thiercelin, M., "Fracture Toughness and Hydraulic Fracturing", Int. J. Rock Mech. Min. Sci. &Geomech. Abstr., Vol. 26, pp. 177-183, 1989.

Thiercelin, M., Roegiers, J. C., "Fracture Toughness Determination with the Modified Ring Test", International Symposium on Engineering in Complex Rock Formations (ECRF), Beijing, China, 1986.

Van de Steen, B., Vervoort,A., "Non-local StressApproach to Fracture Initiation in Laboratory Experiments with a Tensile Stress Gradient", Mechanics of Materials, Vol. 33, pp. 729-740, 2001.

Wang, Q. Z., Jia, X. M., Kou, S. Q., Zhang, Z. X., Lindqvist, P. A., "The Flattened Brazilian Disc Specimen Used for Testing Elastic Modulus, Tensile Strength and Fracture Toughness of Brittle rocks: Analytical and Numerical Results", International Journal of Rock Mechanics and Mining Sciences, Vol. 41, Issue 2, pp. 245-253, 2004.

Wang, Q. Z., Xing, L., "Determination of Fracture Toughness KIC by Using the Flattened Brazilian Disc Specimen for Rocks", Engineering Fracture Mechanics, Vol. 64, Issue 2, pp. 193-201, 1999.

Wang, Q. Z., Wu, L. Z., " The Flattened Brazilian Disc Specimen Used for Determining Elastic Modulus, Tensile Strength and Fracture Toughness of Brittle Rocks: Experimental Results", International Journal of Rock Mechanics and Mining Sciences, Vol. 41, Supp. 1, pp. 26-30, 2004.

Yan, J., Mecholsky J. J., Clifton, J. and Clifton, K. B., "How Tough is Bone? Application of Elastic–Plastic Fracture Mechanics to Bone" , Department of Materials Science and Engineering, University of Florida, USA Department of Physiological Sciences, University of Florida, USA, 2006.

Yan, X., "An Emprical Formula for Stress Intensity Factors of Cracks Emanating from a Circular Hole in a Rectangular Plate in Tension", Engineering Failure Analysis, Vol. 14, pp. 935-940, 2007.

Zhao, X. L., Roegiers, J. C., "Determination of In Situ Fracture Toughness", International Journal of Rock Mechanics Mining Sciences & Geomechanics Abstracts, Vol. 30, No. 7, pp. 837-840, 1993.

APPENDIX A

A. LOAD – DISPLACEMENT GRAPHS OF SPECIMENS

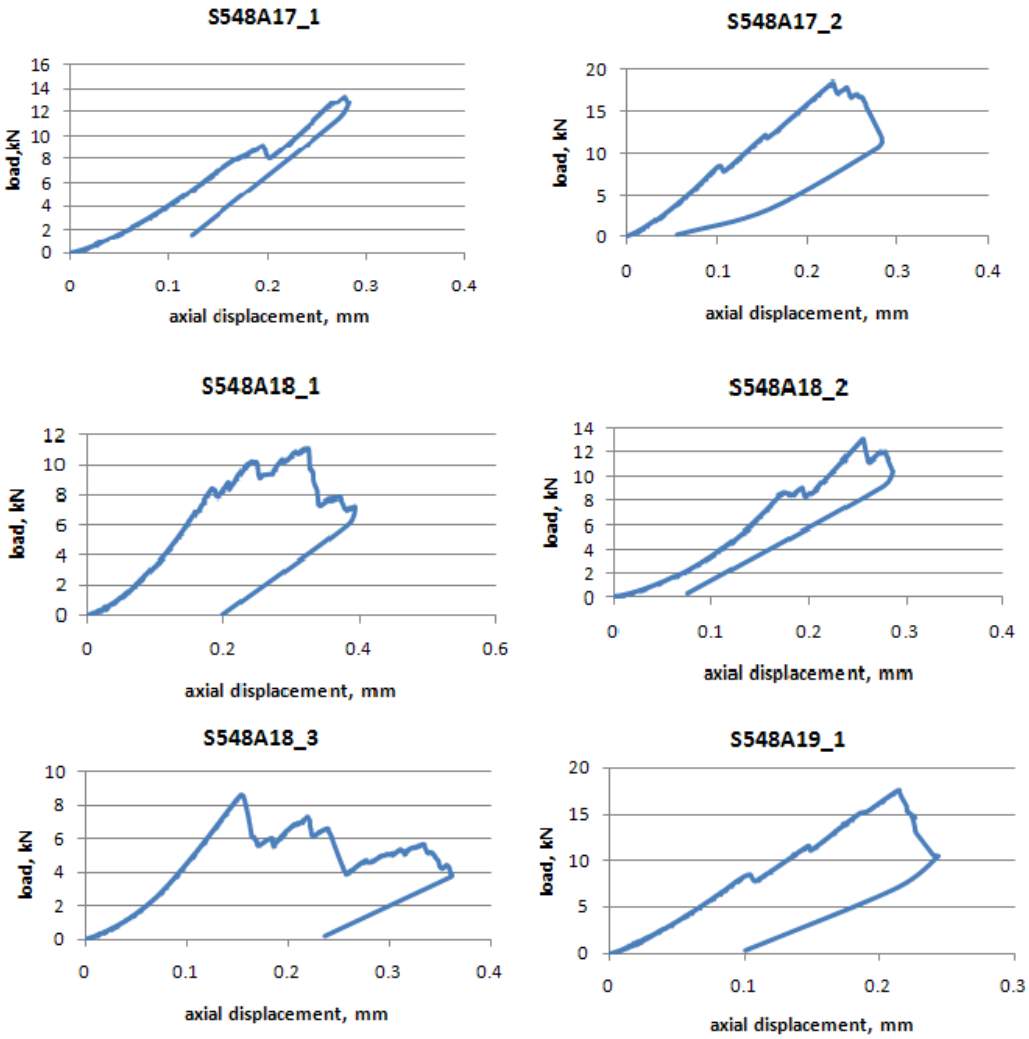

Figure A.1 Load-displacement graphs of MR tests

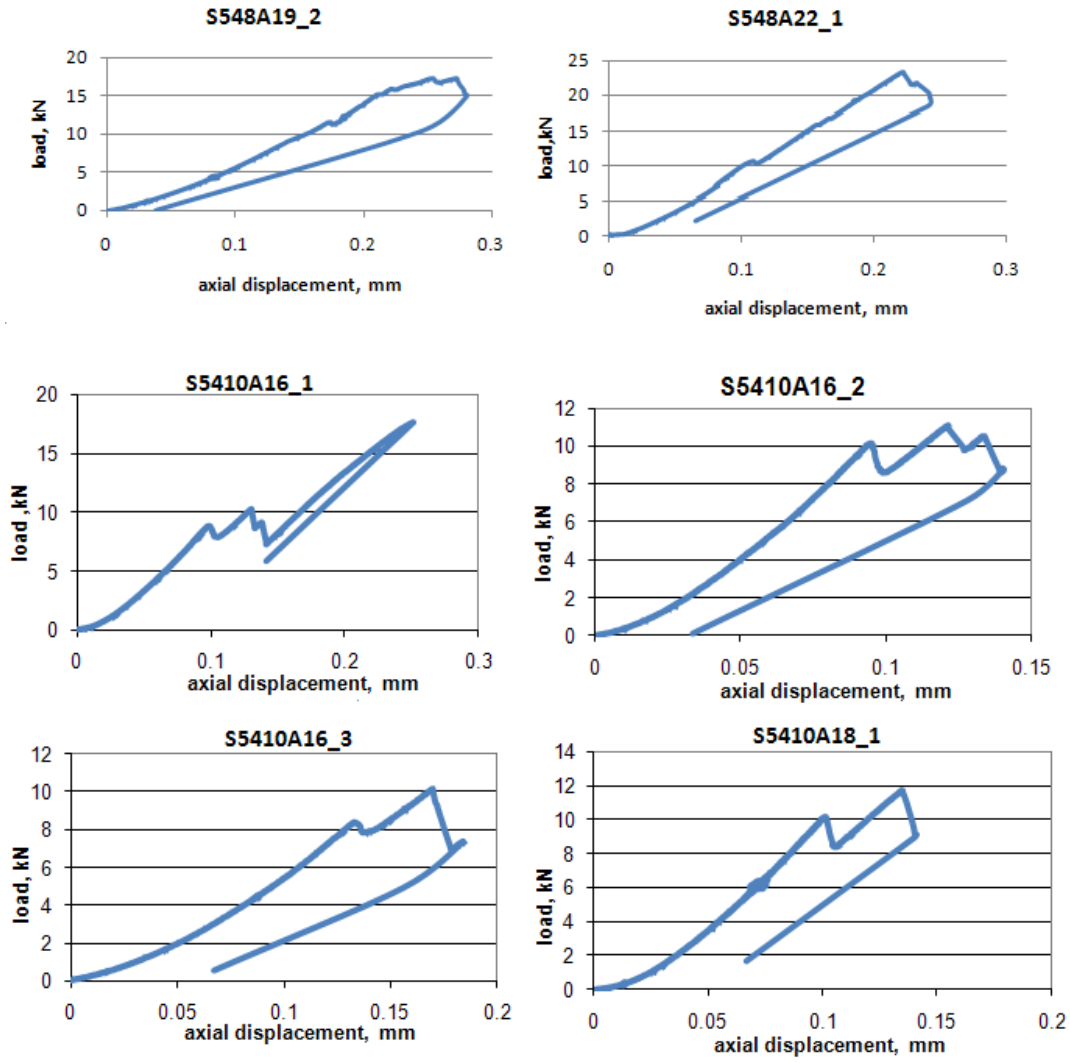

Figure A.1(cont'd) Load-displacement graphs of MR tests

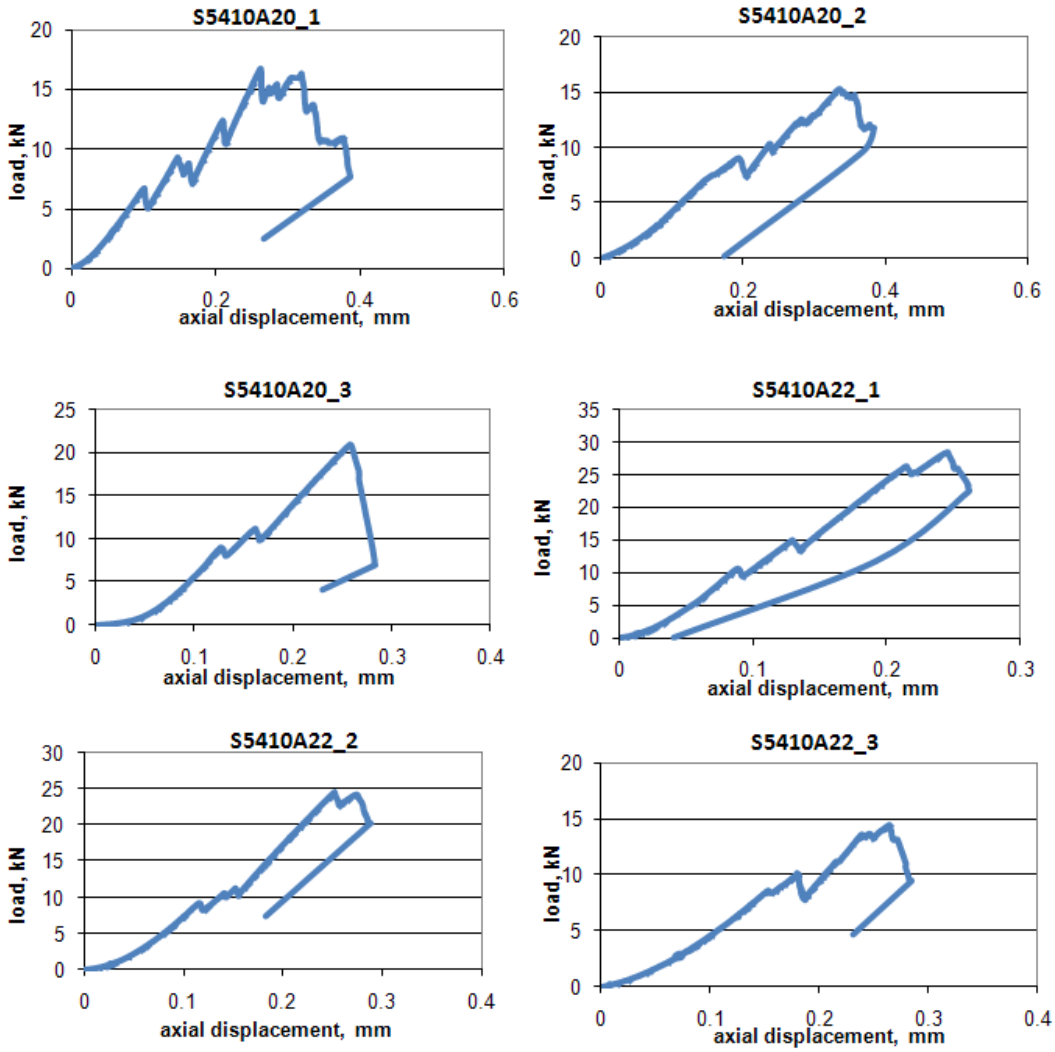

Figure A.1(cont'd) Load-displacement graphs of MR tests

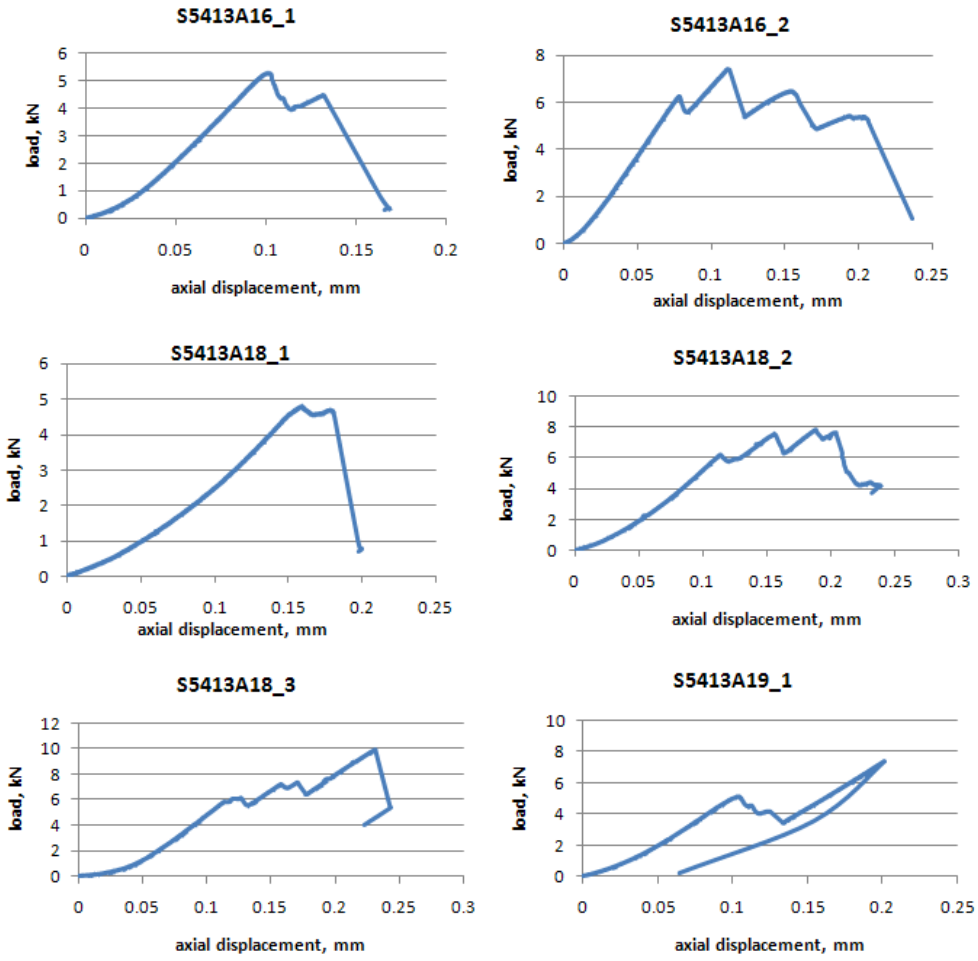

Figure A.1(cont'd) Load-displacement graphs of MR tests

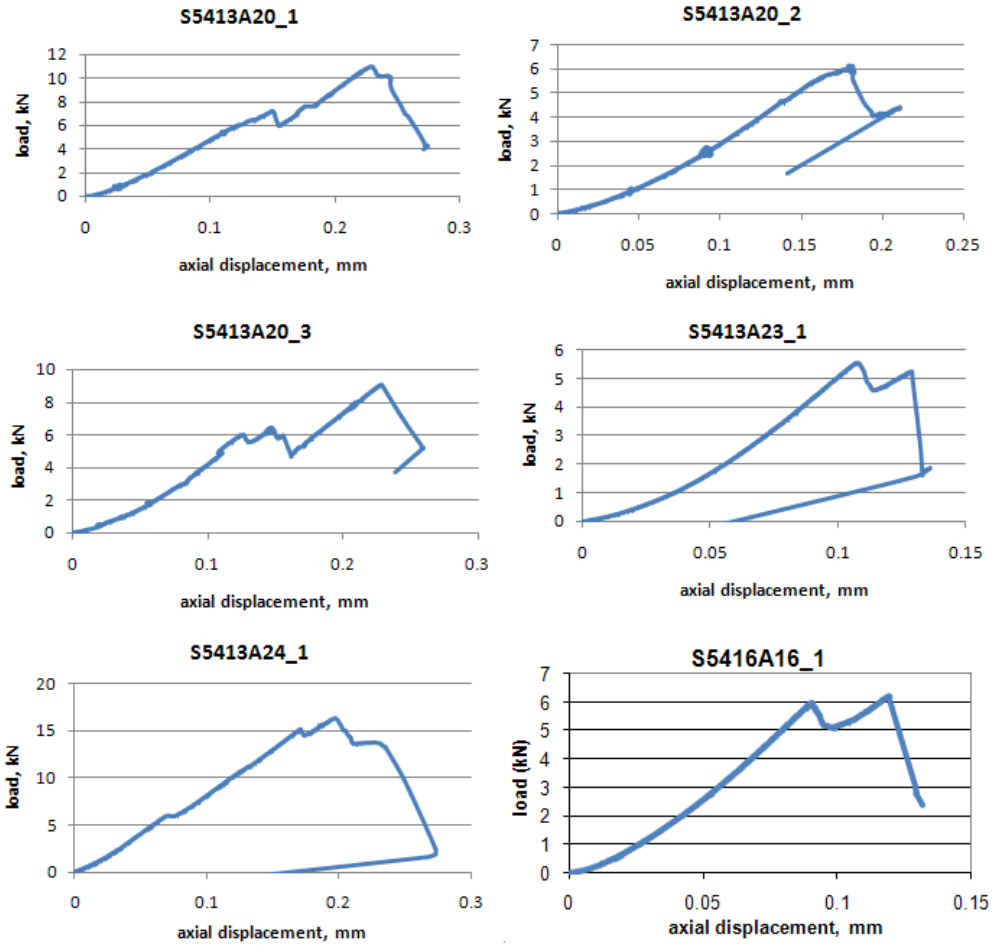

Figure A.1(cont'd) Load-displacement graphs of MR tests

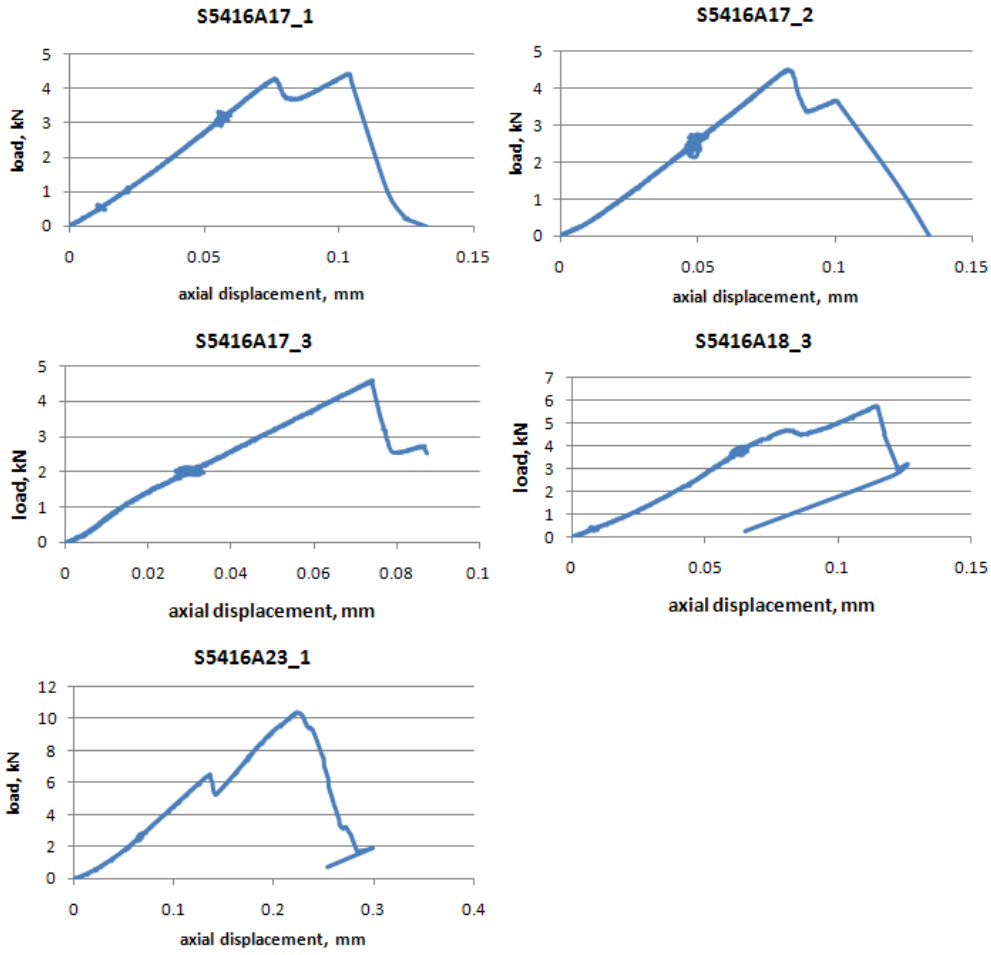

Figure A.1(cont'd) Load-displacement graphs of MR tests

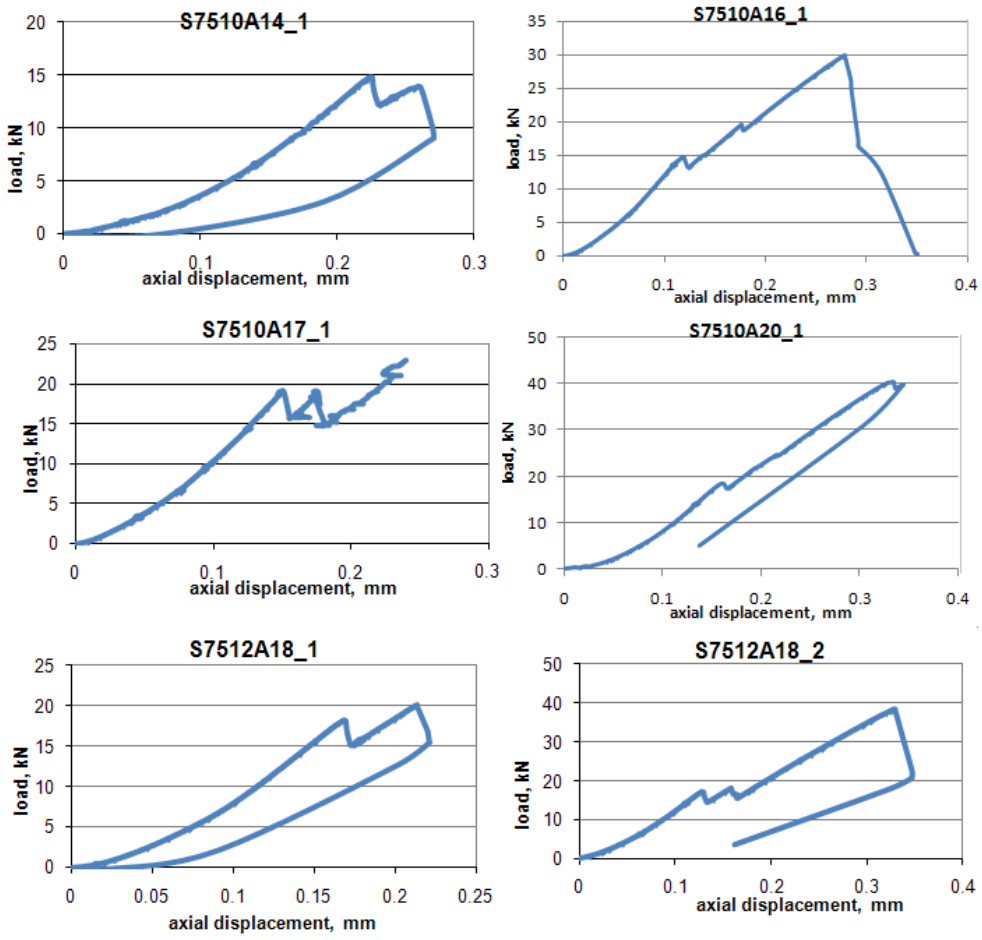

Figure A.1(cont'd) Load-displacement graphs of MR tests

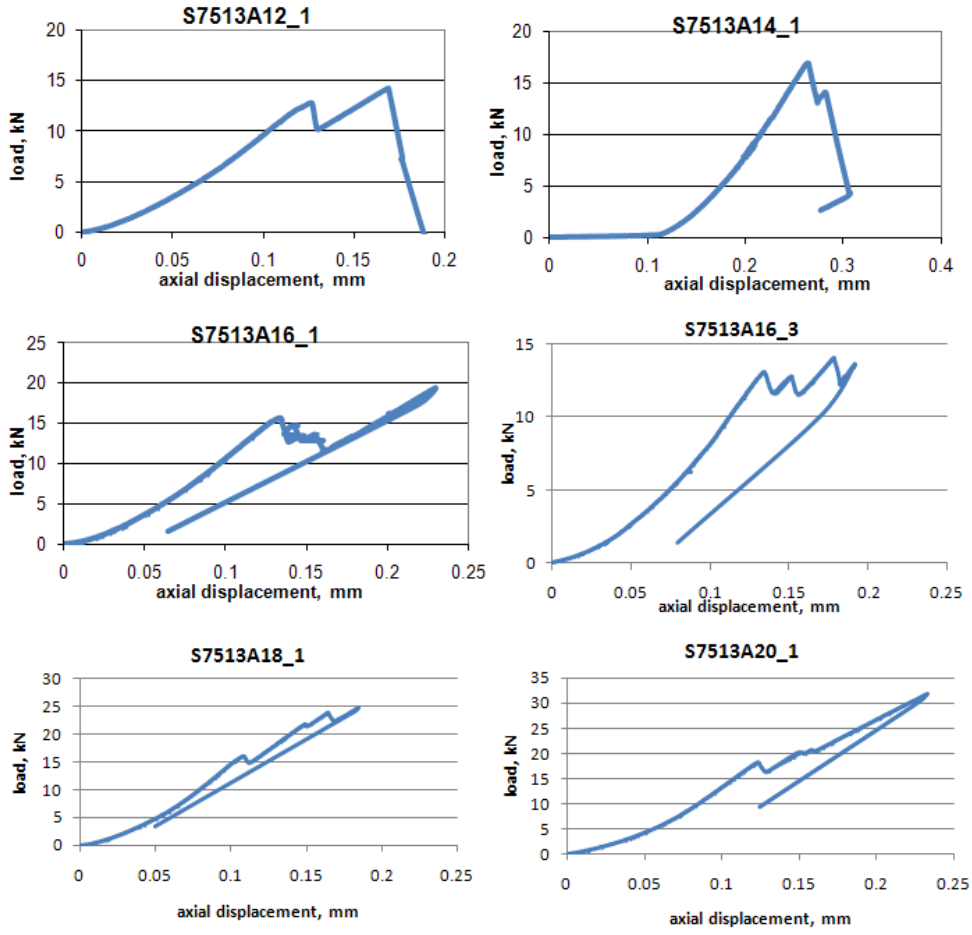

Figure A.1(cont'd) Load-displacement graphs of MR tests

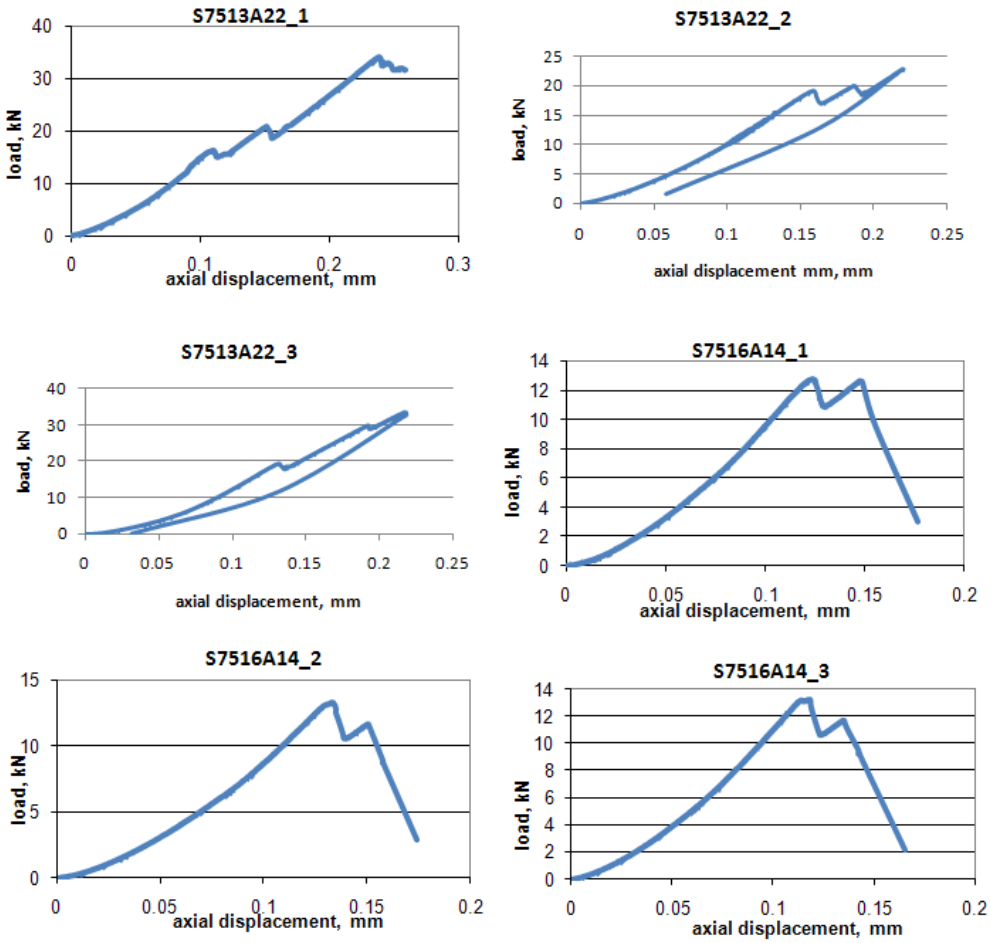

Figure A.1(cont'd) Load-displacement graphs of MR tests

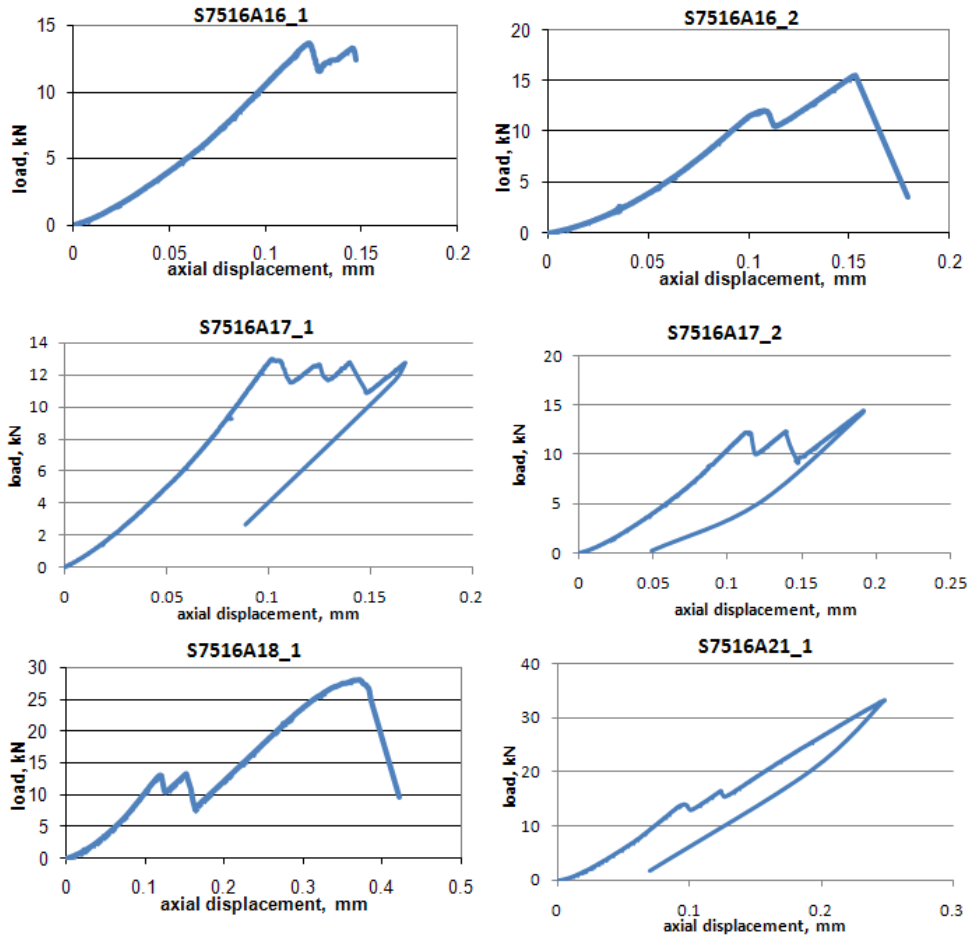

Figure A.1(cont'd) Load-displacement graphs of MR tests

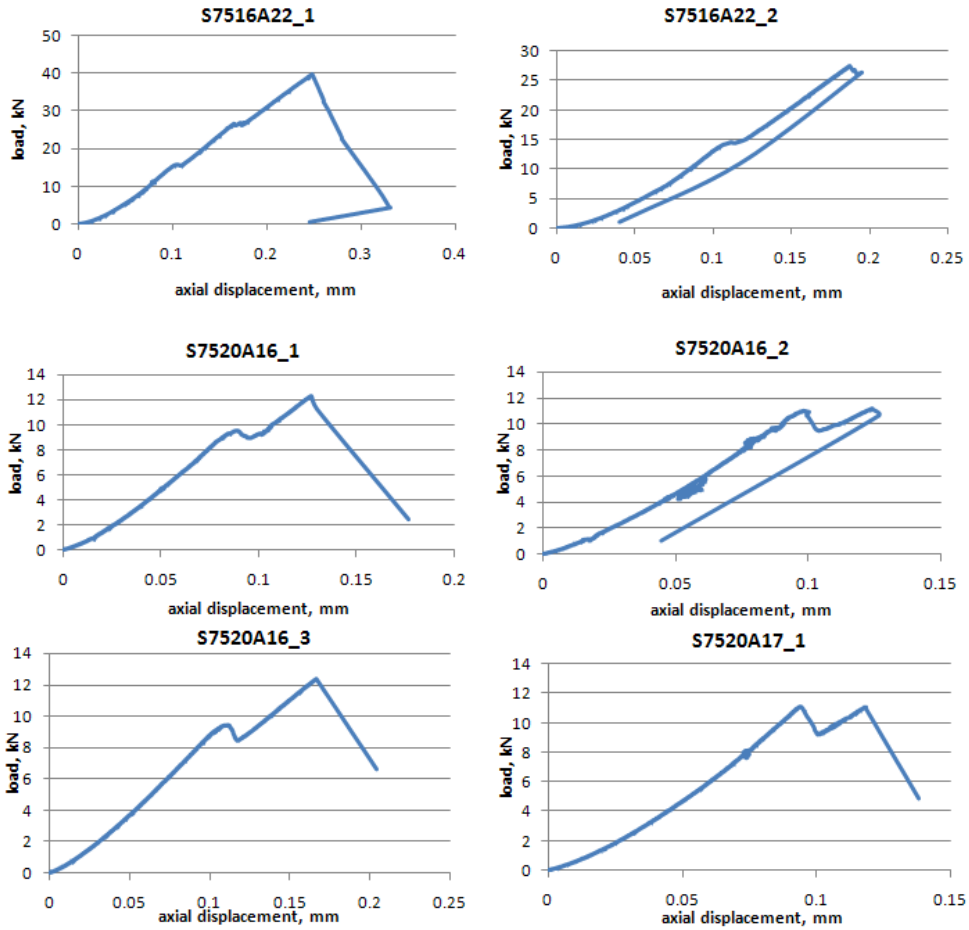

Figure A.1(cont'd) Load-displacement graphs of MR tests

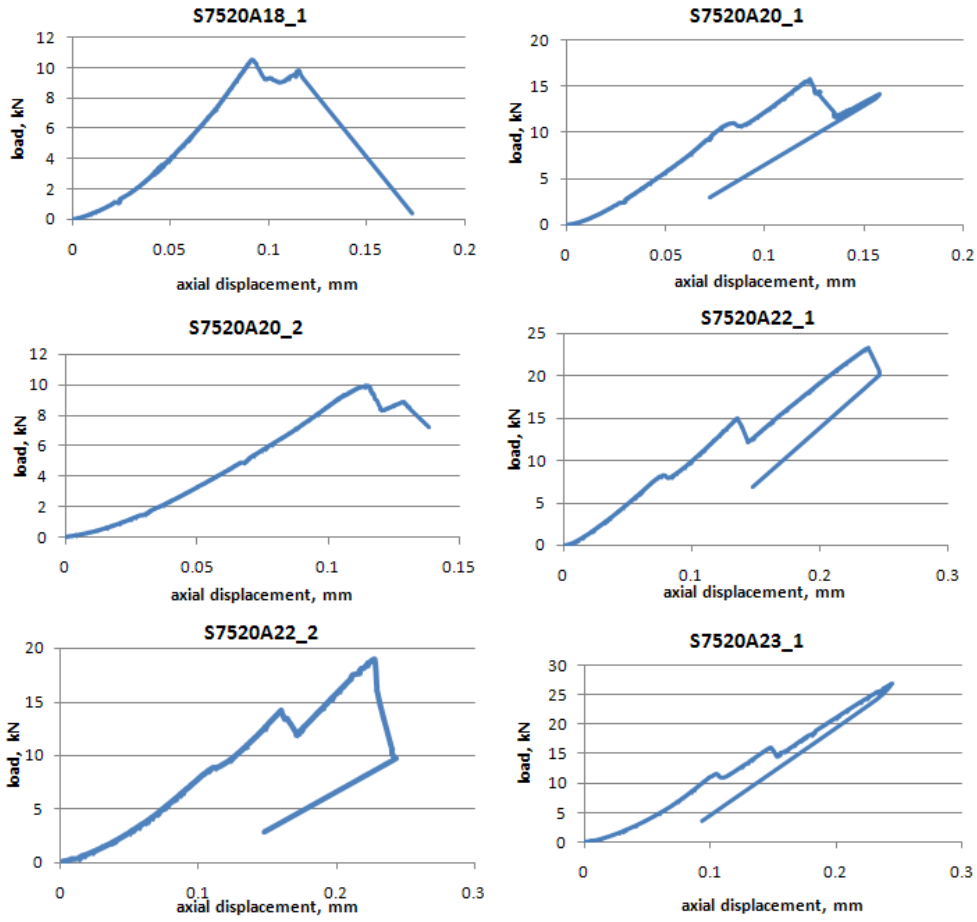

Figure A.1(cont'd) Load-displacement graphs of MR tests

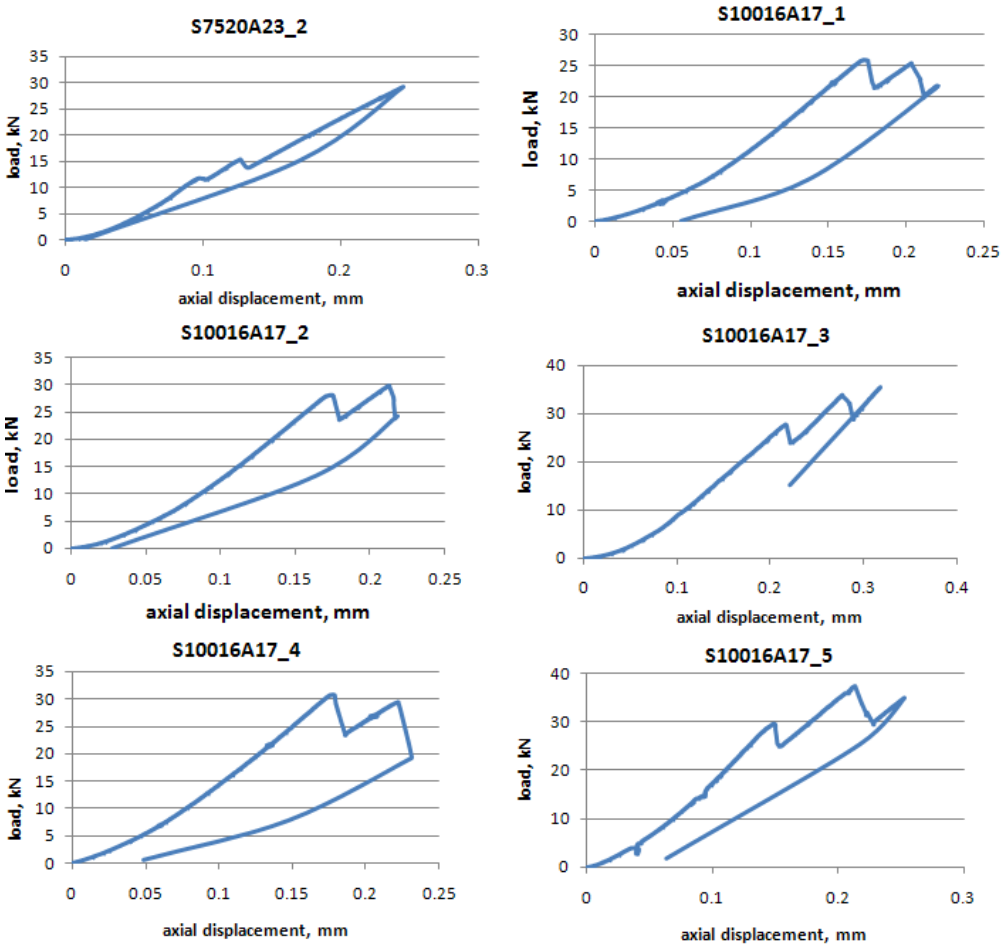

Figure A.1(cont'd) Load-displacement graphs of MR tests

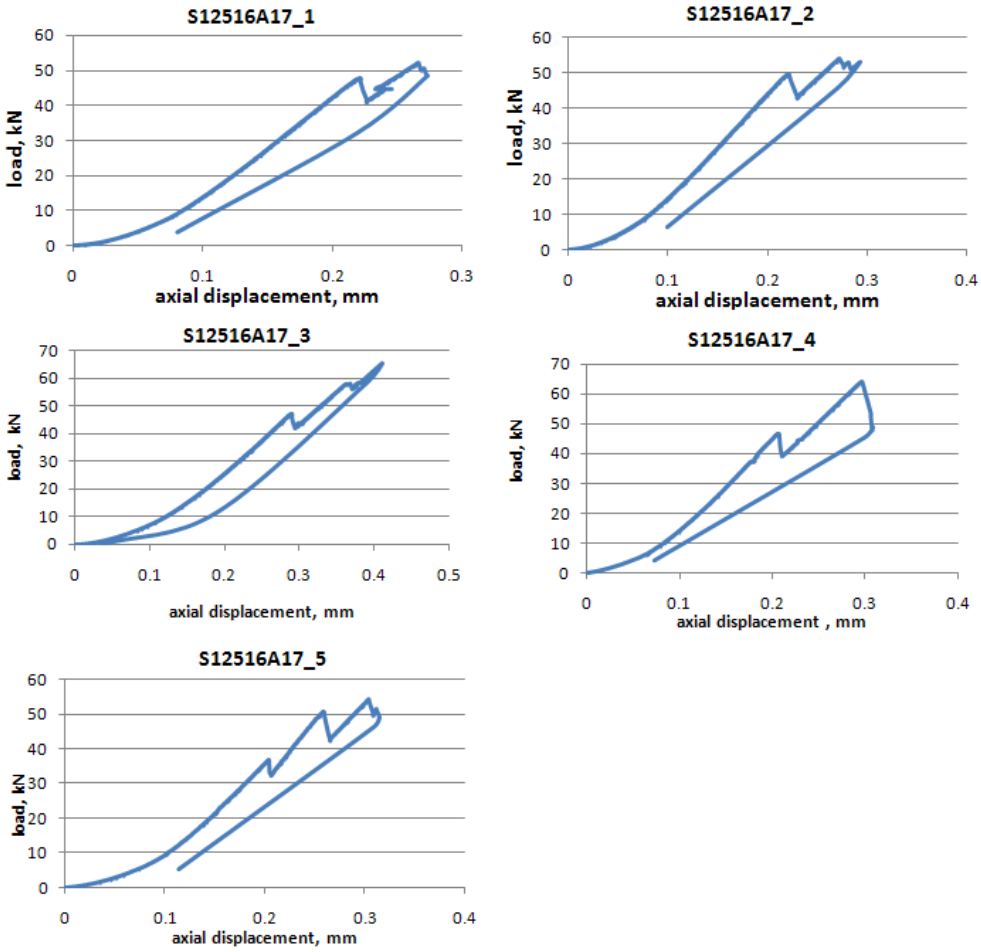

Figure A.1(cont'd) Load-displacement graphs of MR tests

APPENDIX B

B. SPECIMEN PHOTOS AFTER EXPERIMENTS

Figure B.1 Some of the 54 mm specimen photos after the experiments

Figure B.2 Some of the 75 mm specimens after the experiments

Figure B.3 100 and 125 mm specimens after the experiments